Upgrading waste heat streams with wet compression

Gudjonsdottir, Vilborg

DOI
10.4233/uuid:53822efe-863f-4708-b0d4-37f76fcd8a8e

Publication date
2020

Document Version
Final published version

Citation (APA)
Gudjonsdottir, V. (2020). *Upgrading waste heat streams with wet compression*. [Dissertation (TU Delft), Delft University of Technology]. https://doi.org/10.4233/uuid:53822efe-863f-4708-b0d4-37f76fcd8a8e

VILBORG GUÐJÓNSDÓTTIR

UPGRADING WASTE HEAT STREAMS WITH WET COMPRESSION

UPGRADING WASTE HEAT STREAMS WITH WET COMPRESSION

PROEFSCHRIFT

ter verkrijging van de graad van doctor
aan de Technische Universiteit Delft,
op gezag van de Rector Magnificus Prof. dr.ir. T. H. J. J. van der Hagen,
voorzitter van het College voor Promoties,
in het openbaar te verdedigen op maandag 9 maart 2020 om 10:00 uur

door

Vilborg GUÐJÓNSDÓTTIR

Werktuigkundig ingenieur
Technische Universiteit Delft, Nederland
geboren te Reykjavik, IJsland.

Dit proefschrift is goedgekeurd door de promotors:

Promotor: Dr. ir. C. A. Infante Ferreira

Promotor: Prof. dr. ir. T. J. H. Vlugt

Samenstelling promotiecommissie:

Rector Magnificus,	voorzitter
Dr. ir. C. A. Infante Ferreira,	Technische Universiteit Delft, promotor
Prof. dr. ir. T. J. H. Vlugt,	Technische Universiteit Delft, promotor

Onafhankelijke leden:

Prof. dr. A. A. Kiss,	The University of Manchester
Prof. dr. A. Kovacevic,	City University of London
Prof. dr. D. M. J. Smeulders,	Technische Universiteit Eindhoven
Prof. dr. L. C. M. Itard,	Technische Universiteit Delft
Prof. dr. B. J. Boersma,	Technische Universiteit Delft

ISPT
Institute for Sustainable Process Technology

TU Delft Delft University of Technology

The author would like to thank the members of the ISPT "Upgrading waste heat streams with compression resorption heat pumps" project for their financial and in kind contributions. This project was supported by the following organizations: ISPT, TU Delft, DOW, Nouryon, Atlas Copco, IBK, Frames. This project received funding from TKI E&I with the supplementary grant 'TKI-Toeslag' for Topconsortia for Knowledge and Innovation (TKI's) of the Ministry of Economic Affairs and Climate Policy.

Printed by: Gildeprint - Enschede

ISBN 978-94-6384-113-9
An electronic version of this dissertation is available at
http://repository.tudelft.nl/.

Þetta reddast

CONTENTS

SUMMARY

One of the most important steps we can take to minimize global warming is to become more energy efficient. An important example with potential for improvement is the large amount of energy wasted through waste heat streams in industry. For a long time there has already existed a solution that can efficiently upgrade waste heat streams to useful levels – heat pumps. However, heat pumps are rarely applied in industry. There are various reasons for this, including lack of knowledge and increased complexity. Another major reason is the long payback periods. This work focuses on a promising option that, for certain applications, can outperform traditional technologies by having a higher Coefficient of Performance (COP) and reaching higher temperatures: compression-resorption heat pumps (CRHP) using wet compression.

CRHP in its simplest form is similar to the traditionally used vapor-compression heat pump (VCHP), except that the working fluid is a mixture rather than a pure refrigerant. The most commonly used working fluid is NH_3-H_2O. However, alternative working fluids can potentially improve the COP further. In this research the focus is on two ways CRHP can be further improved. First, investigation of an alternative working fluid, NH_3-CO_2-H_2O. Second, assessment of the compressor performance when applying wet compression. In VCHP the compression process takes place entirely in the vapor region. Contrarily to pure vapor compression, wet compression occurs in the two-phase region. By compressing in the two phase region, superheating at the compressor outlet is eliminated, consequently CRHP are an excellent candidate for high temperature applications. However, the performance is only increased if the compression process is efficient enough.

To achieve the first goal of this research, a suitable thermodynamic property model for the NH_3-CO_2-H_2O mixture is identified. A new fit was developed of the e-NRTL model, already existing in the Aspen Plus software. The solid-liquid equilibrium (SLE) was improved and additional experimental data was used to extend the model range from 30 wt% NH_3 to around 50 wt% NH_3. This model was used to study the impact of adding CO_2 to NH_3-H_2O in CRHP using wet compression. The results showed that, for an application where a waste heat stream is heated from 60 to 105 °C, the COP could be increased by 5 % with the added CO_2. To partly validate the results, absorption experiments were performed in a mini-channel heat exchanger with both mixtures. Even though pumping instabilities limited the operating range with the added CO_2, an increase in transferred heat of approximately 5 % was observed compared to only NH_3-H_2O. The results indicate that specialized absorbers might be necessary to ensure that the absorption process is completed. It was also confirmed, that absorption of ammonia in NH_3-H_2O or NH_3-CO_2-H_2O in mini-channel heat exchangers is optimal when (1) the mixture is on the tube side, and (2) downward absorption is used.

At present, commercial compressors utilizing wet compression are not available. Therefore, a twin screw compressor model including entropy production was developed to identify the location of the main irreversibilities during that process. Another aim was to identify the operating ranges that will result in isentropic efficiencies above 70 %. From the model results it is clear that the operating conditions largely affect the efficiency of the compressor, and that for CRHP assuming a fixed efficiency will result in inaccurate estimations. For a fixed pressure ratio, the efficiency increased with increased NH_3 concentration, decreased vapor quality and clearance size. The efficiency also increases, up to a certain limit, with increasing rotational speed. The results indicate that, for certain operating ranges, the goal of reaching an isentropic efficiency of 70 % should be attainable. A simplified version of this model, that operates either with NH_3-CO_2-H_2O or NH_3-H_2O, was developed as well to speed up heat pump cycle estimations. To summarize this study, the thermodynamic and economic performance were investigated of two specific applications with CRHP utilizing wet compression, and operating with both NH_3-CO_2-H_2O and NH_3-H_2O. The payback time, when replacing a boiler, was investigated for two high temperature applications; upgrading a waste heat stream from 90 to 130 °C and from 60 to 140 °C. Regarding the NH_3-CO_2-H_2O mixture, even though for certain cases the thermodynamic performance can be improved significantly, there might not be any economic advantage compared to NH_3-H_2O. The results were also highly affected by the gas and electricity prices and especially the cost of CO_2 emissions; the latter has increased dramatically in the last two years. In the current climate it is crucial to take it into account when analyzing the business case for heat pumps. This investigation showed that CRHP are a very promising economical option for applications with a temperature glide. Even for high glides of 80 K, the payback time can be within acceptable limits: three years in most cases.

This research has shown that CRHP are ideal candidates to upgrade waste heat streams with a temperature glide. Still, some questions remain unanswered. Current work aims to validate the compressor performance. Wet compression experiments using NH_3-H_2O have been initiated at the Delft University of Technology. These experiments need to be finalized, and subsequently a pilot heat pump plant should be constructed. Further experiments should be conducted to investigate the NH_3-CO_2-H_2O mixture performance, especially the compressor performance. Nevertheless, the business case for heat pumps in general keeps on improving, and in the coming years we hopefully will see a steep increase of heat pumps installed at industrial sites.

SAMENVATTING

Eén van de belangrijkste stappen die we kunnen zetten tegen de opwarming van de aarde is het efficiënter omgaan met energie. De grote hoeveelheid energie die verloren gaat in industriële reststromen is een belangrijk voorbeeld van energie waar we efficiënter gebruik van zouden kunnen maken. Een oplossing hiervoor bestaat al een lange tijd: warmtepompen. Warmtepompen worden echter zelden gebruikt in de industrie. Hiervoor zijn verschillende redenen zoals het gebrek aan kennis, complexiteit en de lange terugverdientijd. Het onderzoek in dit proefschrift richt zich op compressie-resorptie warmtepompen (CRHP) die in bepaalde toepassingen betere resultaten behalen dan traditionele systemen in termen van een hogere warmtefactor (Coefficient of Performance, COP) en het bereiken van hogere temperaturen.

CRHP's lijken op de traditionele dampcompressie-warmtepompen (VCHP). In plaats van een zuiver koudemiddel wordt een mengsel als werkmedium gebruikt. Het meest gebruikte mengsel is NH_3-H_2O. Andere werkmedia zouden de COP echter verder kunnen verbeteren. Dit onderzoek beschouwt twee manieren om de prestaties van CRHP's te verbeteren. Ten eerste, door te kijken naar een alternatief mengsel: NH_3-CO_2-H_2O. Ten tweede, door de prestaties van compressoren die gebruik maken van natte compressie te analyseren. In VCHP's gebeurt de compressie volledig in de gasfase en in CRHP's daarentegen gebeurt de (natte) compressie volledig in het twee-fasen gebied. Door de compressie te laten plaatsvinden in het twee-fasen gebied is oververhitting in de uitlaat van de compressor niet mogelijk. Dit maakt CRHP's geschikt voor toepassingen bij hoge temperaturen. De prestaties nemen echter alleen toe als de compressie efficiënt genoeg is.

In het eerste deel van dit onderzoek wordt gezocht naar een bruikbaar thermodynamisch model voor het mengsel NH_3-CO_2-H_2O. Uitgaande van het e-NTRL model in Aspen Plus wordt een nieuw model afgeleid. Het vaste stof-vloeistof evenwicht (SLE) wordt beter voorspeld en additionele experimentele data is gebruikt om het model bruikbaar te maken voor massaconcentraties van 30 % NH_3 tot ongeveer 50 % NH_3. Dit model is gebruikt om te onderzoeken hoe het toevoegen van CO_2 aan NH_3-H_2O de CRHP met natte compressie beïnvloedt. Resultaten laten zien dat de COP met 5 % kan worden verhoogd door CO_2 toe te voegen aan een systeem waarmee een afvalstroom werd verwarmd van 60 °C tot 105 °C. Om dit resultaat (gedeeltelijk) te valideren zijn experimenten uitgevoerd met beide mengsels in een mini-channel warmtewisselaar. Deze experimenten laten een toename van 5 % in de warmteoverdracht zien wanneer CO_2 wordt toegevoegd, vergeleken met alleen NH_3-H_2O. Deze resultaten laten ook zien dat speciale absorbers nodig kunnen zijn zodat het absorptieproces volledig kan plaatsvinden. De absorptie van ammoniak in NH_3-H_2O of NH_3-CO_2-H_2O in mini-channel warmtewisselaars bereikt een optimum als (1)

het mengsel zich aan de pijpenzijde bevindt en (2) het absorptieproces van boven naar beneden plaatsvindt.

Op dit moment zijn commerciële compressoren die gebruik maken van natte compressie niet beschikbaar. In deze studie is daarom een schroefcompressor model ontwikkeld dat de lokale entropieproductie (de irreversibiliteiten) van dat proces in kaart kan brengen. Dit model is ook gebruikt om de condities te bepalen waarvoor de isentropische efficiëntie hoger is dan 70 %. Uit de resultaten blijkt dat de werkcondities een grote invloed hebben op de efficiëntie van de compressor en dat we niet kunnen aannemen dat de CRHP een constante efficiëntie heeft aangezien dit tot onnauwkeurige voorspellingen leidt. Bij een vaste drukverhouding wordt de efficiëntie hoger bij een toenemende concentratie van NH_3, lagere dampfractie en lagere toleranties. De efficiëntie neemt ook toe, tot een bepaalde hoogte, bij een hogere rotatiesnelheid. Deze resultaten laten zien dat het haalbaar zou moeten zijn om een isentropische efficiëntie van 70 % te behalen. Om snellere voorspellingen te kunnen doen wat betreft de warmtepompcycli van de CRHP is een versimpelde versie van het model ontwikkeld voor NH_3-CO_2-H_2O of NH_3-H_2O. De thermodynamische en economische prestaties zijn geanalyseerd voor twee toepassingen van de CRHP met natte compressie, voor zowel NH_3-CO_2-H_2O als NH_3-H_2O. De terugverdientijd is berekend voor twee toepassingen bij hoge temperaturen (waarbij een ketel is vervangen), namelijk het opwaarderen van een reststroom van 90 °C naar 130 °C en van 60 °C naar 140 °C. Hoewel in sommige gevallen het gebruik van het mengsel NH_3-CO_2-H_2O de thermodynamische prestatie significant kan verbeteren is er meestal geen economisch voordeel ten opzichte van NH_3-H_2O. Bovendien werden deze resultaten sterk beïnvloed door de gas- en elektriciteitsprijzen en vooral de kosten voor CO_2-uitstoot die de laatste twee jaar flink hoger zijn geworden. Dit is tegenwoordig een belangrijk aspect bij economische analyses van warmtepompen. Dit onderzoek laat zien dat de CRHP een aantrekkelijk alternatief kan zijn voor toepassingen met een glijdend temperatuurprofiel. Zelfs voor grote temperatuurveranderingen van 80 K blijft de terugverdientijd in de meeste gevallen beperkt tot drie jaar.

Het werk in dit proefschrift laat zien dat de CRHP een aantrekkelijke optie is voor het opwaarderen van industriële reststromen met een glijdend temperatuurprofiel. Een aantal vragen blijven echter onbeantwoord. Op dit moment richt het werk zich op het valideren van de werking van de compressor. Bij de TU Delft zijn er experimenten gestart met NH_3-H_2O. Wanneer deze experimenten zijn afgerond kan een eerste warmtepompsysteem worden gebouwd. Aanvullende experimenten zijn nodig om de werking van NH_3-CO_2-H_2O te analyseren en dan vooral van de compressor. Desalniettemin zal de economische haalbaarheid voor warmtepompen blijven verbeteren en zullen we de komende jaren hopelijk een toename zien van het gebruik van warmtepompen in de industrie.

NOMENCLATURE

A	Area	m^2
aq	Aqueous	
a, b	Constants for Blasius equation	
Bi	Biot number	
C	Dynamic bearing load	N
c	Specific energy cost	€ kWh^{-1}
c_p	Isobaric heat capacity	J kg^{-1} K^{-1}
CRF	Capital recovery factor	
d	Diameter	m
FC	Annual fuel consumption cost	€
G	Gas	
g	Gaseous	
Gz	Graetz number	
H	Enthalpy	J
H	Yearly operating time	h
h	Specific enthalpy	J kg^{-1}
hc	heat transfer coefficient	W m^{-2} K^{-1}
i	Interest rate	
i_L	Inflation rate	
L	Length	m
l/L	Liquid	
m	Mass	kg

$\dot{m}$	Mass flow	kg s^{-1}
mol%	Mole percent	
m_1	Number of male lobes	
N	Number of tubes	
n	Rotation speed	rpm
N_m	Number of measurements	
Nu	Nusselt number	
OMC	Operation and maintenance cost	€
P	Pressure	Pa
p	Tube pitch	m
PBP	Payback period	years
PEC	Purchased Equipment Cost	€
Pr	Pressure ratio	
Q	Heat	J
q	Vapor quality	
$\dot{Q}$	Heat duty	W
r	Radius	m
s	Solid	
s	Specific entropy	J kg^{-1} K^{-1}
T	Temperature	K
TCI	Total Capital Investment	€
U	Overall heat transfer coefficient	W m^{-2} K^{-1}
u	Uncertainty	
V	Volume	m^3
v	Specific volume	m^3 kg^{-1}

$\dot{V}$	Volume flow rate	$m^3\ s^{-1}$
V	Vapor	
W	Work	J
w	Velocity	$m\ s^{-1}$
$\dot{W}$	power	W
X	Component size or capacity	
x	Mass concentration	$kg\ kg^{-1}$
z	Axial position in the heat exchanger	m

Greek Symbols

α	Nonrandomness factor / Dimensionless spacing between tubes	
β	Pitch-to-tube diameter ratio	
Δ	Difference	
η	Efficiency	
γ	Cost function exponent	
λ	Thermal conductivity	$W\ m^{-1}\ K^{-1}$
μ	Coefficient of friction	
μ	Dynamic viscosity	$Pa\ s^{-1}$
ω	Angular rotation speed	s^{-1}
ϕ	Male rotor turning angle	
ϕ_t / ϕ_s	Weight factors	
ρ	Density	$kg\ m^{-3}$
σ	Standard deviation	
$\dot{\sigma}$	Entropy production rate	$W\ K^{-1}$
τ	Asymmetric binary interaction energy parameter	
ζ	Flow coefficient	

Sub and superscripts

2st	2 stage
avg	Average
b	Bearings
calc	Calculated
comb	Combined
comp	Compressor
cw	Waste stream
d	Discharge
des	Desorber
down	downstream
driving	Driving
eff	Effective
el	Electricity
exp	Experimental
h	Hydraulic
high	Higher
HP	Heat Pump
i,j	Component
id	Ideal
in	Inlet
interm	Intermediate
is	Isentropic
lm	Logarithmic mean
low	Lower

LT	Technical life time	years
max	Maximum	
mech	Mechanical	
motor	Motor	
NG	Natural Gas	
opt	Optimum	
out	Outlet	
p	Derived variable	
real	Real	
res	Resorber	
s	Shell side/Suction/Constant entropy	
seal	Seal	
t	Tube side	
th	Theoretical	
total	Total	
up	Upstream	
vol	Volumetric	
W	Equipment with known cost	
x,z	Measured variables	
Y	Equipment with calculated cost	

Abbreviations

CFD	Computation fluid dynamics
CHX	Coiled heat exchangers
COP	Coefficient of Performance
CRHP	Compression-resorption heat pumps

e-NRTL	Electrolyte Non Random Two Liquid
EOS	Equation of State
GHG	Greenhouse gas
GWP	Global warming potential
HP	Heat Pump
HTHP	High temperature heat pump
IEA	International Energy Agency
LMTD	Logarithmic mean temperature difference
MCGP	Magnetically coupled gear pumps
PC-SAFT	Perturbed Chain Statistical Association Fluid Theory
PHX	Plate heat exchangers
RK	Redlich-Kwong
SLE	Solid-liquid equilibrium
SRK	Soave-Redlich-Kwong
UNIQUAC	Universal Quasi Chemical
VCHP	Vapor compression heat pumps
VLE	Vapor-liquid equilibrium

1

INTRODUCTION

1.1 BACKGROUND

As the Swedish 16 year old Greta Thunberg keeps reminding us, global warming is a real threat to our society [1]. Drastic changes and large efforts on many fronts are necessary so that the Paris agreement – keeping the global temperature increase during this century well below 2 °C – can be fulfilled [2]. One important example is the urgent need to switch from fossil fuels to renewable energy sources. However, that alone will not suffice to keep the temperature increase within the set limit.

One of the measures of the European Council to reduce greenhouse gas emissions is to improve energy efficiency [3]. In Europe, industry is responsible for approximately a quarter of the total energy consumption [4]. Heat pumps have the potential to drastically reduce energy requirements in industry and in that way reduce emissions [5]. Wolf and Blesl [6] estimated the technical potential, of heat pumps delivering heat up to 100 °C, to be 1,717 PJ in the EU-28 industrial sector. This corresponds to 17 % decrease in CO_2 emissions in that sector. However, the use of industrial heat pumps is still quite limited. According to the International Energy Agency (IEA), there are various reasons why heat pumps are not applied to a greater extent, such as lack of knowledge and low awareness of heat consumption. Another major reason is long payback periods, often in the range of 5-8 years or even more [7]. By increasing the efficiency of industrial heat pumps, the payback period might decrease sufficiently for industry to start applying heat pumps to a greater extent.

1.2 COMPRESSION-RESORPTION HEAT PUMPS

A mechanically driven heat pump is a device that can upgrade low-temperature waste heat to useful high-temperature heat using mechanical work. In recent years, several review articles investigate the use of industrial heat pumps [8–11]. As these reviews mention, the most widely studied and used heat pump technology is the vapor compression heat pump (VCHP). Many research directions have been taken to improve its performance, including investigation of alternative refrigerants, cascade systems and 2-stage cycles [8, 10]. Furthermore, other heat pump systems have been considered such as absorption heat pumps and hybrid heat pumps [10, 11]. Another alternative that shows potential to have increased performance compared to traditional technologies is the compression-resorption heat pump (CRHP) [12].

For many industrial applications where there is a temperature glide of the heat source and/or sink, CRHP are a very promising option to upgrade waste heat streams, especially when using wet compression. Traditional VCHP have four components: compressor, condenser, expansion valve and evaporator. A compression-resorption heat pump has a resorber and a desorber instead of the condenser and evaporator (see figure 1.1). In CRHP, the working fluid is a mixture, such as NH_3-H_2O. This ensures that the phase transition of

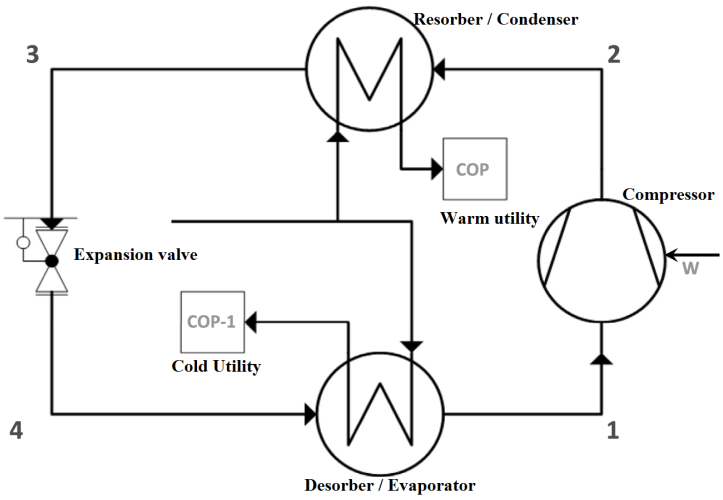

Figure 1.1: A schematic of a heat pump; splitting a waste heat stream into a warm and cold utility stream. If only heat is required the COP is the ratio of heat delivered to an application (in the resorber/condenser) and the work required by the compressor. If there are cooling demands then the cooling delivered to an application (in the desorber/evaporator) is added to the heat delivered for calculating the COP. Compared to VCHP, the condenser is replaced by a resorber and the evaporator by a desorber in CRHP.

the mixture in the heat exchangers at constant pressure is non-isothermal. Therefore, the temperature glide of the mixture can be fitted to the temperature glide of the heat source and/or sink by varying the mixture composition. Additionally, by using wet compression, instead of the traditional vapor compression, superheating is eliminated (see figure 1.2). This means that the source temperature can be upgraded to higher levels and the temperature fit can be further improved. These factors can result in a Coefficient of Performance (COP) higher than that of conventional technologies [12]. This will, however, depend on each specific application as pointed out by Itard and Machielsen [13].

Potential industrial applications where CRHP can be applied are various. Arpagaus et al. [9] identified various applications in the paper, food and chemical industry such as drying processes, pasteurizing and production of low-pressure steam. In Europe alone, the authors estimated the technical potential as "113 PJ for process heat between 100 and 150 °C". As the study mentioned, increased interest has been on high temperature heat pumps (HTHP), defined as delivering heat above 100 °C. As mentioned above, since superheating is eliminated with CRHP utilizing wet compression, they are ideal candidates for high temperature applications.

There are a couple of limitations when it concerns HTHP. One of the main challenges is to find a suitable working fluid that has a low global warming potential (GWP). Common working fluids are R245fa, R717 (ammonia), R744 (CO_2), R134a, and R1234ze(E) [9]. Both R134a and R245fa have a high global warming potential of 1300 and 858, respec-

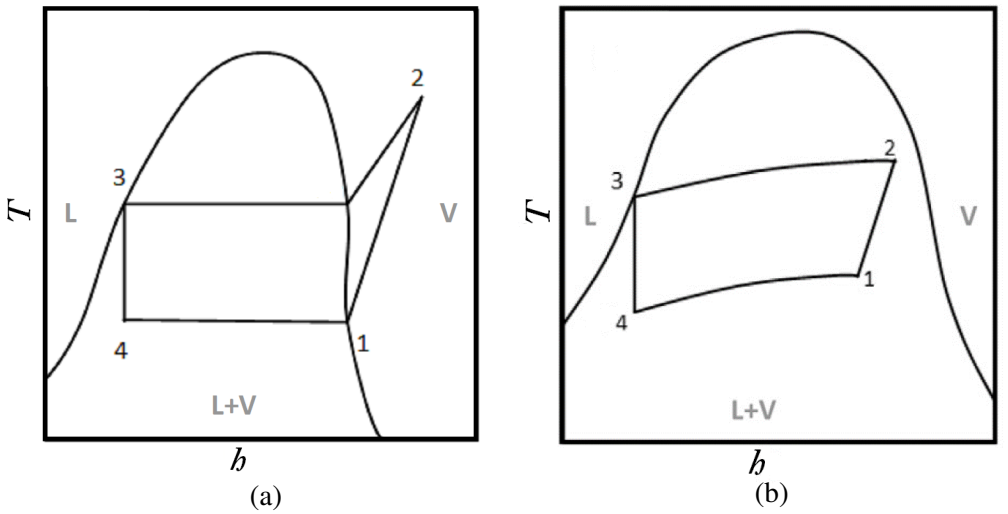

Figure 1.2: Typical *Th*-diagrams for (a) VCHP, and (b) CRHP utilizing wet compression [12]. The state points correspond to figure 1.1. By compressing in the two state region, superheating is eliminated at the compressor outlet (state point 2).

tively. Some studies have been conducted to find low GWP alternatives, in all cases only pure refrigerants have been researched [14–16]. Limited number of studies have looked at mixtures for high temperature applications and in two recent cases the thermodynamic properties are not reported [17, 18]. For CRHP the working fluid is normally NH_3-H_2O. Both NH_3 and H_2O have 0 GWP. One of the main problems of operating a heat pump with water is that the vapor density is very low, resulting in a high volume flows. Additionally, the lower pressure level can be significantly below atmospheric pressure. On the other hand, ammonia as an operating fluid requires special high pressure equipment at high temperatures, resulting in additional costs. Other mixtures can potentially further increase the performance of CRHP. In this study a promising mixture is investigated or NH_3-CO_2-H_2O. Similarly, operating a heat pump with CO_2, with a GWP of 1, the operating pressures are high. Operating a CRHP with an NH_3-H_2O mixture or NH_3-CO_2-H_2O can solve the low and high pressure problems. By choosing the mixture concentration carefully, the operating pressures can stay within reasonable limits.

However, the benefits of CRHP utilizing wet compression are only brought about if the isentropic efficiency of the compressor is high enough. That limit has been identified by several authors to be above 70 % [12, 19, 20]. Additionally, no commercial solution utilizing wet compression is available. If such a compressor could be manufactured, payback periods could be significantly shortened compared to VCHP, especially for applications with temperature glides and high temperature lifts [21]. This makes this solution attractive for the industry, with significant energy savings and associated major reduction in GHG emissions.

1.3 PROBLEM STATEMENT AND METHODOLOGY

The goal of this thesis is to investigate the potential of CRHP utilizing wet compression with the goal of upgrading industrial waste heat streams. An additional aim is to discover how the system performance can be further improved, both in energetic and economic points of view.

To achieve this goal, a preliminary study is made into a potential application and an alternative working fluid for CRHP. As mentioned above, a typical working fluid for CRHP is NH_3-H_2O. This mixture is beneficial due to not only its non-isothermal behavior during phase transition, but also to its very low global warming impact. However, other working fluids can potentially increase the benefits of CRHP even further. A possible candidate investigated in this study is NH_3-CO_2-H_2O. A suitable thermodynamic property model is identified and its operating range is extended. Then the performance of a particular application case is investigated for both mixtures. To partly validate the potential of the mixture, absorption experiments are performed in a mini-channel heat exchanger with NH_3-H_2O and NH_3-CO_2-H_2O. Thereafter, the focus is shifted to the compressor itself, and a model is developed of a twin screw compressor suitable for wet compression. The approach is based on Zaytsev's homogeneous model for mass and energy conservation [20]. The model is modified to include entropy production to identify where the main irreversibilities are located in the compressor. A simplified version of that model was developed as well that can operate with both NH_3-H_2O and NH_3-CO_2-H_2O. That model allows the heat pump performance to be more easily investigated. Subsequently, a model of the entire heat pump cycle with the simplified version of the compressor model is developed to evaluate its overall performance operating with both NH_3-H_2O and NH_3-CO_2-H_2O. It should be noted that the optimal thermodynamic performance does not necessarily correspond to the optimal economic performance. As mentioned above, it is important to shorten payback periods of heat pumps to ensure that they will be applied in industry. Therefore, both the energetic and economic performance of CRHP are compared to that of a conventional technology, namely a boiler.

1.4 OUTLINE OF THIS THESIS

The thesis outline is visualized in Figure 1.3 and is organized as follows. Succeeding this introduction, Chapter 2 investigates the potential of NH_3-CO_2-H_2O in CRHP. The results from Chapter 2 indicate a 5 % increase in the COP compared to only NH_3-H_2O for heating applications. This potential is partly confirmed with absorption experiments in Chapter 3, where a 5 % increase in heat transfer was observed with the added CO_2. However, pumping instabilities limited the operating range suggesting that specialized absorbers might be necessary when operating with the NH_3-CO_2-H_2O mixture. Next, in Chapter 4, a more detailed study into wet compression in a twin screw compressor is performed. The focus

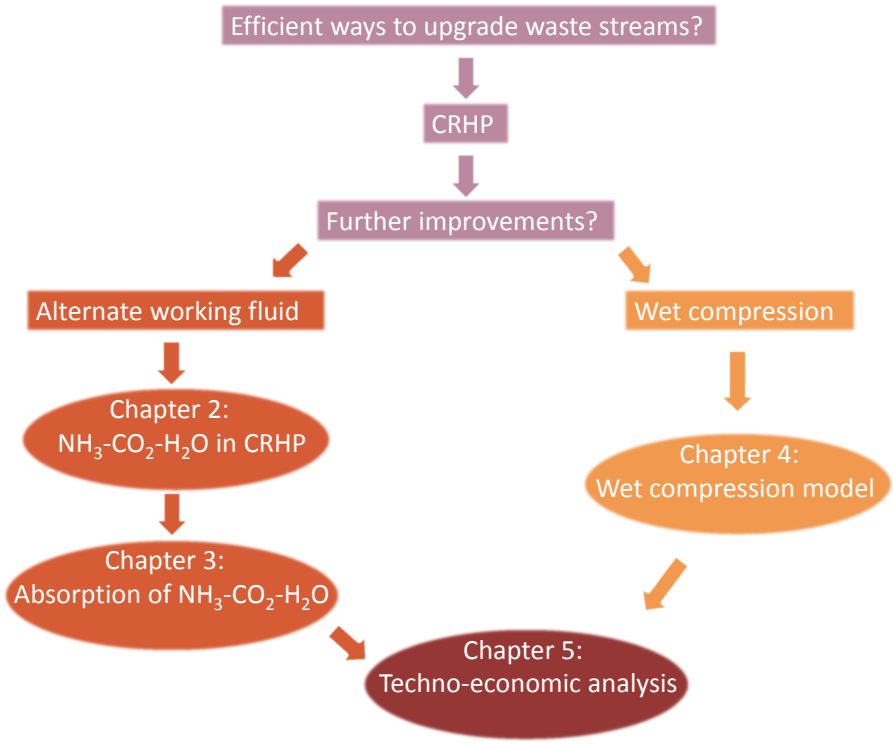

Figure 1.3: Goal of this thesis and outline. Two ways are explored in this thesis to further improve the performance of CRHP, that are a promising option to upgrade industrial waste heat streams. First, the benefits of using NH_3-CO_2-H_2O as a working fluid are explored (Chapter 2 and 3). Secondly, wet compression is investigated (Chapter 4). The thesis is summarized with a techno-economic analysis of a CRHP system (Chapter 5).

is on entropy production and the performance of the compressor when operating within the conditions that are preferable in a CRHP. This chapter shows that the losses during the compression process are closely linked to the operating conditions, therefore, it is important to account for them when evaluating the entire heat pump performance. In Chapter 5, a simplified version of the model presented in Chapter 4 is combined with the other components of a CRHP to investigate the energetic and economic performance compared to a boiler. The findings are highly sensitive to the operating conditions, as well as the gas, electricity and CO_2 emission price. Nevertheless, in most cases the payback time is within acceptable limits. Finally, in Chapter 6, the main conclusions are summarized and recommendations for further work are proposed.

2

ENHANCING THE PERFORMANCE OF CRHP WITH NH_3-CO_2-H_2O

The introduction mentions that ammonia-water is a common working fluid for CRHP. However, the efficiency of CRHP can be further improved by using alternative working fluids. This chapter investigates the addition of carbon dioxide to aqueous ammonia solutions for application in CRHP. The previously published thermodynamic models for the ternary mixture are evaluated by comparing their results with experimental thermodynamic data, thus assessing their advantages and disadvantages. Then the models are used to study the impact of adding CO_2 to NH_3-H_2O in wet compression resorption heat pump applications. For an application where a waste heat stream is heated from 60 to 105 °C, the COP can be increased by 5 % by adding CO_2 to the ammonia-water mixture, without any risk of salt formation. Additional advantages of adding CO_2 to the ammonia-water mixture in that case include decreased pressure ratio, and increased lower pressure level. When practical pressure restrictions are considered, the benefits of the added CO_2 intensify, resulting in around a 25 % increase in the COP. Nonetheless, when the waste heat stream was additionally cooled down, no significant benefits were observed.

This chapter is adapted from Gudjonsdottir, V., Infante Ferreira, C. A., Rexwinkel, G. and Kiss, A. A. „Enhanced performance of wet compression-resorption heat pumps by using NH_3-CO_2-H_2O as working fluid." In: *Energy* 124 (2017), pp. 531–542.

2.1 INTRODUCTION

The absorption of carbon dioxide in aqueous ammonia has been proposed in the past years as an improved carbon capture technology [23]. Preliminary studies by ten Asbroek and Rexwinkel [24] have indicated that this ternary mixture may also lead to positive effects when applied to compression resorption cycles. In the past several working fluids have been investigated for application in CRHP [19, 25], however, this ternary mixture has not been previously proposed. This is actually the motive for the present investigation.

To further investigate the performance of the CRHP with NH_3-CO_2-H_2O mixture as a working fluid, an accurate thermodynamic model is needed, as the solid base of any process simulation is represented by the physical properties models. Missing or inadequate physical properties can undermine the accuracy of a model or even prevent one from performing the simulation [26]. Different thermodynamic models have been used and developed for calculating the thermodynamic properties of NH_3-CO_2-H_2O. These models are normally activity coefficient models for the liquid phase and an equation of state (EOS) for the vapor phase calculations. The activity coefficient models that have been most commonly used are electrolyte models such as: the Pitzer model [27], the extended UNIQUAC model originally developed by Thomsen and Rasmussen [28] and the more commonly used e-NRTL model proposed by Chen et al. [29]. Darde et al. [30] compared a built in e-NRTL model from Aspen Plus to an upgraded version of the extended UNIQUAC model described by Darde et al. [31]. Their findings were that the extended UNIQUAC model generally performed better than the e-NRTL model from Aspen Plus, especially for the partial pressure of NH_3 and the solubility of ammonium bicarbonate. Darde [32] mentions that if the binary interaction parameters were better fitted to experimental data for NH_3-CO_2-H_2O mixture, the e-NRTL model might become more competitive compared to the extended UNIQUAC model. Since then, the e-NRTL model has been modified in this way by a couple of authors, including Que and Chen [33] and Niu et al. [34]. Both of the adjusted models have been used by other authors, for process modeling. For example, Zhang and Guo [35] used the model with adjusted parameters from Niu et al. [34] and Liu et al. [36] used the modified model from Que and Chen [33].

The extended UNIQUAC model has previously not been compared to the modified model from Que and Chen [33] over a large range of operating conditions. Therefore, in this chapter these models are compared together to see if a modified e-NRTL model can perform with similar accuracy as the extended UNIQUAC model. The e-NRTL models that are built into Aspen Plus are used as a reference. Additionally, a new fit of the e-NRTL model was developed with an extended application range to be able to more accurately evaluate the impact of added CO_2 to ammonia water in CRHPs. These thermodynamic models are used to predict the COP of wet CRHP systems which operate under conditions similar to the conditions investigated by van de Bor et al. [12]. The set of equations proposed in that paper to predict the cycle performance has been used to determine the different state conditions when the ternary mixture is used instead of ammonia-water. The

results are compared with the performance of the ammonia-water system so that the advantages of the ternary mixture become evident.

Summarizing, this study investigates the effect of adding CO_2 to the working fluid of wet compression resorption heat pumps which work with ammonia-water. For this purpose, first the thermodynamic properties of the ternary mixture NH_3-CO_2-H_2O are investigated by comparing the extended UNIQUAC model with modified and improved e-NRTL models over a large range of operating conditions. These models, especially e-NRTL models, have been the most commonly used models for the thermodynamic properties of the NH_3-CO_2-H_2O mixture in literature. Additionally, a new fit is made to further improve the e-NRTL model (extend its application range). Then these properties are used to predict the performance of the mixture when applied in wet CRHP making use of a model that takes into account the major irreversibility's of the cycle: driving forces for heat transfer and deviation from isentropic compression. A case relevant for the process industry is investigated: bringing a waste heat stream to temperatures above 100 °C.

2.2 THERMODYNAMIC PROPERTY MODELS

In the next subsections the extended UNIQUAC and the e-NRTL models are described in more detail, covering their applicability ranges as well as their benefits and drawbacks.

2.2.1 EXTENDED UNIQUAC MODEL

The extended UNIQUAC model was developed by Thomsen and Rasmussen [28]. The model uses the extended UNIQUAC model to calculate activity coefficients for the liquid phase and the Soave-Redlich-Kwong (SRK) EOS for vapor phase calculations. The model was further developed and described by Darde et al. [31] and implemented as a FORTRAN subroutine in Aspen Plus by Maribo-Mogensen [37]. The original model describes accurately the thermodynamic properties of the NH_3-CO_2-H_2O mixture for ammonia concentrations up to 80 molal NH_3 (80 mole NH_3 per kg solvent, which is water in this case), temperature of 0-110 °C and pressure up to 10 MPa [31]. The newer version of the model describes the thermodynamic properties accurately up to 150 °C. Additionally, the model parameters have been fitted to more experimental data to increase accuracy. The deviation of the experimental data and the model are in general less than 10 % except for pressure data at temperatures around and above 100 °C where it is slightly higher. The extrapolation of equilibrium constants into the supercritical range was also improved using Henry's law instead of the Gibbs-Helmholtz equation. The chemical equilibria that are taken into account in the model are the following.

Vapor-liquid equilibrium

$$CO_2(g) \rightleftarrows CO_2(aq) \tag{R.2.1}$$

$$NH_3(g) \rightleftarrows NH_3(aq) \tag{R.2.2}$$

$$H_2O(g) \rightleftarrows H_2O(aq) \tag{R.2.3}$$

Speciation equilibrium

$$NH_3(aq) + H_2O \rightleftarrows NH_4^+ + OH^- \tag{R.2.4}$$

$$CO_2(aq) + H_2O(l) \rightleftarrows HCO_3^- + H^+ \tag{R.2.5}$$

$$HCO_3^- \rightleftarrows CO_3^- + H^+ \tag{R.2.6}$$

$$H_2O\ (l) \rightleftarrows H^+ + OH^- \tag{R.2.7}$$

$$NH_3\ (aq) + HCO_3^- \rightleftarrows NH_2COO^- + H_2O\ (l) \tag{R.2.8}$$

Liquid-solid equilibrium

$$NH_4^+ + HCO_3^- \rightleftarrows NH_4HCO_3\ (s) \tag{R.2.9}$$

$$NH_4^+ + NH_2COO^- \rightleftarrows NH_2COONH_4\ (s) \tag{R.2.10}$$

$$2NH_4^+ + CO_3^{2-} + H_2O \rightleftarrows (NH_4)_2CO_3 \cdot H_2O\ (s) \tag{R.2.11}$$

$$H_2O(l) \rightleftarrows H_2O(s) \tag{R.2.12}$$

$$4NH_4^+ + CO_3^{2-} + 2HCO_3^- \rightleftarrows (NH_4)_2CO_3 \cdot 2NH_4HCO_3\ (s) \tag{R.2.13}$$

2.2.2 E-NRTL MODELS

The e-NRTL model (electrolyte Non Random Two Liquid) [29] is built into the Aspen Plus software [38]. In this study, version 8.8 of Aspen Plus is used. A data package for NH_3-CO_2-H_2O mixture using the e-NRTL method and the Redlich-Kwong (RK) EOS for the vapor phase is included in the software. This model will be called e-NRTL1 from here on. A modified version of the model and the one that Darde et al. [30] used for their comparison are included in a carbon capture example [39] also included in the Aspen Plus v8.8 software. Additionally, this model (called here e-NRTL2) has been regressed to vapor-liquid equilibrium (VLE), solid-liquid equilibrium (SLE), speciation and heat capacity data.

The thermodynamic model proposed by Que and Chen [33] is included in another carbon capture example available in the Aspen Plus software [40]. The main difference be-

tween that model and the e-NRTL2 model is that the PC-SAFT (Perturbed Chain Statistical Association Fluid Theory) EOS is used for vapor phase calculations instead of the RK EOS and the model parameters have been fitted to more experimental data. As mentioned in the introduction, the e-NRTL model has also been modified by other authors like Niu et al. [34]. The model modified by Que and Chen [33] was, however, chosen since more experimental data are used for data regression of the model parameters. The model by Que and Chen [33] is reported to be accurate for systems with temperatures up to 473 K, pressures up to 7 MPa, NH_3 concentration up to 30 wt%, and CO_2 loading (molar ratio between CO_2 and NH_3) up to unity. The average relative deviations between the experimental data and the model results were reported to be lower than 5 % for the pressure, NH_3 and CO_2 composition.

In the e-NRTL model, only the formation of ammonium bicarbonate (NH_4HCO_3) is considered for SLE and not ammonium carbonate ($(NH_4)2CO_3 \cdot H_2O$), ammonium carbamate (NH_2COONH_4) and ammonium sesqui-carbonate ($(NH_4)2CO_3 \cdot 2NH_4HCO_3$). However, researchers have shown that ammonium bicarbonate is dominant in the total amount of ammonium salts once the CO_2 absorption reaches steady state [41, 42]. Therefore, the e-NRTL model might still be a good option. However, since no solid formations are wanted in the CRHP, since they will cause blockage in the system components, further investigation of this point is needed.

These versions of the e-NRTL models are compared to the extended UNIQUAC model as well as a new fit in the following section, where it is demonstrated that the model developed by Que and Chen [33] shows satisfactory results except for SLE at temperatures above 50 °C and for high ammonia concentrations (the reported maximum limit is 30 wt% NH_3). The new fit is, therefore, based on the model from Que and Chen [33], except the e-NRTL model binary interaction parameters - see equation 2.1 - associated with the major species of the electrolyte. That is, during the fitting procedure the initial values of the interaction parameters were the ones developed by Que and Chen [33] and then they were refitted to additional SLE and VLE ternary NH_3-CO_2-H_2O experimental data. The application range of the new fit is therefore similar to the model from Que and Chen [33] as well as it should give a better indication for higher ammonia concentrations (above 30 wt%). As explained by Que and Chen [33] the e-NRTL model requires a non-randomness factor α_{ij}, and asymmetric binary interaction energy parameters τ_{ij}, calculated with the next equation:

$$\tau_{i,j} = \tau_{1,ij} + \frac{\tau_{2,ij}}{T} \tag{2.1}$$

where i and j stand for the components, either ionic species, water, ammonia or carbon dioxide. An overview of the experimental data is listed in Table 2.1 and the refitted parameters are listed in Table 2.2.

Table 2.1: Additional experimental data used for regression of the NH_3-CO_2-H_2O system to generate an improved fit of the e-NRTL model developed by Que and Chen [33].

Data Type	***T*, K**		**wt% NH_4HCO_3**			**Source**
SLE	273-363		2.4-14.4			[43]
Data Type	***T*, K**	**mol% NH_3**	**mol% CO_2**	***P* (MPa)**	**Deviation (%)**	**Source**
VLE	393.15	1.2 - 17.7	0.3 – 9.9	0.3 – 5	6.6	[44]
VLE	393.15	4 - 18	0.4 – 7.6	0.1 – 1.3	7.1	[45]
VLE	343-371	47.5 – 62.8	6.5 – 13.5	1.96	7.7	[46]
VLE	303-333	10.8 – 66.3	1.8 – 6.1	0.02 – 2.1	12.7	[47]

Table 2.2: The adjusted NRTL binary interaction parameters of the new fit developed in this study.

Component *i*	**Component *j***	$\tau_{1,ij}$
H_2O	(NH_4^+, HCO_3^-)	-4.27128
H_2O	(NH_4^+, CO_3^{-2})	3.29344
(NH_4^+, CO_3^{-2})	H_2O	-2.82125
H_2O	(NH_4^+, NH_2COO^-)	9.73284
(NH_4^+, NH_2COO^-)	H_2O	-4.39773
NH_3	(NH_4^+, NH_2COO^-)	7.82722
(NH_4^+, NH_2COO^-)	NH_3	-4.58504

2.3 COMPARISON OF THERMODYNAMIC PROPERTY MODELS

The selected model should be able to describe the VLE, the SLE, speciation and enthalpy change over a large range of temperatures and concentrations of NH_3 and CO_2 to be able to accurately simulate an NH_3-CO_2-H_2O heat pump system. Comparison of the models mentioned previously, are discussed in the following sections.

2.3.1 VAPOR-LIQUID EQUILIBRIUM

The partial bubble point pressures of CO_2 and NH_3 versus the molality of CO_2 based on the different models and the new fit are compared for different temperatures in figure 2.1 (20 °C), figure 2.2 (40 °C), figure 2.3 (120 °C) and figure 2.4 (150 and 160 °C). Additionally, the VLE experimental data from Shen [47] and Yanagisawa et al. [46] are compared to the model results from Que and Chen [33], the extended UNIQUAC model and the new fit in figure 2.5.

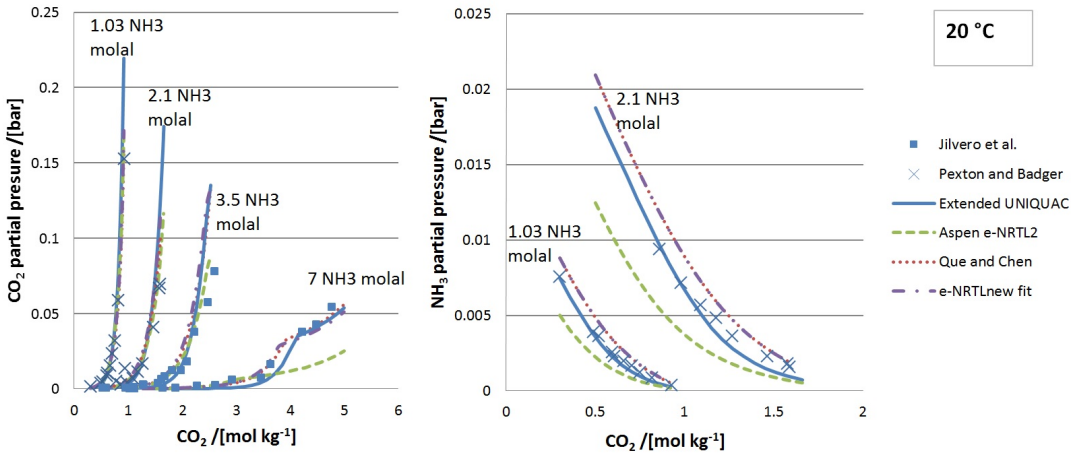

Figure 2.1: Comparison of the experimental data from Pexton and Badger [48] and Jilvero et al. [49] for partial bubble point pressures of CO_2 and NH_3 at 20 °C with the model correlations.

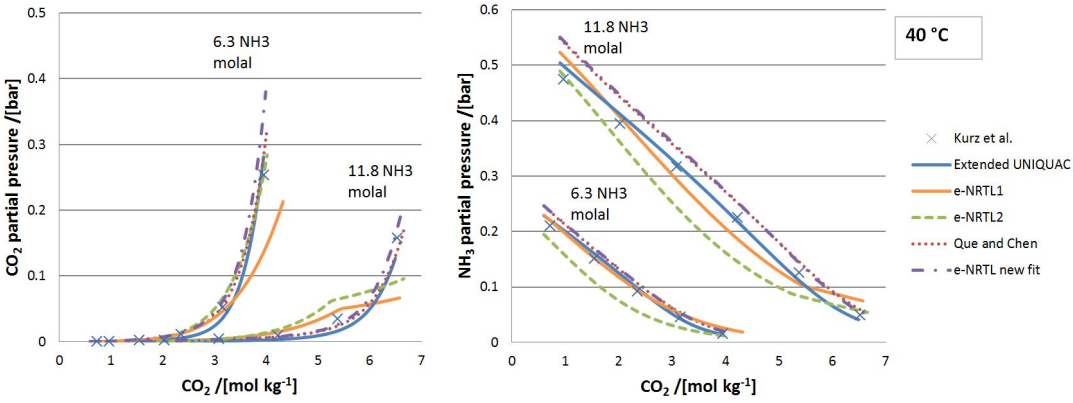

Figure 2.2: Comparison of the experimental data from Kurz et al. [27] for partial bubble point pressures of CO_2 and NH_3 at 40 °C with the model correlations.

The e-NRTL1 model is generally inaccurate at high temperatures and high loadings, as previously reported by Darde [32]. The e-NRTL2 model is in most cases an improvement from the e-NRTL1 model, but it generally underestimates the partial bubble point pressure of NH_3, as well as inaccurately portrays the CO_2 pressure at high loadings at 20 and 40 °C. The model by Que and Chen [33], the new fit and the extended UNIQUAC model quite accurately portray the partial pressures at low molalities of NH_3. Jilvero et al. [49] even reported that the model by Que and Chen [33] fits their experimental data of CO_2 partial bubble point pressures, for 10-40 °C, even more accurately than the extended UNIQUAC model. At higher molalities of NH_3 the models start to underestimate the pressure as can be seen most clearly from figure 2.3 and figure 2.5. As mentioned before the limit of the

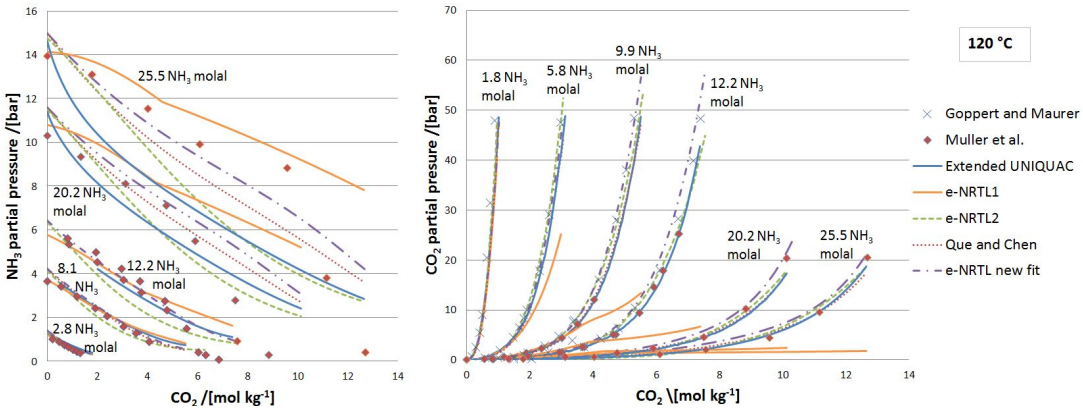

Figure 2.3: Comparison of the experimental data from Göppert and Maurer [44] and Müller et al. [45] for partial bubble point pressures of CO_2 and NH_3 at 120 °C with the model correlations.

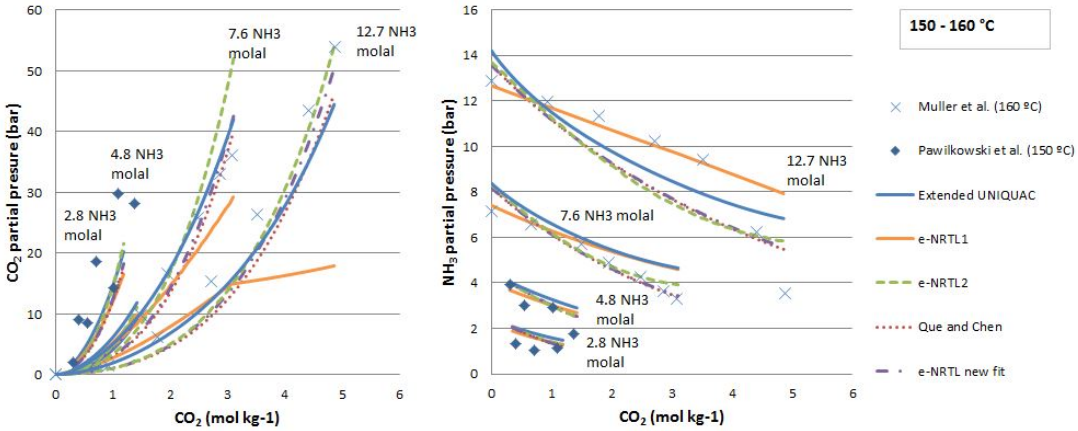

Figure 2.4: Comparison of the experimental data from Müller et al. [45] and Pawilkowski et al. [50] for partial bubble point pressures of CO_2 and NH_3 at 150 °C and 160 °C with the model correlations.

model by Que and Chen [33] is reported to be 30 wt% NH_3 (approximately 24 molal NH_3). The limit of the original extended UNIQUAC model was reported by Darde [32] as 80 molal NH_3. Darde's improved model is, however, refitted with data that does not come close to that limit [32]. And it is quite clear, especially from figure 2.5, that Darde's improved model under predicts the pressure at concentrations above approximately 30 wt% NH_3. The new fit developed in this study predicts most accurately the experimental data at these higher concentrations.

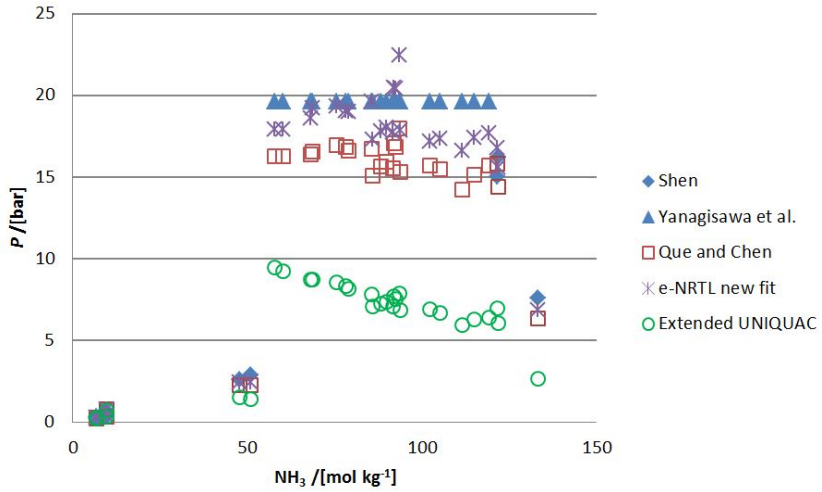

Figure 2.5: Comparison of the experimental data from Shen [47] and Yanagisawa et al. [46] for bubble point pressure with the model correlations.

2.3.2 SOLID-LIQUID EQUILIBRIUM

The comparison of the models for solubility of ammonium bicarbonate (NH_4HCO_3) in water versus temperature is shown in figure 2.6. The models are compared to experimental data from Janecke [43], Trypuc and Kielkowska [51] and Toporescu [52]. Assuming that the experimental data from Janecke [43] is accurate, the extended UNIQUAC model, as well as the new fit are the most accurate at high temperatures or above approximately 50 °C. At higher temperatures, the e-NRTL2 and the model proposed by Que and Chen [33] overestimate the solubility of NH_4HCO_3. The e-NRTL1 model, similar to the trend seen from the VLE data, deviates from the experimental data at high temperatures and high loadings, in this case around 70 °C. In the case of e-NRTL2 and the model from Que and Chen [33] the reason for this difference can be easily explained since the experimental data used for the regression for both models was the one from Trypuc and Kielkowska [51]. The experimental data from them reaches to temperatures of 50 °C. Also, their value at 50 °C is slightly higher than the one from Janecke [43] and Toporescu [52]. Since, more experimental data at high temperatures was not found in literature it is questionable which of the data sets corresponds best to reality. Additionally, in practice for the CRHP application the concentration of NH_3 and CO_2 is unlikely to come close to the concentration necessary for ammonium bicarbonate formation at high temperatures. For example the reported concentration by Janecke [43] of CO_2 at approximately 60 °C is around and above 30 wt% (depending on the NH_3 concentration). The data from Trypuc and Kielkowska [51] suggest that this limit might be even higher and therefore either model should give satisfying results if the application concentration does not reach this limit.

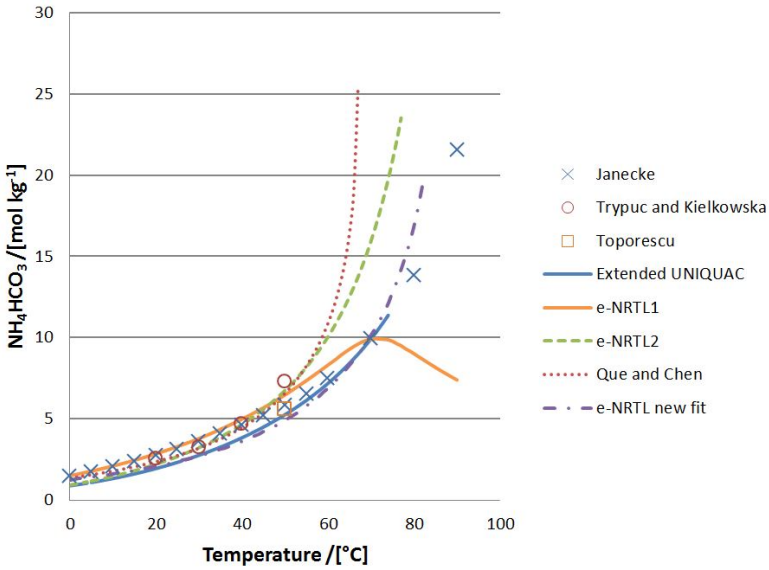

Figure 2.6: Comparison of the experimental data from Janecke [43], Trypuc and Kielkowska [51] and Toporescu [52] for solubility of NH_4HCO_3 in water with the model predictions.

2.3.3 SPECIATION EQUILIBRIUM

Comparison of speciation calculations of the models and experimental data from Lichtfers [53] is shown in figure 2.7 and figure 2.8. All the models are able to quite accurately describe the speciation at both temperatures (60 and 120 °C, respectively) except the e-NRTL2 model. The e-NRTL2 model overestimates the concentration of ammonia and bicarbonate and underestimates the carbamate concentrations. In the two previous subsections, the e-NRTL2 model was in general an improvement of the original model (e-NRTL1). This shows the importance of using a wide range of experimental data for parameter fitting for the NH_3-CO_2-H_2O system.

2.3.4 ENTHALPY CHANGE UPON PARTIAL EVAPORATION OF THE NH_3-CO_2-H_2O MIXTURE

In figure 2.9, figure 2.10 and figure 2.11 the models are compared to experimental data from Rumpf et al. [54] for enthalpy change upon partial evaporation of the NH_3-CO_2-H_2O mixture. The temperature range of the experiments was from 40 to 137 °C with a typical temperature increase of 5-15 °C. The concentration range for NH_3 was up to 12 molal and up to 6 molal for CO_2. The reported temperatures and pressures from Rumpf et al. [54] are used to calculate the inlet enthalpy. At the outlet, however, the reported vapor fraction is used instead of the pressure since the accuracy of the weight of the liquid and vapor

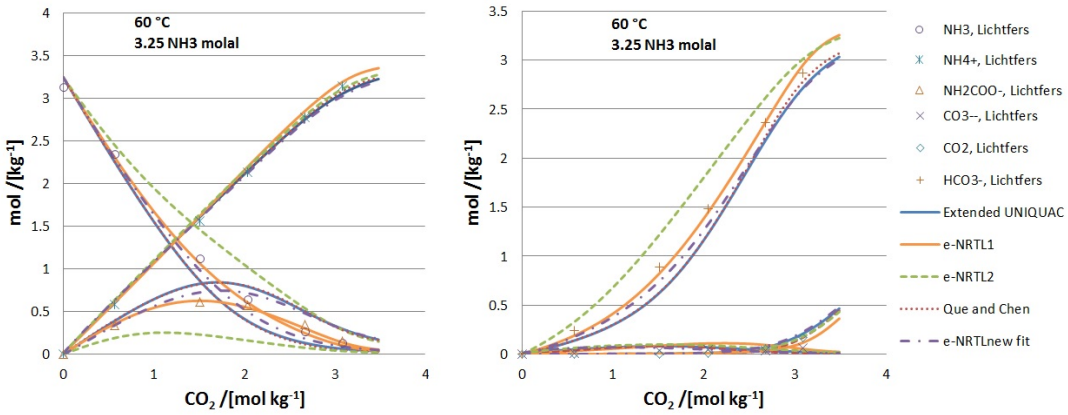

Figure 2.7: Comparison of the experimental data from Lichtfers [53] for speciation at 60 °C and molality of 3.25 mol/kg NH_3 with the model correlations.

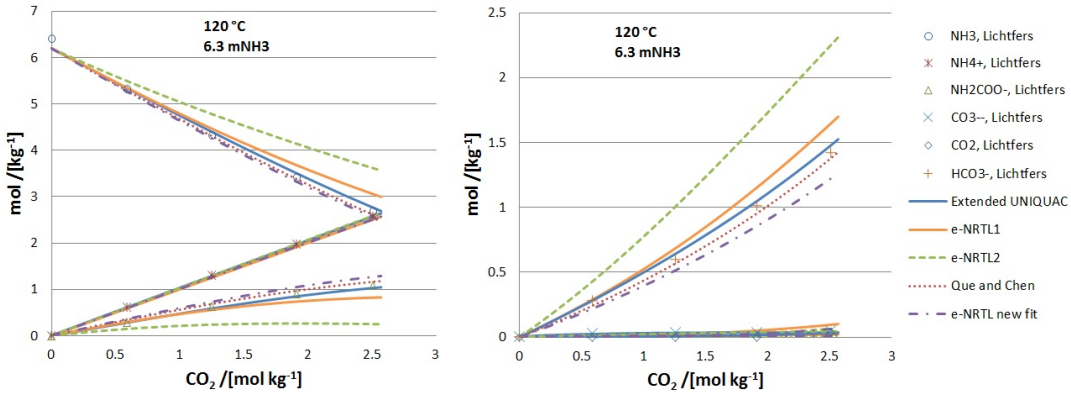

Figure 2.8: Comparison of the experimental from Lichtfers [53] data for speciation at 120 °C and molality of 6.3 mol/kg NH_3 with the model correlations.

part is higher than that of the measured pressure. All correlations show good matches to the experimental data, on average the deviation is less than 3%, with the only exception of two points for the e-NRTL1 correlation. These two points were at the highest reported temperature and CO_2 loading. This deviation corresponds to the previous shown results of VLE and SLE data.

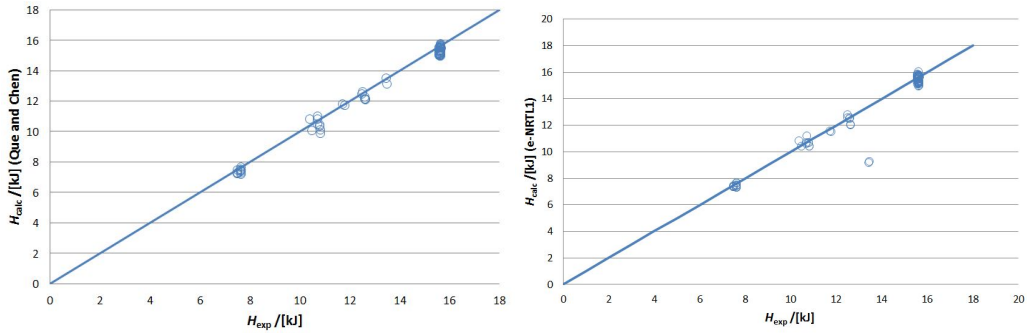

Figure 2.9: Comparison of the experimental data from Rumpf et al. [54] for heat of partial evaporation of the NH_3-CO_2-H_2O mixture: (left) Que and Chen [33] and (right) e-NRTL1 correlation.

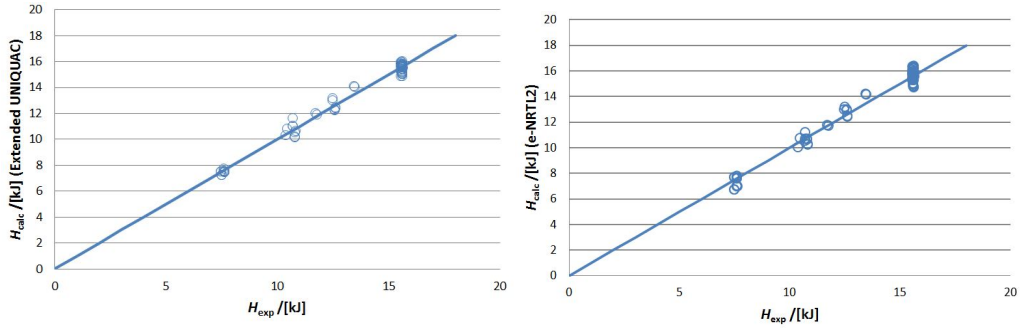

Figure 2.10: Comparison of the experimental data from Rumpf et al. [54] for heat of partial evaporation of the NH_3-CO_2-H_2O mixture: (left) extended UNIQUAC and (right) e-NRTL2 correlation.

2.4 APPLYING NH_3-CO_2-H_2O MIXTURE TO WET COMPRESSION RESORPTION HEAT PUMP

2.4.1 MODEL OF A COMPRESSION-RESORPTION HEAT PUMP

The process for the compression-resorption heat pump is presented in the temperature-enthalpy diagram illustrated in figure 2.12 [12]. Figure 2.12 gives a representation of the cycle, where T_3 is fixed at the waste heat stream inlet temperature (for instance 60 °C) plus 5 K driving force, while T_1 is fixed at the waste heat stream inlet temperature minus 5 K driving force. The desorber and resorber are additionally divided into 100 control volumes to ensure that the pinch temperature does not become smaller than 5 K. The isentropic efficiency of the compressor is assumed 70 %. Infante Ferreira et al. [55] have reported experimental data for wet compression of ammonia-water and have obtained isentropic efficiency up to 35 % with a prototype screw compressor. It is expected that further

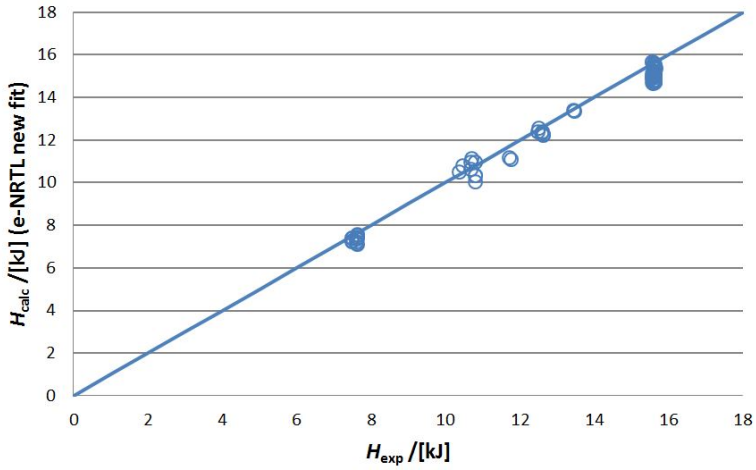

Figure 2.11: Comparison of the experimental data from Rumpf et al. [54] for heat of partial evaporation of the NH_3-CO_2-H_2O mixture and the e-NRTL new fit correlation.

improvement of such a compressor will allow for efficiencies of 70 % and higher. The optimal vapor quality at the outlet of the compressor for wet compression was investigated by van de Bor et al. [56] for 50 different industrial cases. The optimal solution is to have saturated vapor at the compressor outlet. Therefore, for the wet compression cycle, P_1 is initially guessed, from which h_1, s_1, h_{2s}, and h_2 are calculated, while P_1 is iterated until h_2 matches the value for saturated vapor at P_2. For convenience, a summary of equations used to determine the COP of compression resorption heat pumps is given in Table 2.3. Note that, for what concerns ammonia-water, the model was developed using NIST RefProp version 9.1 (Lemmon et al., [57]). For the NH_3-CO_2-H_2O calculations the extended UNIQUAC (Darde et al., [31]), the modified model by Que and Chen [33] and the new fit based on their model are used.

2.4.2 OPERATING CONDITIONS OF THE REFERENCE HEAT PUMP

The case considered concerns the heating of a water waste heat stream flow from 60 °C to 105 °C while part of the stream is cooled down in the desorber. The flow is assumed to be sufficient to achieve the desired temperature levels. Figure 1.1 illustrates the situation. In the first example the focus is only on heating (with a temperature lift of 55 K), while in the second example this case is expanded to consider additionally that the waste heat stream is partly cooled down from 60 °C to 15 °C.

Table 2.3: Equations used to model the CRHP cycle. State points correspond to figure 1.1

$$T_1 = [T_{cw} - \Delta T_{driving}]$$
$$T_3 = [T_{cw} + \Delta T_{driving}]$$
$$P_2, P_3, h_3, h_4 = f(T_3, q = 0)$$
$$T_2, h_2 = f(P_3, q = 1)$$
$$h_1, s_1 = f(P_1, T_1)$$
$$h_{2s} = f(P_3, s_1)$$
$$h_2 = \frac{h_{2s} - h_1}{\eta_{is}} + h_1$$
$$COP = (h_2 - h_3)/(h_2 - h_1)$$

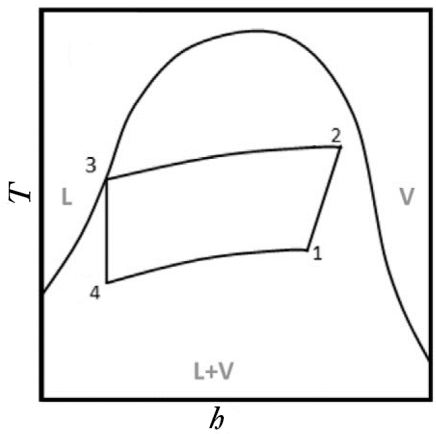

Figure 2.12: Typical temperature-enthalpy diagram for compression-resorption heat pumps. Position 1 indicates the process conditions after the desorber, 2 indicates the conditions at the outlet of the compressor, 3 indicates the conditions at the outlet of the resorber and 4 indicates the conditions after the expansion valve [12].

2.4.3 COMPARISON OF CYCLE PERFORMANCE

2.4.3.1 *Heating case*

The benefits of adding CO_2 to the ammonia-water mixture of the case where a waste heat stream is heated from 60 °C to 105 °C are illustrated in figure 2.13 and figure 2.14 and an example of the cycle calculations results are listed in Table 2.4 and Table 2.5. The observed trend in the cycle performance with an ammonia water mixture is that an optimum exists when the working fluid temperature glide is fitted to the heat sink rather than the heat source. This same trend was observed by van de Bor et al. [56] where 50 industrial cases

Table 2.4: Mixture composition, temperature and pressure results for the CRHP cycle for the heating case; waste heat stream is heated from 60 to 105 °C.

	wt%			T_1	T_2	T_3	T_4	P_{low}	P_{high}
Model	**NH_3**	**H_2O**	**CO_2**	**(°C)**	**(°C)**	**(°C)**	**(°C)**	**(bar)**	**(bar)**
Refprop	19.1	80.9	0	55	110	65	24.8	0.202	1.77
Refprop	39.3	60.7	0	55	143.2	65	3.5	0.3	6.42
Extended UNIQUAC	31.2	48.8	20	55	110	65	20.8	0.3	2.5
Que and Chen [33]	24.6	55.4	20	55	110	65	26.7	0.269	2.26
Que and Chen [33]	29.2	50.8	20	55	119.7	65	17.5	0.3	3.345
New fit	22.8	57.2	20	55	110	65	28.9	0.259	2.185
New fit	28.7	51.3	20	55	123.9	65	16	0.3	3.79

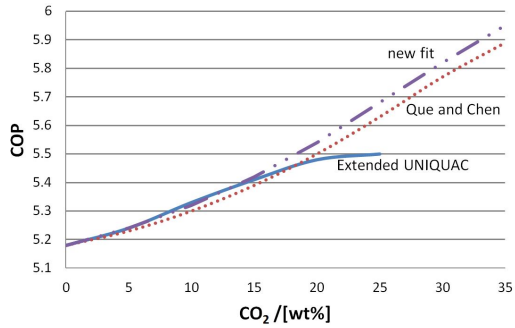

Figure 2.13: COP vs CO_2 weight fraction, heating case; waste heat stream is heated from 60 to 105 °C. Results from the extended UNIQUAC model are shown with continuous line, the model of Que and Chen [33] with dotted line, and the new fit with dashed line.

were investigated. This optimum is in this case for an ammonia weight fraction of 19.1 %. When CO_2 is added the ammonia concentration has to be increased to achieve the optimum cycle performance. For example, at 20 wt% CO_2 the NH_3 concentration is 31.2 % according to the calculations with the extended UNIQUAC model and 24.6 % with the model from Que and Chen [33], see Table 2.4.

Figure 2.13 plots the COP versus the CO_2 weight fraction. The models show the same trend: the COP increases with increased CO_2 concentration. However, the extended UNIQUAC model predicts salt formation (ammonium carbonate) around 18 wt% CO_2 in the stream after the valve (at the lowest temperature in the cycle). At this point the increase in COP reduces. In practice, any salt formation is unwanted in the cycle since it will eventually cause a blockage. The modified e-NRTL models predict no salt formation until above 35 wt% CO_2. As mentioned earlier the e-NRTL models only predict if there is a formation of ammonium bicarbonate. If there is indeed ammonium carbonate forming this shows a

Table 2.5: Mixture composition, enthalpy and COP results for the CRHP cycle for the heating case; waste heat stream is heated from 60 to 105 °C.

		wt%		h_1	h_2	h_3	h_4	COP
Model	**NH_3**	**H_2O**	**CO_2**	**(kJ/kg)**	**(kJ/kg)**	**(kJ/kg)**	**(kJ/kg)**	
Refprop	19.1	80.9	0	2081.9	2533.2	194.7	194.7	5.18
Refprop	39.3	60.7	0	1780.7	2413.8	187.6	187.6	3.52
Extended UNIQUAC	31.2	48.8	20	-9442.9	-9047.9	-11211.3	-11211.3	5.48
Que and Chen [33]	24.6	55.4	20	-10156.6	-9763.3	-11926.7	-11926.7	5.5
Que and Chen [33]	29.2	50.8	20	-9704.4	-9259.4	-11396.9	-11396.9	4.8
New fit	22.8	57.2	20	-10348.5	-9955.1	-12135.0	-12135.0	5.54
New fit	28.7	51.3	20	-9773.1	-9307.3	-11452.6	-11452.6	4.61

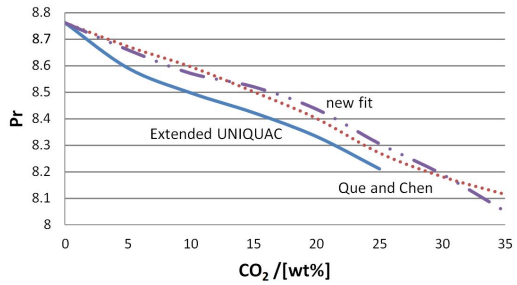

Figure 2.14: Pressure ratio vs CO_2 weight fraction, heating case; waste heat stream is heated from 60 to 105 °C. Results from the extended UNIQUAC model are shown with continuous line, the model of Que and Chen [33] with dotted line, and the new fit with dashed line.

clear advantage of the extended UNIQUAC model over the e-NRTL models. The increase in COP with added CO_2 before any salt formation is predicted is around 5 %. A traditional VCHP operating with ammonia would have a COP around 4 in this case. The improvement of a CRHP operating with ammonia and water is already around 30 % and with the addition of CO_2 the improvement comes close to 40 %. That is, if it is assumed that a compressor efficiency of 70% will be attainable.

The pressure ratio is plotted versus the CO_2 weight fraction in figure 2.14 and the absolute pressure results are listed in Table 2.4. From the figure and the table it is clear that the benefits of adding CO_2 is not only the increase in COP, but also the pressure ratio decreases and the lower pressure level increases. For the ammonia-water case the lower pressure level is about 0.2 bar for the optimum case, which can be difficult to achieve in practice. The pressure can be increased at higher ammonia concentration, but then the

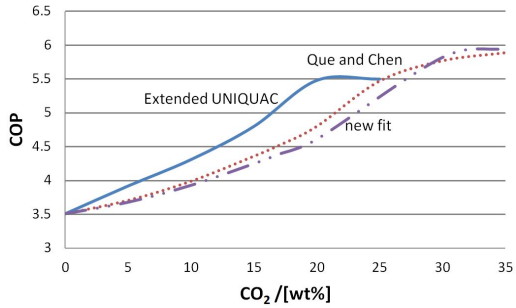

Figure 2.15: COP vs CO_2 weight fraction, 0.3 to 25 bar pressure limit; waste heat stream is heated from 60 to 105 °C. Results from the extended UNIQUAC model are shown with continuous line, the model of Que and Chen [33] with dotted line, and the new fit with dashed line.

COP decreases. The benefits of the added CO_2 can be even greater if there are pressure restrictions of the lower pressure level.

Figure 2.15 plots the COP versus the CO_2 weight fraction when the pressure level is restricted from 0.3 bar (shaft seal requirements limitation) to 25 bar (equipment cost limitation), a pressure range which is more easily reached in practice. The higher pressure restriction is included since another local optimum exists when the temperature glide is fitted to the heat source rather than the heat sink. This local optimum is found at higher ammonia weight fraction where the pressure levels become way higher which would require specialized and more expensive equipment. From figure 2.15 it is clear that the benefits of the added CO_2 are now much larger. It should be noted that the ammonia weight fraction is around and above 30 wt%, see Table 2.5, and therefore the modified model by Que and Chen [33] and the extended UNIQUAC model are reaching their limits. The new fit estimates an improvement of 25 % in the COP compared to the ammonia water system before the extended UNIQUAC model predicts solid formations (around 18 wt% CO_2).

When CO_2 is added to the ammonia-water mixture the heat exchanger area decreases for the same heat output for the optimized case. The pressure ratio and electricity cost are also lower therefore the payback period should be shorter than for a CRHP operating with ammonia-water.

In the case where the lower pressure is restricted the area increases slightly with added CO_2. The reason is that the temperature difference in the resorber is smaller with the added CO_2 which means that the needed heat transfer area is larger. However, the decrease in pressure ratio and the increase in COP are even higher in this case. Therefore, the payback period should still be shorter in this case compared to an CRHP operating with ammonia-water.

The corrosion risk might however increase with the added CO_2. In water - CO_2 system the largest cause for corrosion is carbonic acid, H_2CO_3 [58]. With enough ammonia included, as is the case here, this acid should however not be formed. Also, according to

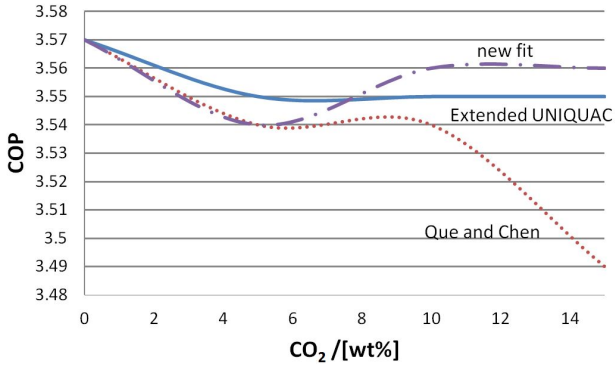

Figure 2.16: COP vs CO_2 weight fraction, cooling case; waste heat stream is heated from 60 to 105 °C and partially cooled down to 15 °C. Results from the extended UNIQUAC model are shown with continuous line; the model of Que and Chen [33] with dotted line, and the new fit with dashed line

Krzemień et al. [59] the main causes for corrosion in amine-based CO_2 capture processes are oxidizing acid species like NOx and SOx and heavy metals in the amine solution. Therefore, the risk of corrosion for this mixture might be comparable to that of ammonia-water. Further investigation is however needed to confirm this.

2.4.3.2 *Additional cooling case*

The same case is now considered except that now an extra cooling demand is assumed. That is the waste water stream is assumed to be partly cooled down to 15 °C. Since the same heat sink is assumed the optimum ammonia weight fraction is still 19.1 %, for an ammonia water mixture, and the acquired COP is 3.57 (see table 2.7). However, to reach the required cooling demand the lower pressure level is significantly lower or around 0.057 bar. This pressure level is quite difficult to reach in practice. If the lower pressure level is restricted to 0.3 bar the necessary ammonia weight fraction increases to 49 wt% NH_3 and the COP decreases to 2.97 (see table 2.7). However, in that case the temperature glide of the ammonia water mixture is of course not fitted optimally to the heat sink. In this case the optimal weight fraction will actually become 91.1 wt% NH_3 which results in a COP of 3.29, in this case the temperature glide of the ammonia water mixture is fitted to the heat source rather than the heat sink. Adding CO_2 will not be beneficial with an ammonia weight fraction this high, since there is not enough water. This is, therefore, not the optimal application case for adding CO_2, it is however interesting to test the boundaries of the models and to investigate the potential benefits of added CO_2. Figure 2.16 plots the COP versus the CO_2 weight fraction when it is assumed that there are no limits to the lower pressure level. In this case the models all predict a decrease in the COP with added CO_2 and additionally the pressure ratio increases. This is likely due to the fact that the

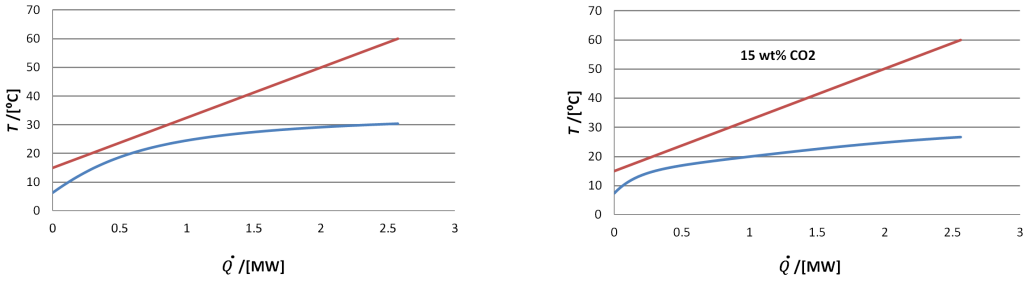

Figure 2.17: Temperature profiles in the desorber as a function of the heat load. Left: profiles for the ammonia water mixture. Right: added CO_2 (15 wt%) calculated with the new fit.

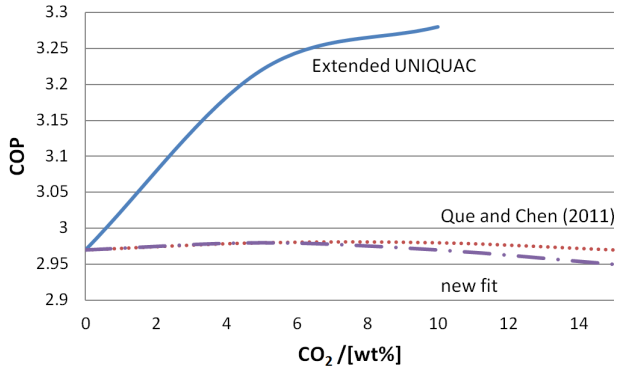

Figure 2.18: COP vs CO_2 weight fraction, cooling included and 0.3 bar lower pressure limit. Results from the extended UNIQUAC model are shown with continuous line; the model of Que and Chen [33] with dotted line, and the new fit with dashed line.

temperature glide of the NH_3-CO_2-H_2O mixture does not fit as well to the temperature glide in the desorber as that of the ammonia water mixture (see figure 2.17).

Figure 2.18 plots the COP versus the CO_2 weight fraction when there is a 0.3 bar limit for the lower pressure level and an example of the cycle calculations results are listed in Table 2.6 and Table 2.7 with and without pressure limits. The models from Que and Chen [33] and the new fit show similar results as before, that is there is hardly any improvement of the cycle performance with added CO_2. In contrast, the extended UNIQUAC model in this case shows an improvement of the COP. However, as was shown in section 3.1 the model does not accurately predict experimental data for these ammonia weight fractions (approximately 50 wt% NH_3). It is therefore highly unlikely that the model results are accurate. However, it can give an indication of the formation of solids. For the present condition, the model predicts ammonium carbonate formation before 10 wt% of CO_2. This is not surprising since now the lowest temperature level in the cycle is lower than for the case when only heating is considered. It should be noted that also for conventional heat pumps the simultaneous delivery of hot and cold output leads to higher pressure ratios and

Table 2.6: Mixture composition, temperature and pressure results for the CRHP cycle for the cooling case; waste heat stream is heated from 60 to 105 °C and partially cooled down to 15 °C.

		wt%		T_1	T_2	T_3	T_4	P_{low}	P_{high}
Model	**NH_3**	**H_2O**	**CO_2**	**(ºC)**	**(ºC)**	**(ºC)**	**(ºC)**	**(bar)**	**(bar)**
Refprop	19.1	80.9	0	30.4	110	65	6.3	0.057	1.77
Refprop	91.1	0.09	0	55	144.8	77.6	10	5.4	35.2
Refprop	49	51	0	49.2	154.3	65	-9.1	0.3	10.2
Extended UNIQUAC	20.3	74.7	5	28.9	110	65	3.99	0.055	1.831
Extended UNIQUAC	44	51	5	48.1	138.7	65	-5.7	0.3	7.209
Que and Chen [33]	19.2	75.8	5	29.0	110	65	5.68	0.055	1.826
Que and Chen [33]	48.6	46.4	5	47.9	152.6	65	-11.3	0.3	10.307
New fit	18.6	76.4	5	28.9	110	65	6	0.054	1.809
New fit	48.2	46.8	5	48	153.2	65	-11.3	0.3	10.389

Table 2.7: Mixture composition, enthalpy and COP results for the CRHP cycle for the cooling case; waste heat stream is heated from 60 to 105 °C and partially cooled down to 15 °C.

		wt%		h_1	h_2	h_3	h_4	**COP**
Model	**NH_3**	**H_2O**	**CO_2**	**(kJ/kg)**	**(kJ/kg)**	**(kJ/kg)**	**(kJ/kg)**	
Refprop	19.1	80.9	0	1878.9	2533.2	194.7	194.7	3.57
Refprop	91.1	0.09	0	1533.0	1929.5	623.8	623.8	3.29
Refprop	49	51	0	1629.1	2346.1	216.4	216.4	2.97
Extended UNIQUAC	20.3	74.7	5	-11507.0	-10854.4	-13169.9	-13169.9	3.55
Extended UNIQUAC	44	51	5	-8167.2	-7531.0	-9577.0	-9577.0	3.22
Que and Chen [33]	19.2	75.8	5	-11648.7	-11005.8	-13284.0	-13284.0	3.54
Que and Chen [33]	48.6	46.4	5	-8488.2	-7794.6	-9863.2	-9863.2	2.98
New fit	18.6	76.4	5	-11714.5	-1107.8	-13352.0	-13352.0	3.54
New fit	48.2	46.8	5	-8529.43	-7833.63	-9909.88	-9909.88	2.98

very low COPs. For instance, a butane heat pump would require a pressure ratio of 12.4 and have a COP of only 1.8. Therefore, an CRHP operating with ammonia water mixture can already improve the process significantly.

2.5 RESULTS, ANALYSIS AND DISCUSSION

The comparison of the thermodynamic models shows that the modified e-NRTL models are generally an improvement of the original model. The model modified by Que and Chen [33] and the new fit are especially compatible with the extended UNIQUAC model at low ammonia concentrations. The model developed by Que and Chen [33] is even more accurate for the partial pressure of CO_2 at low temperatures (10-40 °C) as reported by Jilvero et al. [49] and at high ammonia concentrations. Their model also improves the partial pressure of NH_3 and speciation compared to the e-NRTL2 model. The exception is the SLE. The model further underestimates the pressure at high ammonia concentrations. The extended UNIQUAC model under predicts the pressure at high NH_3 concentrations even more seriously. The new fit that was developed in this work, based on the model by Que and Chen [33], solves these problems, and the new model is able to represent the experimental data, in general, satisfactorily. The new fit should therefore be applicable for the same range and applications as the model developed by Que and Chen [33] as well as to give a better indication for higher ammonia concentrations (above 30 wt%). However, ammonium bicarbonate is, as mentioned before, the only solid formation that is predicted by the e-NRTL models. The NH_3-CO_2-H_2O mixture shows great potential for certain CRHP applications (e.g. heating only). As was shown with the cooling case, not all applications will benefit significantly from adding CO_2. Each potential application case should, therefore, be investigated beforehand. A known fact is that there is a larger chance of solid formations at lower temperature levels and the potential benefits of adding CO_2 will therefore be smaller. It should also be noted that the calculations were pushing the reported limits of the models, around and above 30 wt% NH_3. Also, the available experimental data in this range is limited and the data sets are not consistent. Therefore, it is difficult to evaluate the error of the predicted COP with the added CO_2.

2.6 CONCLUSIONS

From the model comparison it is clear that the modified e-NRTL models are in general an improvement of the original model. The model modified by Que and Chen [33] and the new proposed fit are especially compatible with the Extended UNIQUAC model for ammonia concentrations below 30 wt%. The exception is the SLE. All models additionally under predict the pressure at higher ammonia concentrations. The new fit, that was developed to include experimental data at higher concentrations, fits the data with comparable or higher accuracy than the other models. However, since there is a risk of formation of other solids than ammonium bicarbonate, the extended UNIQUAC model is in general recommended for ammonia concentrations below 30 wt%. The NH_3-CO_2-H_2O mixture shows great potential for certain CRHP cycles with wet compression; both the COP can increase as well as the pressure levels and pressure ratio can become more favorable. The

benefits of the NH_3-CO_2-H_2O mixture for CRHP will depend on each application case. For the heating case discussed in this study a COP increase of approximately 5 % can be attained compared to a cycle operating with only ammonia water without any risk of solid formation. When there are additionally practical pressure restrictions the benefits can become even higher for this application case or around 25 % increase in the COP. When the heat pump must also deliver low temperature heat, the benefit of added CO_2 appears to become insignificant.

3

EXPERIMENTAL ABSORPTION PROCESS OF NH_3-CO_2-H_2O IN A MINI-CHANNEL HEAT EXCHANGER

The previous Chapter showed the potential of CRHP when CO_2 is added to NH_3-H_2O. In this Chapter this potential is further explored by performing heat exchanger experiments. A mini-channel heat exchanger with 116 tubes of inside diameter of 0.5 mm is used for this purpose. For the NH_3-H_2O experiments overall heat transfer coefficients of 2.7 to 6 kW/(m^2K) were reached for mixture mass flows of 0.71 - 2.5 kg/h. For the NH_3-CO_2-H_2O mixture pumping instabilities limited the operating range which resulted in higher pressures and higher mixture mass flows compared to NH_3-H_2O. The overall heat transfer coefficients were lower in the case of the added CO_2, with the maximum of 3 kW/(m^2K) corresponding to a mixture mass flow of 4.2 kg/h. However, for the testing conditions an increase in heat transfer of approximately 5% was reached with the added CO_2. Additionally, limited research has been conducted on upward versus downward absorption and, therefore, these two configurations have also been tested in the mini-channel heat exchanger. Even though the pumping instabilities vanished with upward absorption it was confirmed that downward absorption with the mixture in the tube side is the most beneficial configuration for absorption of ammonia in NH_3-CO_2-H_2O or NH_3-H_2O in a mini-channel heat exchanger. The performance increased by approximately 10 % in the downward absorption mode.

This chapter is adapted from Gudjonsdottir, V., Shi, L. and Infante Ferreira, C. A. „Experimental investigation of the upward or downward absorption process of NH_3-CO_2-H_2O in a mini-channel heat exchanger." In: *International Journal of Heat and Mass Transfer* (2019). Under review.

3.1 INTRODUCTION

The previous chapter shows, with simulations, that the thermodynamic performance of the heat pump can be increased by approximately 5% with the NH_3-CO_2-H_2O mixture compared to only NH_3-H_2O. In this chapter, the absorption process in the resorber of a CRHP is investigated experimentally to partly confirm the potential of the NH_3-CO_2-H_2O mixture. The absorption process is studied in a mini-channel heat exchanger for NH_3-H_2O and then the NH_3-CO_2-H_2O mixture.

The mini-channel heat exchanger was chosen since compact heat exchangers can decrease energy requirements and costs compared to traditional heat exchangers [61]. Mini/micro-channels can have even better heat transfer performance, and be even more compact than conventional compact heat exchangers like plain-fins, wavy fins and fin-tubes [61, 62]. A comprehensive review is given by Khan and Fartaj [62] on microchannel heat exchangers, defined to have channels ≤ 1 mm. As they mention the potentials are great, however, more research is necessary. There is especially limited research for large scale thermal and energy applications of micro-channel heat exchangers.

For NH_3-H_2O absorption, the most common methods are bubble or falling film absorption [63]. A comprehensive review is given by Amaris et al. [63], as they mention the falling film absorption has been more commonly applied and is the preferred option for many researchers [64, 65]. As mentioned by Trichè et al. [64] the performance varies greatly depending on the absorption method and the specific geometry. According to their prediction the falling film mode is the preferred one. It is clear that very limited studies in the open literature compare directly the two absorption modes, especially experimentally. Kang et al. [66] investigated analytically the two different absorption modes and concluded that the local absorption rate was always higher for the bubble mode. Castro et al. [67] investigated experimentally the two modes for air-cooled absorption systems. The bubble absorption was generally more efficient, especially for low solution flow rates because of the low wetted area of the falling film. As mentioned by van Leeuwen [68] the flow patterns in mini-channel heat exchangers are significantly different from in traditional absorbers. Therefore, in this study we use the terms downward and upward absorption rather than falling film and bubble absorption. One of the goals of this study is, therefore, to study which mode is more effective.

When it comes to absorption of NH_3-H_2O in micro- or mini-channel heat exchangers several studies have been conducted. Garimella et al. [69] studied the absorption process in a microchannel heat exchanger. They improved an existing design and reached overall heat transfer coefficients in the range of 0.54 to 1.16 kW/(m^2K). In mini-channels the absorption process of NH_3-H_2O has previously been studied by Van Leeuwen [68] and van de Bor et al. [70]. Van Leeuwen [68] performed experiments with single tube mini-channel heat exchanger using tube diameters of about 1.1 and 2.0 mm. His conclusion was that the overall heat transfer coefficient increased with decreased diameter and that the overall heat transfer coefficient was significantly higher than for conventional heat exchangers. This is

similar to the findings of Amaris et al. [71] for tubular bubble absorbers and Yoon et al. [72] for falling film absorbers. According to the VDI Heat Atlas [73] conventional heat exchangers, like shell and tube and plate heat exchangers, have an overall heat transfer coefficient in the range from 1 to 4 kW/(m^2K). Van Leeuwen [68] reached values from approximately 6 to 13 kW/(m^2K) for a tube diameter of 1.1 mm and predicted values up to 25 kW/(m^2K) for 0.5 mm tubes.

The heat exchanger used in this study is a multi-tube (116 tubes) mini-channel heat exchanger with an inside diameter of 0.5 mm. As was mentioned before, there is a need to scale up micro- and minichannel heat exchangers [62]. This heat exchanger was designed as a first step in scaling up mini-channel heat exchangers. Experimental results with the current heat exchanger have previously been reported for water-water experiments [74] and with NH_3-H_2O [75]. The heat transfer performance was, unfortunately, lower than expected with the highest overall heat transfer coefficients only around 2 kW/(m^2K). It was concluded that the decrease in performance was due to hydrodynamic instabilities. In the study by van de Bor [75] the NH_3-H_2O mixture was either on the shell side or both on shell and tube side of the heat exchanger. These results were still considerably higher than reported by Lee at al. [76] where NH_3-H_2O bubble absorption was performed in a plate heat exchanger with a maximum overall heat transfer coefficient of around 0.6 kW/(m^2K). The results from van de Bor [75] were also slightly higher than the results reported by Lee et al. [77] for horizontal tube falling-film flow where the overall heat transfer coefficient ranged from 0.7-1.9 kW/(m^2K). Various other researches for either bubble absorption or falling film flow with NH_3-H_2O have been reported for plate heat exchangers [64, 78, 79]. In these cases the heat transfer performance was also worse than for the mini-channel reported by van de Bor [75]. In all the cases mentioned above the temperature difference was calculated with the log mean temperature difference (LMTD), except in the case of van de Bor [75] and Trichè et al. [64] where the absorber was divided into control volumes and the average of the calculated local temperature difference was used. Even though the mini-channel heat exchanger could be further optimized, it is well suitable for comparing the absorption process of NH_3-H_2O and the NH_3-CO_2-H_2O mixtures.

In this study first water-water experiments are performed with the current mini-channel heat exchanger, then the water on the tube side is replaced by NH_3-H_2O and, finally, CO_2 is added to the NH_3-H_2O mixture. The water-water experiments are compared with existing prediction methods for both sides of similar heat exchanger arrangements. In the NH_3-H_2O experiments as well as in the initial NH_3-CO_2-H_2O experiments downward absorption is taking place. In the last set of experiments, the effects of upward absorption are investigated.

3.2 EXPERIMENTAL SETUP

The design of the mini-channel heat exchanger is illustrated in figures 3.1 and 3.2. The heat exchanger was designed as a first step in scaling up mini-channel heat exchangers for industrial use [75]. The heat exchanger is oven-brazed and the length of the heat exchanger was limited by the physical dimensions of the brazing oven, resulting in total heat exchanger length of 0.8 m [80]. This size was still considered a good first step before further scale up. The tube diameter and number of tubes were the results of an optimization study done by Ozgur [80]. He investigated which size would lead to acceptable pressure drops, resulting in an inner diameter of 0.5 mm and 116 tubes. To guarantee pure counter current flow fractal distribution is used on both tube and shell sides. The main geometrical characteristics of the heat exchanger are listed in Table 3.1. The reader is referred to Nefs et al. [74] for additional details regarding the design of the heat exchanger.

A simplified process and instrumentation diagram of the experimental setup is shown in figure 3.3. The setup consists of two almost identical loops. One for the shell side of the mini-channels and the other for the tube side. In each loop the flow is driven by magnetically coupled gear pumps (MCGP) that are coupled to a Coriolis flow meter that, additionally to the flow, provides density and temperature measurements. To reach the desired conditions at the inlet of the heat exchanger the flow circulates through coiled heat exchangers (CHX), in which hot oil from a thermostatic bath circulates through the annulus side. There is a slight temperature fluctuation in the oil bath. Therefore, to reach a better accuracy, the flow is additionally heated by an electric tracing to the desired conditions. After exiting the mini-channel heat exchanger the fluid is cooled by the means of cooling water in a plate heat exchanger (PHX) to subcooled conditions. This is to prevent cavitation in the pumps. Temperature sensors are located both at the in- and outlet of both the tube and shell sides of the mini-channel heat exchanger. Pressure and differential pressure sensors are also located at the in- and outlet to provide the pressure drop over the tube and shell sides. The specifications and accuracy of all the sensors are listed in Table 3.2. Additionally, there are ten temperature sensors located along the shell of the mini-channel heat exchanger. These have rather low accuracy, around ± 1 °C. They still give a good idea of the temperature profile along the heat exchanger. As shown in figure 3.3, the set-up is configured in such a way that both downward and upward absorption are possible. Figure 3.4 shows three photographs of the set-up where the locations of the main components are highlighted. The water/shell side loops are located in one fume hood and the mini-channel heat exchanger in another one next to it. The photograph of the mini-channel shows how the temperature sensors are located along the shell of the heat exchanger.

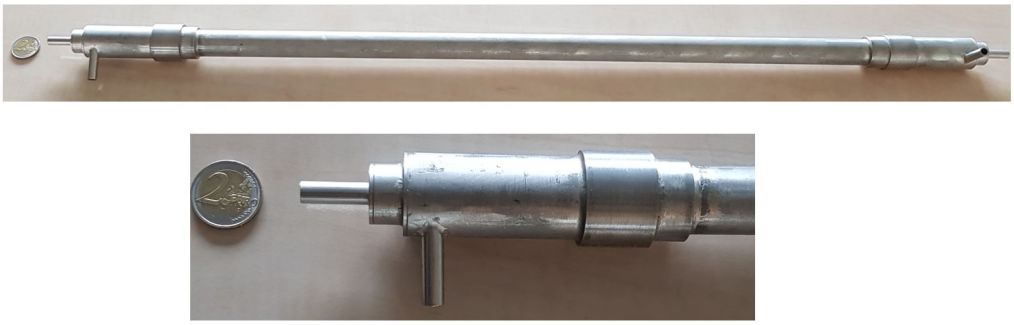

Figure 3.1: Photographs of the investigated mini-channel heat exchanger. The 2 € coin clarifies the dimension of the heat exchanger.

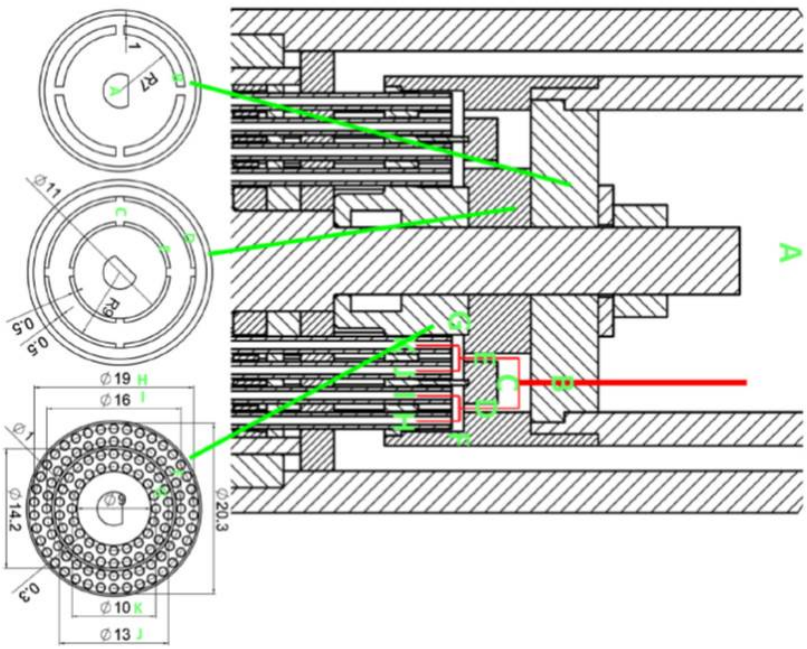

Figure 3.2: Illustration of the fractal distribution that is used both on tube and shell sides of the mini-channel heat exchanger to guarantee pure counter current flow of the heat exchanger fluids [74]. The bottom left figure shows how the tubes are arranged in the shell of the heat exchanger. Dimensions are in mm.

Table 3.1: The mini-channel heat exchanger main geometrical characteristics. Additonal details can be found in the study by Nefs et al. [74].

Number of tubes	116
Heat exchanging length, mm	652
Total length of heat exchanger, mm	800
Inner tube diameter, mm	0.5
Outer tube diameter, mm	1.0
Inner shell diameter, mm	21
Outer shell diameter, mm	25
Shell hydraulic diameter, mm	1.8
Tube pitch, mm	0.78
Tube side heat exchanging area, m^2	0.146

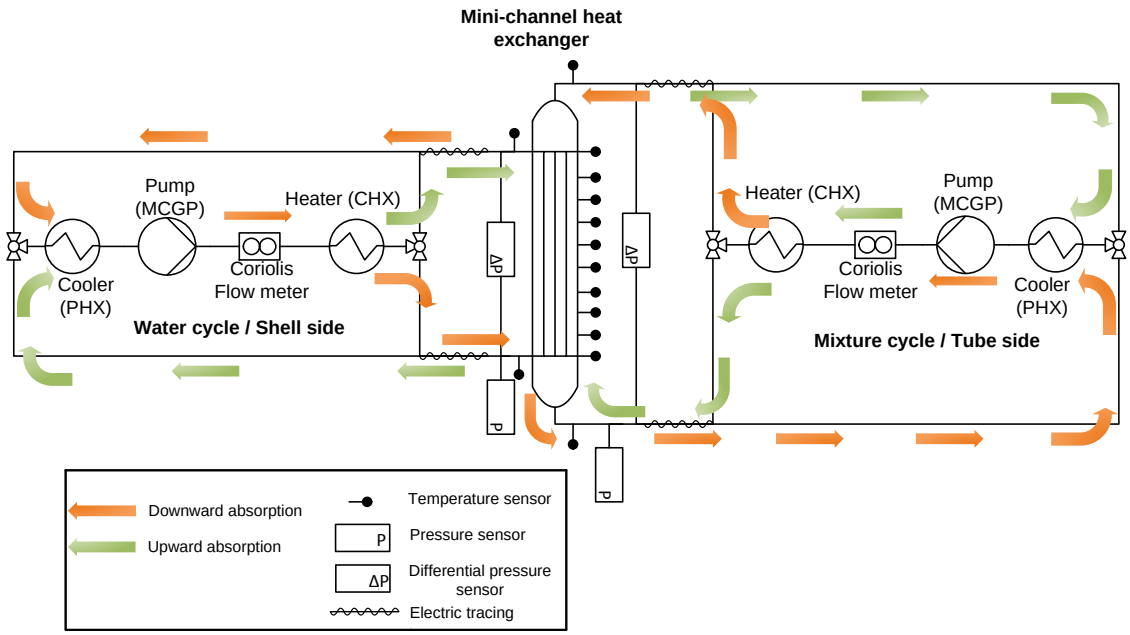

Figure 3.3: A simplified process and instrumentation diagram of the mini-channel test setup. On the left hand side, water is heated up by the means of a coiled heat exchanger and electrical tracing before entering the shell side of the mini-channel heat exchanger. After exiting the heat exchanger the water is subcooled before entering the pump and flow meter. The right hand side is identical, except the mixture enters the tube side of the mini-channel heat exchanger. It is possible to operate the setup with downward absorption (indicated with orange arrows) or upward absorption (indicated with green arrows).

Table 3.2: Type, range and accuracy of the sensors used in the mini-channel heat exchanger experiments.

Sensor type	Range	Accuracy	Unit
PT-100, Type B, temperature sensors	-50...+200	± 0.05	°C
Mini Cori-Flow, M14, mass flow sensors	0...+20	± 0.04	kg/h
Mini Cori-Flow, M14, density sensors	n. a.	± 5	kg/m^3
Mini Cori-Flow, M14, temperature sensors	0..+70	± 0.5	°C
Sitrans P DS III, 7MF4033, pressure sensors	-1...+15	± 0.13	barg
Sitrans P DS III, 7MF4333, differential pressure sensors	-1600...+1600	± 8	mbar

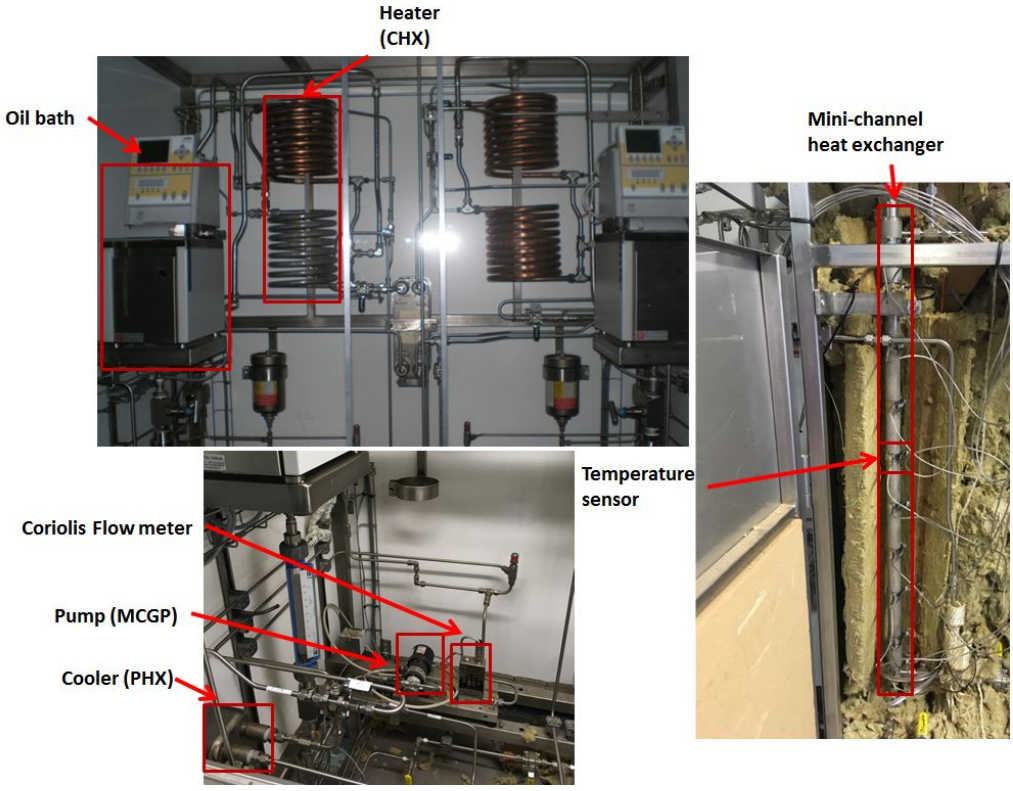

Figure 3.4: Photographs of the experimental set-up. The two photographs on the left are from a fume hood containing the water and mixture cycles. The photograph on the right is from a separate fume hood where the mini-channel heat exchanger is located (see table 3.1 for dimensions).

3.2.1 HEAT TRANSFER CALCULATIONS AND ERROR PROPAGATION

The heat duty of the tube and shell sides are calculated with the following equation:

$$\dot{Q} = \dot{m}(h_{\text{out}} - h_{\text{in}}) \tag{3.1}$$

where the enthalpy for the water and NH_3-H_2O are determined with the Refprop database [57] and the new fit described in the previous chapter is used for the NH_3-CO_2-H_2O mixture. The overall heat transfer coefficient is determined as:

$$U = \frac{\dot{Q}}{A\Delta T_{\text{lm}}} \tag{3.2}$$

where the heat flow is the uncertainty-weighted average of the shell and tube side as described by Park et al. [81]

$$\bar{\dot{Q}} = \phi_{\text{t}}\dot{Q}_{\text{t}} + \phi_{\text{s}}\dot{Q}_{\text{s}} \tag{3.3}$$

where ϕ_{t} and ϕ_{s} are weight factors dependent on the uncertainty of each heat flow, they are described further in this section along with the uncertainty. The contact area is estimated as:

$$A = \pi d N L \tag{3.4}$$

where, d, is the internal tube diameter, N, the number of tubes and, L, is the length of the heat exchanger. The logarithmic mean temperature difference (LMTD) is calculated as:

$$\Delta T_{\text{lm}} = \frac{(T_{\text{t,in}} - T_{\text{s,out}}) - (T_{\text{t,out}} - T_{\text{s,in}})}{ln\left(\frac{T_{\text{t,in}} - T_{\text{s,out}}}{T_{\text{t,out}} - T_{\text{s,in}}}\right)} \tag{3.5}$$

It should be noted that in the case of NH_3-H_2O and NH_3-CO_2-H_2O mixture the thermal properties vary considerably within the mini-channel heat exchanger and, therefore, the actual average temperature difference can differ from the estimated LMTD. The LMTD and overall heat transfer coefficient results should in those cases be taken with caution.

For error propagation the method described by Taylor [82] is used. The general equation for determining the uncertainty of a function, p, can be described as:

$$u_p = \sqrt{\left(\frac{\delta p}{\delta x}u_x\right)^2 + \ldots + \left(\frac{\delta p}{\delta z}u_z\right)^2} \tag{3.6}$$

where $x, \ldots, z$ are measured variables with uncertainties $u_x, \ldots, u_z$. If the relationship of the function is unknown then the uncertainty can be calculated as:

$$u_p = \sqrt{(p(x+u_x,\ldots,z) - p(x,\ldots,z))^2 + \ldots + (p(x,\ldots,z+u_z) - p(x,\ldots,z))^2} \tag{3.7}$$

The uncertainty of each heat flow is, therefore, calculated as follows:

$$u_{\dot{Q}} = \sqrt{\left(\frac{\delta\dot{Q}}{\delta\dot{m}}u_{\dot{m}}\right)^2 + \left(\frac{\delta\dot{Q}}{\delta h_{\text{out}}}u_{h_{\text{out}}}\right)^2 + \left(\frac{\delta\dot{Q}}{\delta h_{\text{in}}}u_{h_{\text{in}}}\right)^2} \tag{3.8}$$

where the uncertainty of the enthalpy is determined as:

$$u_h = \sqrt{(h(T+u_T,P,x)-h(T,P,x))^2+(h(T,P+u_p,x)-h(T,P,x))^2+(h(T,P,x+u_x)-h(T,P,x))^2} \tag{3.9}$$

The weight factors for the uncertainty-weighted average can then be determined as:

$$\phi_{\text{t}} = \frac{u^2_{\dot{Q}_{\text{s}}}}{u^2_{\dot{Q}_{\text{s}}} + u^2_{\dot{Q}_{\text{t}}}} \tag{3.10}$$

$$\phi_{\text{s}} = \frac{u^2_{\dot{Q}_{\text{t}}}}{u^2_{\dot{Q}_{\text{s}}} + u^2_{\dot{Q}_{\text{t}}}} \tag{3.11}$$

And the uncertainty of the weighted average [83]

$$u_{\bar{\dot{Q}}} = \sqrt{\phi^2_{\text{t}}u^2_{\dot{Q}_{\text{t}}} + \phi^2_{\text{s}}u^2_{\dot{Q}_{\text{s}}}} \tag{3.12}$$

The uncertainty of the LMTD and the overall heat transfer coefficient are estimated in a similar way. Additionally, to account for fluctuations during the experiments the standard deviation of the mean is used

$$u_x = \sigma_{\bar{x}} = \sigma_x/\sqrt{N_m} \tag{3.13}$$

It should be noted that in most cases discussed in this study this is negligible compared to the accuracy of the sensors.

3.3 EXPERIMENTAL RESULTS AND ANALYSIS

The following sections display the experimental results. The uncertainty and error bars are included where applicable, except where they would be barely visible. Firstly, experiments were performed with water on both the shell and tube side. Thereafter, with NH_3-H_2O mixture on the tube side of the heat exchanger and, lastly, with NH_3-CO_2-H_2O mixture on the tube side.

Table 3.3: Conditions to be tested during water-water experiments.

Tube side mass flow, $\dot{m}_s$	10 kg/h
Shell side mass flow, $\dot{m}_t$	2.5 - 20 kg/h
Shell side inlet temperature, $T_{s,in}$	60 °C
Tube side inlet temperature, $T_{t,in}$	110 °C

3.3.1 WATER-WATER EXPERIMENTS

Initially, experiments with water on both the shell and tube sides were performed. The water entered at the top of the tube side and at the bottom of the shell side. The operating conditions are listed in Table 3.3. The large temperature glides of the flows correspond to the expected operating conditions in industrial heat pump applications. The operating pressure was around $8 \cdot 10^5$ Pa for the shell side during the experiments and around $6 \cdot 10^5$ Pa at the tube side.

With these experiments it could be determined if sufficient insulation around the mini-channel heat exchanger was used. Initially, additional insulation was added until the difference in the heat flow of the tube and shell side was within 5 % for a mass flow of 10 kg/h. Then other shell side mass flows were tested. Figure 3.5 shows the comparison of the heat flows. In all cases the difference is less than 10 %. It is expected that the shell side heat flow is slightly lower than the tube side since the insulation can not completely hinder some losses to the environment. This is seen for the lower shell side mass flows. At the higher mass flows an opposite trend is seen. The uncertainty of the measurements is very low in these cases, only around ± 2 W, while the difference in the most extreme case, at 20 kg/h, is 63 W. Figure 3.6 illustrates how the shell side flow is collected and flows through an annulus space along the tube side inlet flow before leaving the heat exchanger. The temperature difference between the two flows in this region may explain the additional temperature rise of the shell side flow which is detected by the outlet temperature sensor just after the heat exchanger.

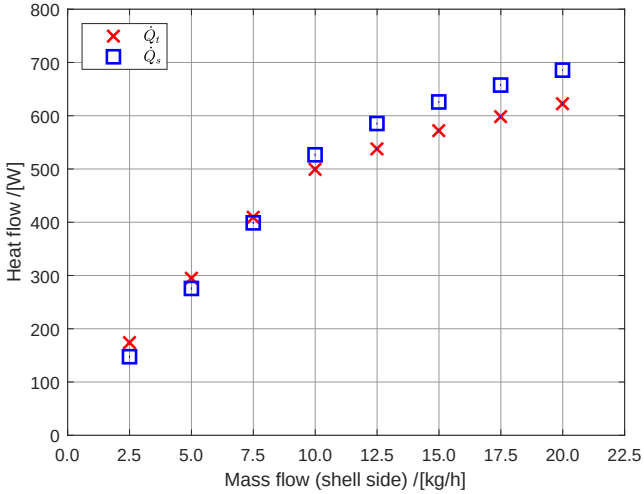

Figure 3.5: Heat flow of the shell side, $\dot{Q}_s$, and tube side, $\dot{Q}_t$, for the water-water experiments.

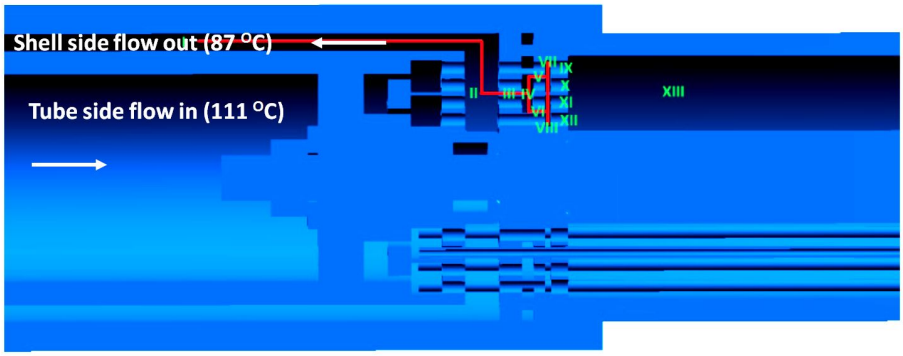

Figure 3.6: Illustration of the shell side outlet of the mini-channel heat exchanger. The temperatures correspond to the measured temperature values of the water-water experiments when the shell side mass flow is kept at 20 kg/h.

For the water-water experiments the method provided by Nefs et al. [74] for the prediction of the heat transfer performance of the heat exchanger has been applied. There the heat transfer coefficient is a function of the Nusselt number:

$$hc = Nu\frac{\lambda}{d_h} \tag{3.14}$$

The tube side heat transfer coefficient is then calculated with the method proposed by Sparrow and Patankar [84] for laminar single phase flow in tubes (defined for Reynolds

Numbers lower than 2300). In their case the Nusselt number is related to the Biot number of the flow. The Biot number is defined as:

$$Bi = hc_t * r_t / \lambda \tag{3.15}$$

The Nusselt number is then calculated in the following way:

$$\begin{aligned}
&Nu = 4.364 && Bi = 0\\
&Nu = 4.330 && 0 < Bi \leq 0.1\\
&Nu = 4.284 && 0.1 < Bi \leq 0.25\\
&Nu = 4.221 - (Bi - 0.5)(4.221 - 4.112)/0.5 && 0.25 < Bi \leq 0.5\\
&Nu = 4.122 - (Bi - 1)(3.997 - 4.122)/0.5 && 0.5 < Bi \leq 1\\
&Nu = 3.997 && 1 < Bi \leq 2\\
&Nu = 3.840 && 2 < Bi \leq 5\\
&Nu = 3.758 && 5 < Bi \leq 10\\
&Nu = 3.663 && 10 < Bi \leq 100\\
&Nu = 3.657 && Bi > 100
\end{aligned} \tag{3.16}$$

The shell side Nusselt number is calculated by the method provided by Miyatake and Iwashita [85] for a single phase thermally developed laminar flow along a tube bundle.

$$Nu = (c^2 + e^2 \cdot Gz^{2/3})^{1/2} \tag{3.17}$$

where

$$c = \frac{3.1\alpha^{0.1} + 324\alpha^{16}}{1 + 69.5\alpha^{24}} \tag{3.18}$$

$$e = \frac{1.536(1 + 8.24\alpha^{0.39})}{(2\sqrt{3}\beta - \pi)^{1/3}(1 + 6.37\alpha^{0.73})} \tag{3.19}$$

where the local Graetz number, pitch-to-tube diameter ratio and dimensionless spacing between tubes are defined as:

$$Gz = \frac{\dot{m}_s c_p}{N\lambda_s z} \tag{3.20}$$

$$\beta = \frac{2p}{d_{out,t}} \tag{3.21}$$

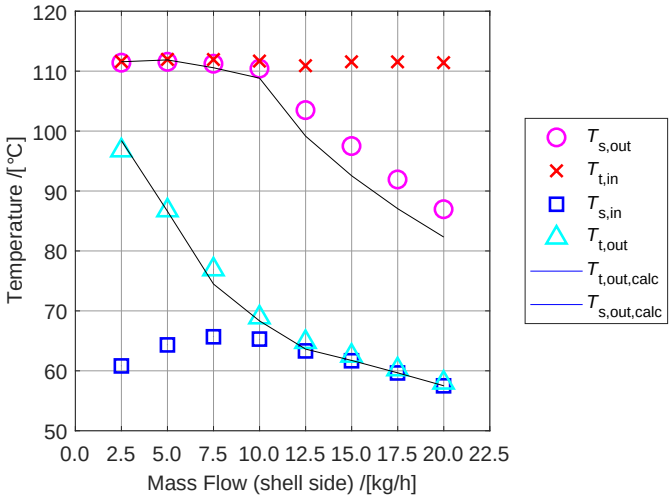

Figure 3.7: In- and outlet temperatures for the water-water experiments. The tube side mass flow is kept constant at 10 kg/h while the shell side mass flow ranges from 2.5 to 20 kg/h. The markers are the experimental values while the solid lines are calculated with the method proposed by Nefs et al. [74] and discussed above.

.

$$\alpha = \beta - 1 \tag{3.22}$$

In all tested cases the flow was laminar with a local Graetz number of less than 500. Therefore, it can be concluded that the shell side flow was indeed thermally developed laminar flow and the method provided by Miyatake and Iwashita[85] should give sufficiently accurate results. Figure 3.7 shows the inlet and outlet temperatures of the different experiments, both the experimental values and the outlet values calculated with the method proposed by Nefs et al. [74]. The calculated values correspond quite well with the measured values. Since the same working fluid is on both sides of the heat exchanger it is not surprising that the optimum shell side mass flow is 10 kg/h, or when it is identical to the tube side mass flow. At these conditions the temperature difference between the shell and tube sides are minimal and the overall heat transfer coefficient is maximized (see figure 3.8). The error for the overall heat transfer coefficient ranges from $\pm$ 4 to 14 $\mathrm{Wm^{-2}K}$ in this case. For different working fluids the mass flow ratio that gives the optimal results will vary. In the following sections a similar procedure will be carried out to attempt to find the optimum mass flow for the different working fluids.

In figure 3.7, the method proposed by Nefs et al. [74], which has been introduced above, has been used to predict the outlet conditions of the tube and shell sides using the inlet conditions as inputs. The calculated values are represented by solid lines while the markers represent the experimental values. It is seen from the figure that the method comes

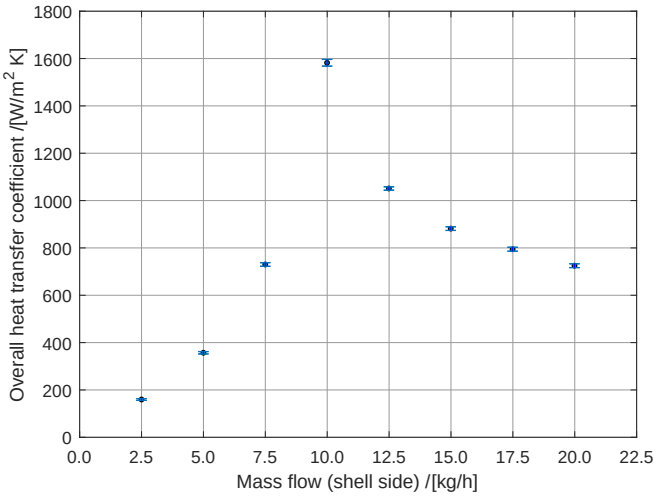

Figure 3.8: Experimental overall heat transfer coefficient based on the tube side area for the water-water experiments. Error bars are included (see section 3.2.1 for details).

very close to predict the outlet conditions of the experiments. Figure 3.9 shows the results of the prediction method (solid lines) compared to the sensors values along the shell (marker values). It is seen that the profiles are very well represented except at the higher temperature where the sensor values are lower than the predicted profiles, although the trend is still the same. Since these temperature sensors are located at the outside of the heat exchanger it is likely that the insulation was insufficient for the sensors to represent accurate values at these temperatures.

Table 3.4: Conditions to be tested during NH_3-H_2O experiments.

Ammonia concentration, x_{NH3}	33.5 wt%
Shell side mass flow, $\dot{m}_s$	5 - 17.5 kg/h
Shell side inlet temperature, $T_{s,in}$	50 °C
Tube side inlet temperature, $T_{t,in}$	130 °C

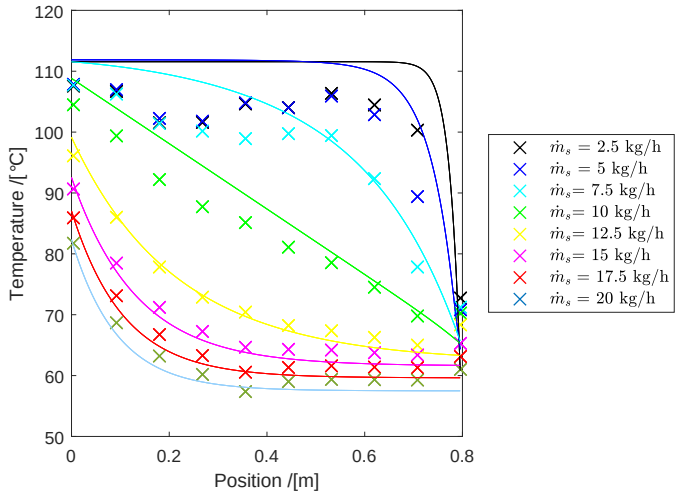

Figure 3.9: Temperatures along the length of the heat exchanger for the water-water experiments. Solid lines are calculated temperatures of the shell side flow with the method proposed by Nefs et al. [74], that is described above, and the marker values are from the temperature sensors along the heat exchanger.

3.3.2 EXPERIMENTS WITH NH_3-H_2O

After the water-water experiments the tube side was filled with an NH_3-H_2O mixture, 33.5 wt% NH_3. This concentration was chosen since at atmospheric conditions the pressure is around $1{\cdot}10^5$ Pa. The theoretical optimum for CRHPs is achieved when the mixture enters the resorber as saturated vapor and leaves as saturated liquid [56]. Reaching these exact conditions in the set-up proved to be quite difficult and if the mixture at the in- or outlet of the heat exchanger was in the two phase region the temperature and pressure measurements were quite unstable. Therefore, it was imposed that the mixture enters slightly superheated and leaves slightly subcooled. To match these conditions the tube side inlet temperature was set around 130 °C and the shell side inlet temperature around 50 °C. The operating conditions are listed in Table 3.4.

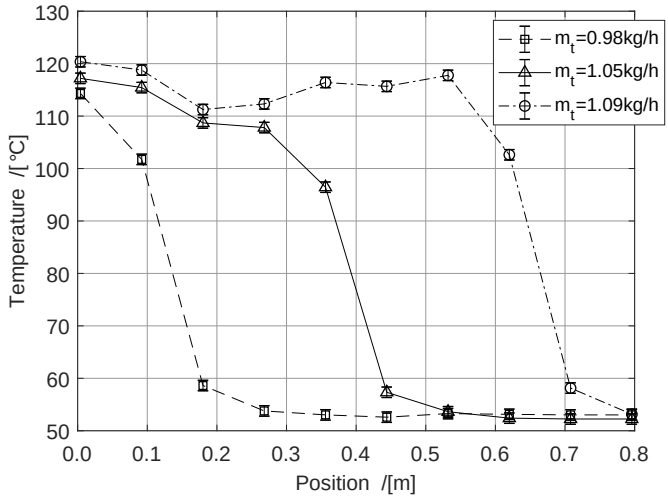

Figure 3.10: Temperature results from the sensors located along the shell side of the mini-channel heat exchanger when the shell side mass flow is fixed at 7.5 kg/h for the NH_3-H_2O experiments. Error bars are included (see section 2.2 for details). The lines serve as visual guidelines for the reader.

For each shell side mass flow an attempt was made to find the optimum tube side mass flow with the procedure described in the previous section. As an example, the results for a shell side mass flow of 7.5 kg/h are shown in Figures 3.10 and 3.11. The optimum tube side mass flow in this case was around 1.05 kg/h. For this condition the superheated and subcooled regions (flatter trend in Figure 3.10) are minimized as well as the temperature difference between the shell and tube sides. From Figure 3.10 it is also clear that the absorption of NH_3 takes up only a small portion of the heat exchanger. The mass flows were limited by the limits of the pumps, however, this indicates that the heat exchanger is oversized for these flows. Figure 3.11 shows that the target temperature difference between in- and outlet of both sides of the heat exchanger is smallest when the tube side mass flow is around 1.05 kg/h.The results for each shell side mass flow follow a linear trend as shown in Figure 3.12 and can be described with the following equation:

$$\dot{m}_t = 0.1467 \cdot \dot{m}_s \qquad for\, 5.0 \leq \dot{m}_s \leq 17.5 kg/h \tag{3.23}$$

Figure 3.13 shows the overall heat transfer coefficient for the experiments where the maximum tube side mass flow was reached. The maximum of 6 kW/(m^2K) is significantly higher than the 2 kW/(m^2K) reported by van de Bor [75] who investigated absorption on the shell side with the same set-up. This confirms that it is beneficial for the absorption process to have the NH_3-H_2O mixture on the tube side and the water on the shell side of the mini-channel. The overall heat transfer coefficient increases with increased shell side mass flow except at mass flows of 12.5 kg/h. This indicates that the tube side mass flow

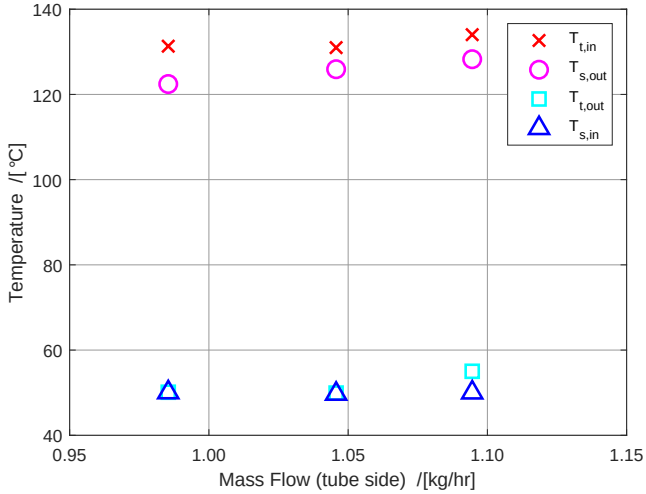

Figure 3.11: In- and outlet temperatures for the NH_3-H_2O experiments at various tube side mass flows when the shell side mass flow is kept constant at 7.5 kg/h.

.

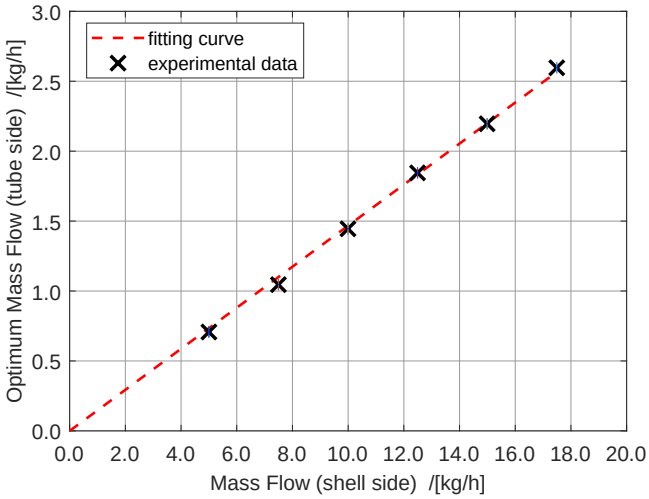

Figure 3.12: The optimum tube side mass flow for each shell side mass flow of the NH_3-H_2O experiments. A clear linear trend can be seen.

has not been properly optimized at this mass flow. Even though the heat load is higher (see Figure 3.14) the LMTD was higher than in the other cases. In this case the LMTD was higher than 3 K while in all others it was less than 2 K. In the previous experiments by van de Bor [75] the temperature sensors along the shell of the mini-channel were not in place. As mentioned above, they show that only a limited section of the heat exchanger is

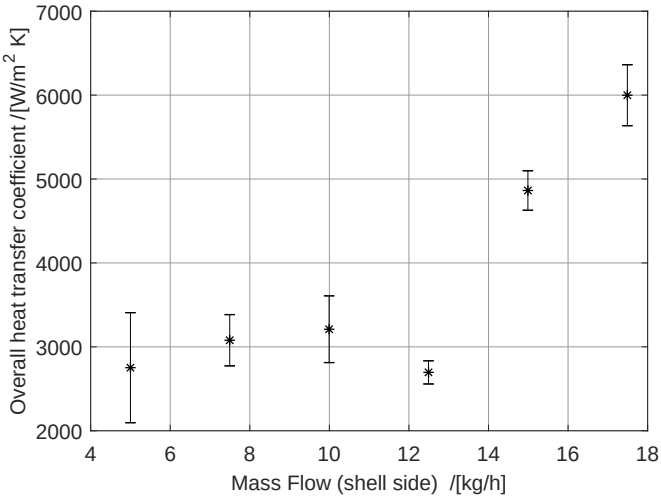

Figure 3.13: The overall heat transfer coefficient for the optimum tube side mass flows of the NH_3-H_2O experiments.

used for the absorption process. With more powerful pumps it is, therefore, a possibility that even higher overall heat transfer coefficients can be reached. Figure 3.14 shows the heat load on the shell and tube sides. For the NH_3-H_2O experiments the heat load of the shell side is always slightly lower than the tube side as expected because of losses to the environment. The difference is small, or always within 3%, with an average of 2.1 %. The phenomenon noticed during the water-water experiments is not noticeable at all, where at higher mass flows the shell side heat load became larger than the tube side. That trend was, however, only detected at higher mass flows, or around 10 kg/h. In the case of NH_3-H_2O the optimum mass flow does not exceed 3 kg/h.

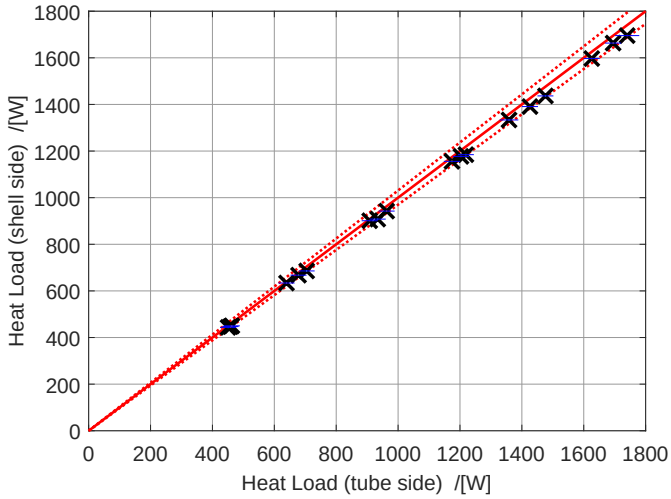

Figure 3.14: The heat load on the shell and tube sides for the NH_3-H_2O experiments. The difference is within 3 % (dotted line) for all the experiments.

The pressure drop over the shell and tube sides of the heat exchanger is shown in figure 3.15. Both of them show a trend of increased pressure drop as a function of the mass flow as expected. The trend is quite linear in both cases, although, the pressure drop on the tube side is more scattered. Since the absorption process is on the tube side it can happen that unabsorbed gas passes the heat exchanger at some point. This will affect the pressure drop over the heat exchanger which could be the reason for the scattered results.

Table 3.5: Conditions to be tested during NH_3-CO_2-H_2O experiments

Ammonia concentration, x_{NH_3}	32.8 wt%
CO_2 concentration, x_{CO_2}	2.1 wt%
Shell side mass flow, $\dot{m}_s$	5 - 17.5 kg/h
Shell side inlet temperature, $T_{s,in}$	50 °C
Tube side inlet temperature, $T_{t,in}$	130 °C

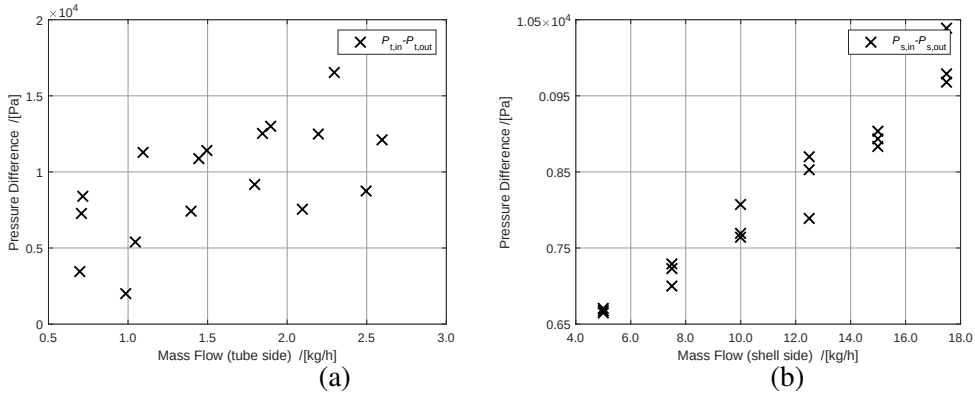

Figure 3.15: Pressure drop over the mini-channel heat exchanger on the tube side (NH_3-H_2O side) (a), and the shell side (water side) (b).

3.3.3 EXPERIMENTS WITH NH_3-CO_2-H_2O

After the NH_3-H_2O experiments a small amount of CO_2 was added to the tube side: 2.1 wt% CO_2. The desired testing conditions are listed in Table 3.5. The inlet shell and tube temperatures are kept the same as in the NH_3-H_2O experiments. The goal was to test the same range of shell side mass flows as in those experiments as well. Unfortunately, for tube side mass flows higher than 4.5 kg/h the conditions became too unstable to reach any kind of steady state. Large fluctuations in the density measured at the pump at random time intervals were observed. This indicates that unabsorbed CO_2 was still in gas phase as it passed the pump. Therefore, it was only possible to get results for shell side mass flows of 5, 7.5 and 10 kg/h. Even though the data is limited, it can give a good indication of the influence of the added CO_2.

For the shell side mass flows of 5, 7.5 and 10 kg/h an attempt was made to find the optimum tube side mass flow with the same method as before. The temperature results for a shell side mass flow of 5 kg/h are shown in Figure 3.16. For this case the optimum tube side mass flow is at around 2.1 kg/h. For each optimum tube side mass flow the

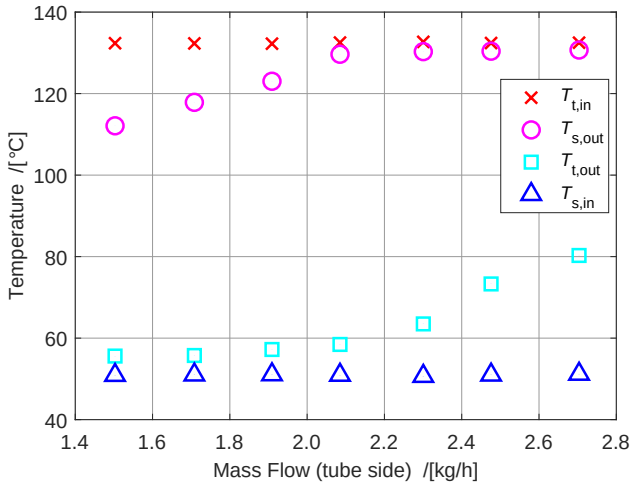

Figure 3.16: The in- and outlet temperatures for the NH_3-CO_2-H_2O experiments at various tube side mass flows when the shell side mass flow is kept constant at 5 kg/h.

temperature values at the in- and outlet are listed in Table 3.6. The optimum mass flow in this case can be described with the following equation:

$$\dot{m}_t = 0.43 \cdot \dot{m}_s \qquad for\, 5.0 \leq \dot{m}_s \leq 10.0 kg/h \tag{3.24}$$

The pressure drop results at the tube and shell sides are shown in Figure 3.17. When compared to Figure 3.15, it can be observed that the pressure drop at the shell side is comparable for similar mass flows. This is expected since in both cases water is at the shell side of the heat exchanger. For the mixture side, or the tube side, the pressure drop is slightly lower with the added CO_2 for similar mass flows. It should be noted that for similar mass flows the NH_3-H_2O mixture goes from being slightly superheated to subcooled. In the case of the NH_3-CO_2-H_2O mixture the mixture enters in the two-phase region and leaves the heat exchanger subcooled with associated decrease in the average velocity, which can explain the pressure drop difference.

With the added CO_2 it can be seen from Table 3.6 that the LMTD as well as the overall heat transfer coefficient becomes worse. On the other hand it was noticed that the heat load increased compared to the NH_3-H_2O experiments as is clear from the shell side temperature results. The heat load for each shell side mass flow is shown in figure 3.18. The increase is around 5% for each case. These are positive results since the main goal of a heat pump is to provide heat to a heat sink. However, the optimum tube side mass flow is significantly higher with the added CO_2 (see figure 3.19). This will have a negative impact on the overall performance of CRHPs since larger mass flow means a larger power input is needed. However, with the added CO_2 the pressure increased significantly (see figure

Table 3.6: Temperature and overall heat transfer coefficient results for various shell side mass flows, with and without added CO_2 before extraction. The uncertainty of the results is obtained according to section 3.2.

Parameter	Without CO_2/with CO_2	Without CO_2/with CO_2	Without CO_2/with CO_2
$\dot{m}_s$ [kg/h]	5.00 ± 0.04/5 ± 0.04	7.5 ± 0.04/7.5 ± 0.04	10 ± 0.04/10 ± 0.04
$T_{t,in}$ [°C]	132.00 ± 0.05/132.46 ± 0.05	130.99 ± 0.05/131.36 ± 0.05	135.35 ± 0.05/134.30 ± 0.05
$T_{s,out}$ [°C]	127.11 ± 0.05/131.31 ± 0.05	125.92 ± 0.05 /130.08 ± 0.05	127.24 ± 0.05/133.42 ± 0.05
$T_{t,out}$ [°C]	50.69 ± 0.05/58.51 ± 0.05	49.94 ± 0.05/58.43 ± 0.05	50.24 ± 0.05/54.75 ± 0.05
$T_{s,in}$ [°C]	50.63 ± 0.05/50.82 ± 0.05	49.72 ± 0.05/50.10 ± 0.05	50.11 ± 0.05/50.21 ± 0.05
ΔT_{lm} [K]	1.1 ± 0.3/3.45 ± 0.05	1.5 ± 0.1/3.77 ± 0.08	1.9 ± 0.2/2.24 ± 0.07
U [kW/(m^{2}K)]	2.7 ± 0.7/0.94 ± 0.02	3.1 ± 0.3/1.280 ± 0.03	3.2 ± 0.4 /3.0 ± 0.1

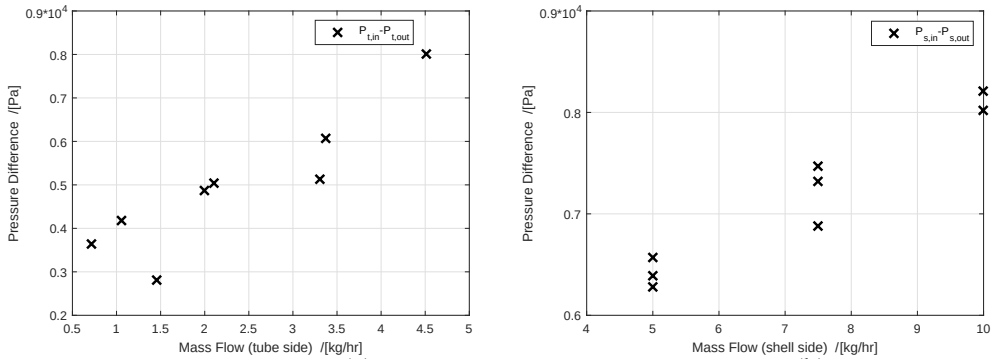

Figure 3.17: Pressure drop over the mini-channel heat exchanger on the tube side (NH_3-CO_2-H_2O side) (a), and the shell side (water side) (b).

3.20). This increase in pressure resulted in the inlet being in the two phase region. To make a fairer comparison between the two mixtures similar pressure levels are desired. Since the system is a closed loop, a part of the mixture needs to be drained to lower the pressure. To reach homogeneous conditions the system was kept at atmospheric conditions and the mixture was kept flowing to keep the same concentration after the draining process. However, when keeping the system at lower temperature the final pressure is unknown. Therefore, a couple of iterations might be needed to reach similar pressure levels.

The pressure level and shell side heat load results before and after extraction are shown in figure 3.21. The pressure during the NH_3-H_2O experiments was slightly lower than $4{\cdot}10^5$ Pa compared to around 8 - $9{\cdot}10^5$ Pa for the first NH_3-CO_2-H_2O experiments. After the first extraction the pressure decreased slightly and the optimum tube side mass flow did indeed decrease, from around 2.1 kg/h to around 1.7 kg/h for a fixed shell side mass flow of 5 kg/h. After the second extraction the results became even better, the pressure level was

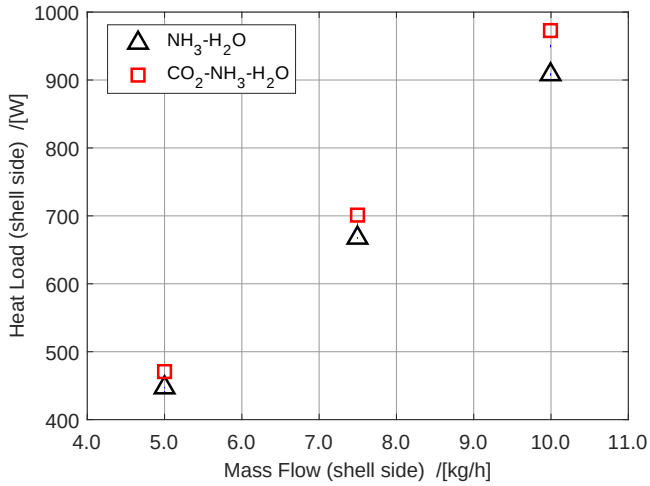

Figure 3.18: Shell side heat load for the NH_3-H_2O and NH_3-CO_2-H_2O experiments.

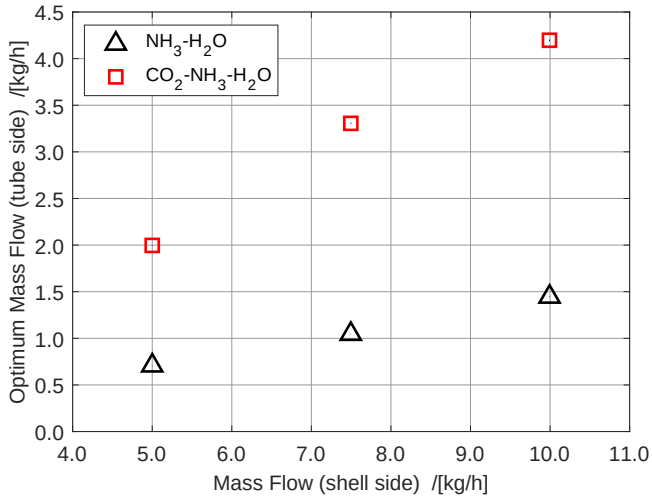

Figure 3.19: Optimum tube side mass flow for the NH_3-H_2O and NH_3-CO_2-H_2O experiments for shell side mass flows of 5, 7.5 and 10 kg/h.

still too high or around $6{\cdot}10^5$ Pa, but the optimum tube side mass flow decreased to around 1.4 kg/h. Unfortunately, after the third extraction the operation became too unstable and no steady state was reached. One plausible cause, as mentioned before, is that part of the CO_2 is unabsorbed. This also shows that the optimum mass flow is highly dependent on the operating pressure. Figure 3.22 shows the shell temperature profile for the NH_3-CO_2-H_2O and NH_3-H_2O at shell side mass flows of 5 kg/h. From the figure it can be seen that the absorption process takes up significantly larger section of the mini-channel for the

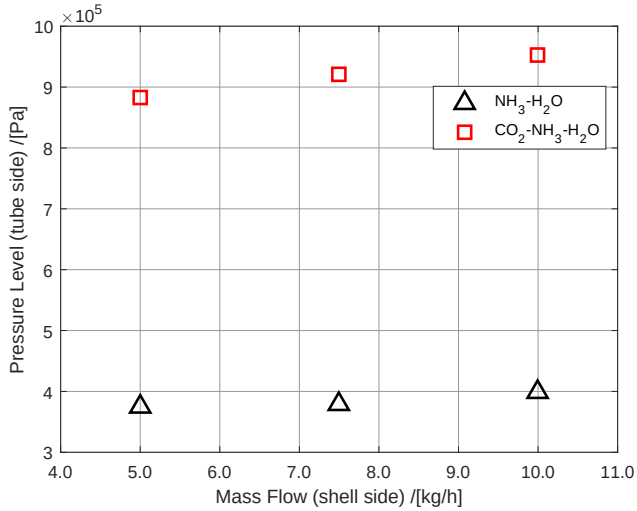

Figure 3.20: Pressure levels for the NH_3-H_2O and NH_3-CO_2-H_2O experiments for shell side mass flows of 5, 7.5 and 10 kg/h.

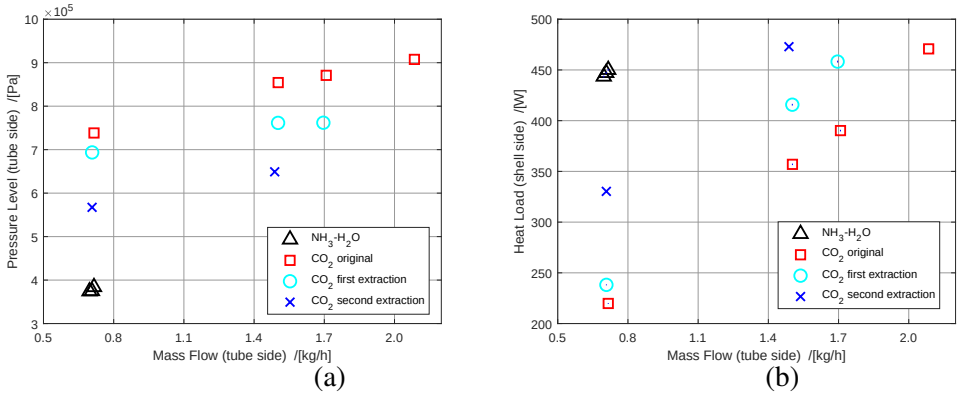

Figure 3.21: Results for a shell side mass flow of 5 kg/h before and after draining of the mixture with added CO_2 compared to the NH_3-H_2O results, the different pressure levels (a), and the shell side heat load (b). It is clear that comparable pressure levels were not reached with the added CO_2. However, with each extraction the performance at similar mass flows approached the performance of the NH_3-H_2O mixture.

NH_3-CO_2-H_2O mixture compared to NH_3-H_2O. The figure also shows clearly that larger mass flows are needed to reach comparable or better performance with the added CO_2 for these specific operating conditions.

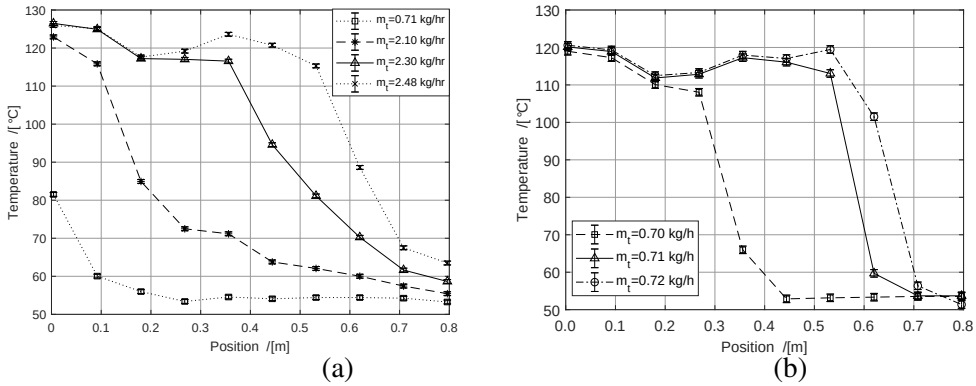

Figure 3.22: Temperature results from the sensors located along the shell side of the mini-channel heat exchanger for a shell side mass flow of 5 kg/h, for the NH_3-CO_2-H_2O mixture (a), and the NH_3-H_2O mixture (b). Error bars are included (see section 2 for details). The lines serve as visual guidelines for the reader.

3.3.4 DOWNWARD VS UPWARD ABSORPTION

The randomness of the spikes in the mass flow after the last extraction pointed to a pocket of CO_2 gas building up somewhere in the system. Likely at the top of the heat exchanger. To further investigate this, experiments were performed where the absorption process is from the bottom to the top of the mini-channel heat exchanger instead of top to bottom. As reported by Bhagwat and Ghajar [86] the flow patterns and void fractions differ quite significantly between vertical two phase downward and upward flow. For the third extraction where no steady state was reached at all when the absorption process was from top to bottom, it was now easily reached for the bottom to top absorption configuration. Figure 3.23 shows the temperature profile from the shell side of the heat exchanger for both upward and downward absorption. From the figure it is clear that the trend differs significantly between the two absorption modes. The mass flows and the heat duties are listed in Table 3.7 and compared to the results from the downward flow without extraction and from the NH_3-H_2O experiments. The optimum tube side mass flow decreased, however, the heat transfer became worse by approximately 10%. This is contradictory to the findings of Kang et al. [66] and Castro et al. [67] where bubble absorption was more favorable than falling film absorption. This indicates that the geometry plays a large role in the absorption process and it is likely that for other compact heat exchangers the findings would be similar as in this case.

This also indicates that the configuration of the heat exchanger becomes very important when operating with an NH_3-CO_2-H_2O mixture. Other heat exchangers might be better suited for NH_3-CO_2-H_2O than the mini-channel heat exchanger used for the experiments. It is unlikely that plate heat exchangers are well suited since the mixture passed through a

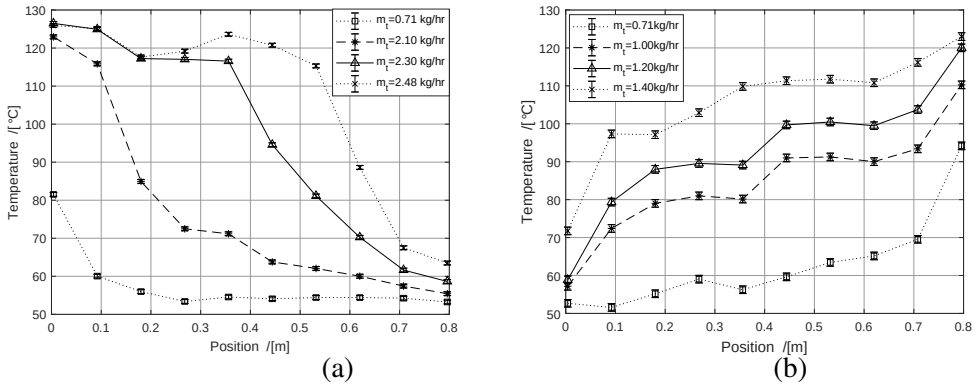

Figure 3.23: Temperature values along the mini-channel for a shell side mass flow of 5 kg/h, for downward absorption of the NH_3-CO_2-H_2O mixture (a), and upward absorption of the NH_3-CO_2-H_2O mixture (b). Error bars are included (see section 3.2 for details). The lines serve as visual guidelines for the reader.

plate heat exchanger before the pump in the setup. In the plate heat exchanger the mixture is subcooled by more than 30 K. Still, the CO_2 was not fully absorbed at certain conditions. The upward absorption experiments resulted in increased stability. Therefore, it might be sufficient to redesign the top part of the heat exchanger in such a way that accumulation of gaseous CO_2 would be eliminated or limited. Another solution would be to increase the absorption rate. Different measures have been done to achieve this. As mentioned in the introduction, it has been shown experimentally that smaller diameters increase the absorption rate [68, 71]. Therefore, it could be beneficial to use a micro-channel heat exchanger with even smaller channels, since this might be sufficient to get rid of gas pockets of CO_2. Another way could be to increase the surface roughness of the tubes, both Kim et al. [87] and Park et al. [83] showed that the absorption performance increased significantly by only increasing the surface roughness. Another important factor to take into account is that in CRHPs there is no pump. The unabsorbed CO_2 might still be a problem for the expansion device after the absorber, however, for the rest of the components, the desorber and the compressor, it isn't.

Table 3.7: Comparison of the tube side optimum mass flow and uncertainty-weighted average heat load when operating at different shell side mass flows for NH_3-H_2O, NH_3-CO_2-H_2O downward absorption and NH_3-CO_2-H_2O upward absorption.

Mixture	$\dot{m}_s$ [kg/h]	$\dot{m}_{t,opt}$ [kg/h]	$\bar{\dot{Q}}$ [W]
NH_3-H_2O	5.00 ± 0.04	0.71 ± 0.04	447 ± 4
	7.50 ± 0.04	1.05 ± 0.04	668 ± 4
	10.00 ± 0.04	1.40 ± 0.04	901 ± 4
NH_3-CO_2-H_2O (downward absorption)	5.00 ± 0.04	2.10 ± 0.04	462 ± 1
	7.50 ± 0.04	3.30 ± 0.04	693 ± 2
	10.00 ± 0.04	4.20 ± 0.04	970 ± 2
NH_3-CO_2-H_2O (upward absorption)	5.00 ± 0.04	1.20 ± 0.04	418 ± 1
	7.50 ± 0.04	1.80 ± 0.04	615 ± 1
	10.00 ± 0.04	2.40 ± 0.04	888 ± 2

3.3.5 MATERIAL COMPATIBILITY WITH ADDED CO_2

The components in the experimental setup have been carefully chosen to be compatible with NH_3-H_2O. Most components are stainless steel. With the added CO_2 it is a question if the setup is still compatible. One of the dangers of adding CO_2 to NH_3-H_2O is the chance of solid formation, mainly of ammonium bicarbonate. Therefore, before initiating the experiments the properties of the NH_3-CO_2-H_2O mixture were investigated by Gudjonsdottir et al. [22] and are discussed in Chapter 2. They developed a new fit of the existing e-NRTL (electrolyte - Non-Random Two-Liquid) method available in the Aspen Plus software [38] suitable for the range that is interesting for CRHP applications. With only 2.1 wt% of CO_2, when the NH_3 concentration is above 30 wt%, there is no danger of solid formation at room temperatures. Much higher concentration of CO_2 is needed, of around 20 wt%. With the same method the pH level of the mixture can be investigated. CO_2 in water results in an acid solution, however, NH_3 in water results in a basic solution. The mixture concentration used in the experiments has much higher concentration of NH_3 than CO_2 and, therefore, the mixture is basic. For the temperature range that is investigated the pH level is in the range of 8 - 10. After conduction of the experiments the setup has been partly taken apart and no corrosion or solid formation of any kind was visible.

3.4 CONCLUSIONS

In this study experiments were performed in a mini-channel heat exchanger to verify the benefits of utilizing NH_3-CO_2-H_2O, rather than NH_3-H_2O, for heat pump applications. Additional goal was to verify which configuration achieves higher absorption performance. That is if the mixture should be on the tube or shell side and if downward or upward absorption should be used. The main conclusions are the following:

- For increased performance the mixture should be on the tube side of the mini-channel heat exchanger. Overall heat transfer coefficients of 6 kW/(m^2K) were reached compared to only 2 kW/(m^2K) when the mixture was kept on the shell side [75].
- Downward absorption mode is preferred. With the present heat exchanger design the performance increased by approximately 10 % compared to upward absorption.
- The mixture mass flow that results in better results in terms of temperature difference and overall heat transfer coefficient is highly dependent on the operating pressure.
- A heat load increase of approximately 5 % was observed for the NH_3-CO_2-H_2O mixture compared to NH_3-H_2O. However, pumping instabilities limited the operating range resulting in limited data and comparable pressure ranges were not accomplished.

The encountered pumping instabilities indicate that specific absorbers might be necessary for optimum performance when operating with NH_3-CO_2-H_2O, such as micro-channel heat exchangers or a mini-channel heat exchanger with a specially designed inlet that minimizes the risk of accumulation of CO_2. It is, therefore, recommended to study the performance of NH_3-CO_2-H_2O in microchannel heat exchangers and over a large operating range. Further, it is recommended to further study the compressor performance with added CO_2 and the performance when implemented in an entire heat pump cycle.

4

WET COMPRESSION MODEL FOR MINIMIZING ENTROPY

As mentioned in the introduction, commercial solutions utilizing wet compression are not yet available. Wet compression is an attractive option for industrial heat pumps if the isentropic efficiency of the compressor is 0.7 or higher, as noted by several authors. In this chapter, we develop a model of a twin screw compressor operating with NH_3-H_2O that is suitable for wet compression. The model is adapted to calculate the entropy production in order to identify where the major irreversibilities are located in the compressor. The effects of clearance size, rotational speed, ammonia concentrations, compressor inlet vapor quality as well as under- and over compression are analysed. The results show that the clearance size and the rotational speed have the largest effects on the entropy production. Additionally, increased ammonia concentration and decreased vapor quality lead to decreased losses. The results indicate that it should be feasible to reach the targeted performance if the clearances size is limited to 50 μm, the rotational speed maintained above 10,000 rpm, the ammonia concentration kept in the range of 30 – 40 wt.%, and the inlet vapor quality in the range 0.5 to 0.7. A simplified version of the model was also developed that shows the same trends as the more detailed model. This model was modified to operate with the NH_3-CO_2-H_2O mixture. The model indicates a slight increase in the isentropic efficiency with the added CO_2, which implies that with added CO_2 the benefits might be even greater than expected from the previous chapters.

This chapter is adapted from Gudjonsdottir, V., Infante Ferreira, C. A. and Goethals, A. „Wet compression model for entropy production minimization." In: *Applied Thermal Engineering* 149 (2019), pp. 439–447.

4.1 INTRODUCTION

As mentioned in the first Chapter, there might be no advantage of wet compression compared to the traditionally used vapor compression heat pump (VCHP) if the compressor efficiency is not higher than 70 %. In wet compression the process is entirely in the two phase region instead of in the vapor region. Zaytsev [20] identified a twin screw compressor as the most suitable type of compressor for wet compression since it is tolerant for liquid carry over and can have a rather high efficiency. He performed experiments with a twin screw compressor utilizing wet compression with additional liquid injection, however, he reached only efficiencies of around 6 – 7 %. Infante Ferreira et al. [55] performed further experiments with a prototype twin screw compressor, and they reached isentropic efficiencies of around 35 %. Since then quite a number of experiments have been performed with twin screw compressors with liquid injection where high efficiencies have been achieved, around or higher than 70 % [89, 90]. In these cases liquid is injected during vapor compression, however, few studies have been performed with ammonia-water. Tian et al. [91] recently performed experiments with ammonia-water mixture in an ammonia refinery, therefore with high concentrations of ammonia. They investigated two sets of compressors, in the first one liquid was injected to a superheated ammonia stream, 98 wt.% NH_3, and it reached an isentropic efficiency of around 75 wt.%. In the second one liquid was injected to a saturated ammonia stream at higher temperature and pressure and an efficiency of 64 % was reached. For CRHP the ideal situation is to compress within the two-phase region at all times. Therefore, it is necessary to further study the influence of compression within the two-phase region and to investigate if isentropic efficiencies above 70 % are still a feasible option. Different modeling approaches have been used in the literature to simulate the performance of twin screw compressors. For the thermodynamic performance most of them are 1 D cavity models with different level of accuracy like the ones used by Cao et al. [89], Chamoun et al. [92], Jianfeng et al. [93], Seshaiah et al. [94], and Tian et al. [95]. In recent years computation fluid dynamics (CFD) models of twin screw compressors have gained increased attention and a comparison was recently made by Kennedy et al. [96] for oil free dry compression. In their study the thermodynamic cavity model gave more accurate results and for wet compression the CFD model will be even more challenging. However, as pointed out by these authors the CFD model gives an idea of the complex internal flow phenomena which can be useful for the design of twin screw compressors though difficult to validate. In this study a 1 D cavity model based on the work of Zaytsev [20] is developed, validated and modified to include entropy production. This model is chosen since it should give sufficient accuracy to evaluate the performance of wet compression in a twin screw compressor. Entropy production allows identification of the locations of irreversibilities in the system. In this study the effects of the clearance size, ammonia concentration, rotational speed, vapor quality at the inlet of the compressor, and location of the discharge port are investigated. The results give an

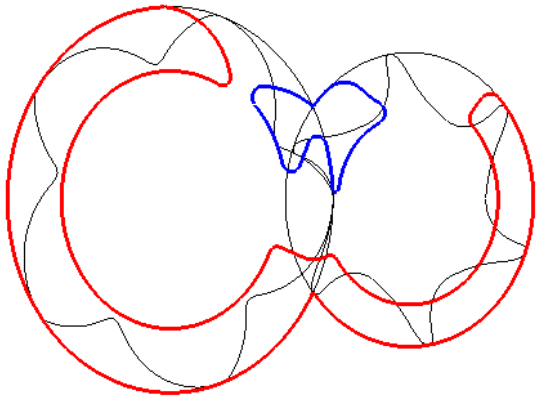

Figure 4.1: The twin screw compressor rotor profiles and shape of the radial suction port in red (there is also an axial suction port) and discharge port in blue.

idea of the optimal operating conditions of such a compressor in a CRHP operating with ammonia-water as a working fluid.

4.2 THE SCREW COMPRESSOR MODEL

The screw compressor model is based on a model described by Zaytsev [20]. The model is divided in a geometry model and a thermodynamic model. The geometry model was developed by Zaytsev [20] and is based on the meshing line between the two rotors. For a detailed description of the geometry model see Zaytsev and Infante Ferreira [97]. Table 4.1 gives some geometrical data of the studied compressor. Additionally, some details of the adopted compressor geometry are illustrated in figure 4.1 to clarify the determination of the port sizes and leakage path areas.

The model is not described here further, however, it does give essential information for further thermodynamic calculations; the cavity volume, the suction area, the discharge area and the leakage areas. The thermodynamic model is described in the following section.

4.2.1 THERMODYNAMIC MODEL

The thermodynamic model is a homogeneous model based on mass and energy conservations [20]. This model is assumed to be of sufficient detail to give reliable results for wet compression. The main reasons are that in contrast to liquid injected process, in wet

compression the liquid and vapor are already at equilibrium at the inlet of the compressor. Additionally, Stosic et al. [98] concluded that for oil injected process the oil follows closely the gas temperature during the compression process in a twin screw compressor for droplet sizes less than 0.5 mm. Therefore, by spraying the liquid into the vapor flow at the compressor inlet, close to homogeneous conditions should be attained. The mass conservation can be defined in the following way:

$$\frac{\mathrm{d}P}{\mathrm{d}\phi} = \frac{1}{\left(\frac{\delta v}{\delta P}\right)_{T,x}} \left[\frac{v}{m} \left(\sum_{k=1}^{n} \left(\frac{\mathrm{d}m_{\mathrm{out}}}{\mathrm{d}\phi} \right)_k - \sum_{k=1}^{n} \left(\frac{\mathrm{d}m_{\mathrm{in}}}{\mathrm{d}\phi} \right)_k \right) + \frac{1}{m} \frac{\mathrm{d}V}{\mathrm{d}\phi} - \left(\frac{\delta v}{\delta T} \right)_{P,x} \frac{\mathrm{d}T}{\mathrm{d}\phi} \right] \tag{4.1}$$

where P is the pressure, ϕ the male rotor turning angle, m mass of the mixture, v the specific volume, V the cavity volume and T the temperature. The energy conservation can be written in the following form:

$$\frac{\mathrm{d}T}{\mathrm{d}\phi} = \frac{T \left(\frac{\delta v}{\delta T}\right)_{P,x} \left[\frac{v}{m} \left(\sum_{k=1}^{n} \left(\frac{\mathrm{d}m_{\mathrm{out}}}{\mathrm{d}\phi} \right)_k - \sum_{k=1}^{n} \left(\frac{\mathrm{d}m_{\mathrm{in}}}{\mathrm{d}\phi} \right)_k \right) + \frac{1}{m} \frac{\mathrm{d}V}{\mathrm{d}\phi} \right]}{\left(\frac{\delta v}{\delta P}\right)_{T,x} \left(\frac{\delta h}{\delta T}\right)_{P,x} + T \left(\frac{\delta v}{\delta T}\right)^2_{P,x}} + \frac{\frac{\delta Q}{\delta \phi} + \sum_{k=1}^{l} (h_{\mathrm{in,k}} - h) \left(\frac{\mathrm{d}m_{\mathrm{in}}}{\mathrm{d}\phi} \right)_k}{m \left(\frac{\delta h}{\delta T}\right)_{P,x} + \frac{mT}{\left(\frac{\delta v}{\delta P}\right)_{T,x}} \left(\frac{\delta v}{\delta T}\right)^2_{P,x}} \tag{4.2}$$

where h is the specific enthalpy. The mass flow rate, depending on the male rotation angle, through both the suction and discharge ports as well as due to the leakages is calculated with the continuity equation:

$$\frac{\mathrm{d}m}{\mathrm{d}\phi} = \frac{\zeta \rho A w}{\omega} \tag{4.3}$$

Where ζ is the empirical flow coefficient, A the leakage area, ρ density of the flow, ω the angular speed of the male rotor and the flow velocity, w, is determined by the converging nozzle model:

$$w = \sqrt{2 \int_{P_{\mathrm{down}}}^{P_{\mathrm{up}}} v \mathrm{d}P} \tag{4.4}$$

With the maximum limit being the local speed of sound

$$w_{\mathrm{max}} = v \sqrt{-\left(\frac{\delta P}{\delta v}\right)_{\mathrm{is}}} \tag{4.5}$$

The overall mass flow rate can then be calculated as

$$\dot{m} = m_1 \frac{n}{60} \int \frac{dm}{d\phi} d\phi \tag{4.6}$$

The model takes into account the main leakage paths in a screw compressor, which are:

1. Through the contact line between the two rotors.
2. Through the sealing line between the tip of the rotors and the housing.
3. Through the cusp blowholes at compression side with high pressure.
4. Through the compression-start blowholes at the suction side.
5. Through the discharge end clearance.

The isentropic efficiency of the compressor is defined as:

$$\eta_{is} = \frac{\dot{m}(h_{id,d} - h_s)}{\dot{W}} \tag{4.7}$$

Where the power input, $\dot{W}$, is defined as

$$\dot{W} = \dot{m} \int V \mathrm{d}P \tag{4.8}$$

The volumetric efficiency is defined as the ratio of the real and theoretical volumetric displacement:

$$\eta_{vol} = \frac{\dot{V}_{real}}{\dot{V}_{th}} \tag{4.9}$$

Where $\dot{V}_{real} = v_s \int \frac{\mathrm{d}m}{\mathrm{d}\phi} \mathrm{d}\phi$ and $\dot{V}_{th}$ is the volume flow that follows from the maximum cavity volume and the rotational speed.

4.2.2 MECHANICAL LOSSES

In the literature it is common to assume a fixed mechanical efficiency [91, 92, 99], normally in the range 0.9 to 0.95. However, as experiments from Arjeneh et al. [100] show the mechanical losses do increase with increased rotational speed. In this work one of the goals is to estimate the effects of the rotational speed and therefore assuming a fixed value for the mechanical efficiency would not result in the most realistic results. It is assumed that the main contributors to the mechanical losses are:

- Bearings
- Seals
- Gears

It is assumed that there are four radial and two axial bearings and the losses are estimated with the following equation [101]

$$\dot{W}_{\mathrm{b}} = 5.25 \cdot 10^{-6} \mu C d_{\mathrm{b}} n \tag{4.10}$$

Where μ is the coefficient of friction and C is the dynamic bearing load, both given by the manufacturer.

To estimate the sealing losses an equation from Parker Hannifin Corporation [102] for elastomer shaft seals is used. As noted by them this should only be used as an estimate and the real value will depend on many factors like the seal design, shaft texture, pressures and time in service.

$$\dot{W}_{\mathrm{seal}} = 7.45 \cdot 10^{-7} d_{\mathrm{seal}} n^{4/3} \tag{4.11}$$

They indicate that the power input needed for a dry running seal will be two to three times the value above. In the calculations it is assumed that the power input will therefore be three times the estimated value.

Further it is assumed that the losses caused by gear meshing and synchronization are 4% [103]. As pointed out by Zaytsev [20] it is difficult to estimate to what degree these losses will affect the process medium itself. Similar to Zaytsev [20] it is assumed that only the sealing losses will have effects on the process medium at the beginning of the compression process, as heat input ($\frac{\delta Q}{\delta \phi}$ in equation 4.2) . The total isentropic efficiency of the system is then defined as the product of the isentropic efficiency and the mechanical efficiency. It should be noted that motor losses are not taken into account.

$$\eta_{\mathrm{is,total}} = \eta_{\mathrm{is}} \eta_{\mathrm{mech}} \tag{4.12}$$

4.2.3 ENTROPY PRODUCTION

The model takes into account the rate of entropy production which for systems operating in steady state can be defined as [104]

$$\dot{\sigma} = \sum_k \dot{m}_k s_k - \sum_j \dot{m}_j s_j - \sum \frac{\dot{Q}_i}{T_i} \tag{4.13}$$

The entropy production is then calculated as a function of the male rotation angle to observe the entropy production throughout the compression process. In each control volume all inlet and outlet mass flows are considered and their respective properties, e.g. if there is a leakage flow from the following cavity the entropy is a function of the conditions of that cavity. The heat losses to the environment are assumed negligible, except for the sealing losses influencing the process medium at the start of the compression process.

$$\frac{\mathrm{d}\sigma}{\mathrm{d}\phi} = \sum_{k=1}^{n} \left(\frac{\mathrm{d}m_{\mathrm{out}}}{\mathrm{d}\phi} s_{\mathrm{out}} \right) - \sum_{k=1}^{n} \left(\frac{\mathrm{d}m_{\mathrm{in}}}{\mathrm{d}\phi} s_{\mathrm{in}} \right) \tag{4.14}$$

The model is implemented in Matlab. The conservation equations are solved with the Heun method. The thermodynamic properties of the ammonia-water mixture needed for the calculations, including the entropy, are calculated with the computational method developed by Rattner and Garimella [105]. To include the leakage calculations first the model is run without any leakages. Then the model is run including the leakages until the solution converges to acceptable tolerances, which was chosen as 0.1 % change in isentropic efficiency. Compared to the model of Zaytsev [20], the model is now implemented in Matlab, a new thermodynamic property method is used and the mechanical loss estimation has been modified. Therefore, a validation is necessary and is implemented in the following section.

4.3 MODEL VALIDATION

A new twin screw compressor prototype is being built that will be used in the near future to test wet compression. Since the prototype is not ready, experimental data from Zaytsev [20] are used for validation purposes, the geometrical characteristics are listed in Table 4.1 and the experimental results and their accuracy are listed in Table 4.2. Although the efficiencies attained during this experiment were quite low, this experiment has been selected since only Zaytsev's work reports oil-free ammonia-water compression in a twin-screw compressor with sufficient detail to be used for validation purposes. The low efficiencies were caused by mainly the use of a labyrinth seal which created a large leakage flow from discharge to inlet nozzle and the large manufacturing tolerances. These processes can be added to the model for validation purposes. Both the compressor used for validation purposes and the compressor studied in this thesis have bearings being oil lubricated outside the process side of the compressor. In the compressor used for validation purposes labyrinth and lip seals were used to separate the oil lubricated and the oil-free process sides of the compressor. In the compressor discussed in this thesis only lip seals separate the process side from the oil lubricated side. Liquid ammonia-water was used as the lubricant in the compressor used for validation purposes. In the present study synchronization gears are used to prevent contact between the two rotors so that no lubrication is required. The main differences between the prototype used by Zaytsev and the current one under study are that Zaytsev [20] used not only wet compression but also liquid injection of ammonia-water. In the new prototype no liquid is injected, the two-phase working fluid (ammonia-water) is compressed directly. Another important factor is that in the new prototype the rotors are kept apart by timing gears and therefore no losses are caused because of friction in contrast to Zaytsev's prototype. Additionally, a labyrinth seal, a seal that lies between the discharge and suction nozzle of the compressor, which caused additional leakage was included in Zaytsev´s prototype.

Liquid injection, added power input caused by friction, and the leakage caused by the labyrinth seal are implemented in the validation, however, they are not applicable for the

new prototype and are therefore not implemented in the analysis in the following sections. Nannan [106] analyzed the leakage flow through the labyrinth seal. The method that gave the best results was the one developed by Eser and Kazakia [107]. The one used by Zaytsev [20], the Blasius equation was, however, not far off and is easier to implement and is therefore used:

$$\dot{m} = \rho A \left(\frac{2 d_h \Delta P}{\rho a L_{\text{seal}}}\right)^{\frac{1}{2+b}} \left(\frac{\rho d_h}{\mu}\right)^{\frac{-b}{2+b}} \tag{4.15}$$

where $a = 0.3164$ and $b = -0.25$. During the experiments of Zaytsev [20] liquid was injected between angles 60 to 384 º. When liquid is added the ammonia concentration changes throughout the control volume which can be expressed with the following equation:

$$\frac{\mathrm{d}x}{\mathrm{d}\phi} = \frac{1}{m}\left[\left(\sum_{k=1}^{n} x_{\text{in,k}} \left(\frac{\mathrm{d}m_{\text{in}}}{\mathrm{d}\phi}\right)_k - x \sum_{k=1}^{n} \left(\frac{\mathrm{d}m_{\text{in}}}{\mathrm{d}\phi}\right)_k\right)\right] \tag{4.16}$$

Also additional terms need to be added to the conservation equations, eq. 4.1 and eq. 4.2. And they can be written in the following form:

$$\frac{\mathrm{d}P}{\mathrm{d}\phi} = \frac{1}{\left(\frac{\delta v}{\delta P}\right)_{T,x}}\left[\frac{v}{m}\left(\sum_{k=1}^{n}\left(\frac{\mathrm{d}m_{\text{out}}}{\mathrm{d}\phi}\right)_k - \sum_{k=1}^{n}\left(\frac{\mathrm{d}m_{\text{in}}}{\mathrm{d}\phi}\right)_k\right) + \frac{1}{m}\frac{\mathrm{d}V}{\mathrm{d}\phi} - \left(\frac{\delta v}{\delta T}\right)_{P,x}\frac{\mathrm{d}T}{\mathrm{d}\phi} - \left(\frac{\delta v}{\delta x}\right)_{P,T}\frac{\mathrm{d}x}{\mathrm{d}\phi}\right] \tag{4.17}$$

And the energy conservation can be written in the following form:

$$\frac{\mathrm{d}T}{\mathrm{d}\phi} = \frac{T\left(\frac{\delta v}{\delta T}\right)_{P,x}\left[\frac{v}{m}\left(\sum_{k=1}^{n}\left(\frac{\mathrm{d}m_{\text{out}}}{\mathrm{d}\phi}\right)_k - \sum_{k=1}^{n}\left(\frac{\mathrm{d}m_{\text{in}}}{\mathrm{d}\phi}\right)_k\right) + \frac{1}{m}\frac{\mathrm{d}V}{\mathrm{d}\phi} - \left(\frac{\delta v}{\delta x}\right)_{P,T}\frac{\mathrm{d}x}{\mathrm{d}\phi}\right]}{\left(\frac{\delta v}{\delta P}\right)_{T,x}\left(\frac{\delta h}{\delta T}\right)_{P,x} + T\left(\frac{\delta v}{\delta T}\right)^2_{P,x}} + \frac{\frac{\delta Q}{\delta \phi} + \sum_{k=1}^{l}(h_{\text{in,k}} - h)\left(\frac{\mathrm{d}m_{\text{in}}}{\mathrm{d}\phi}\right)_k}{m\left(\frac{\delta h}{\delta T}\right)_{P,x} + \frac{mT}{\left(\frac{\delta v}{\delta P}\right)_{T,x}}\left(\frac{\delta v}{\delta T}\right)^2_{P,x}} \tag{4.18}$$

Comparison of the experimental data, the current model and the model developed by Zaytsev is shown in a *P-V* diagram in Figure 4.2, and comparison of the calculated and measured efficiencies are listed in Table 4.3. The estimated uncertainty of the isentropic and volumetric efficiency of the compressor from Zaytsev are 18 % and 12 %, respectively [20]. As can be seen the current model can estimate the overall performance of the compressor within these error boundaries. Since it is similar to the model of Zaytsev it similarly underestimates the pressure during compression and slightly overestimates the pressure at the discharge side. It should be noted that the exact clearances of the compressor are not really known since they were not measured accurately by Zaytsev. He mentions in his work that the main reason for the extremely low efficiencies was caused by large

Table 4.1: Rotor main geometrical characteristics.

Rotor length, mm	172.5
Distance between the axes, mm	77.1
Number of male rotor lobes	5
Number of female rotor lobes	6
Wrap angle of the male rotor, °	314
Diameter of the male rotor, mm	104.9
Diameter of the female rotor, mm	80
Estimated average clearance, μm	200*

*The value used by Zaytsev [20] during his validation.

Table 4.2: Experimental results from wet compression experiments from Zaytsev [20].

Suction pressure, bar(a)	3.70	$\pm$ 0.08 bar
Discharge pressure, bar(a)	9.08	$\pm$ 0.13 bar
Injection pressure, bar(a)	4.19	$\pm$ 0.13 bar
Suction temperature, °C	62.8	$\pm$ 0.5 °C
Discharge temperature, °C	97.6	$\pm$ 0.8 °C
Injection temperature, °C	64	$\pm$ 0.5 °C
Ammonia concentration suction, kg kg^{-1}	0.359	$\pm$ 6 %
Injection concentration, kg kg^{-1}	0.284	$\pm$ 10 %
Injection flow rate, kg s^{-1}	0.14	$\pm$ 1 %
Shaft speed, rpm	3500	$\pm$ 7 rpm

clearances. They were both kept large to ensure safe operation taking into account thermal expansion during operation and also they were increased because of rotor wear. It should also be noted that the flow coefficient used for the leakage flow is kept the same as adopted by Zaytsev or 1.2. The flow coefficients used for the suction and discharge flows are 0.8 and 0.6, respectively. Several authors have investigated flow coefficients including Fujiwara and Osada [108], and Prins and Infante Ferreira [109]. It is clear from those studies that the flow coefficients have quite a large range (in the aforementioned studies values from 0.4 to 1.22) and will depend on the specific geometry, working fluid and operating conditions. Since Zaytsev had similar conditions, his coefficients have been used. It

Table 4.3: Comparison of efficiencies, discharge temperature and discharge flow rate between the experimental data from Zaytsev [20], his model and the current model

	Measured	Zaytsev	Current model
Isentropic efficiency, %	5.2	5.6	5.9
Volumetric efficiency, %	7.4	7.2	7.4
Discharge temperature, °C	97.6	98.2	98.4
Discharge flow rate, kg s^{-1}	0.078	0.070	0.077

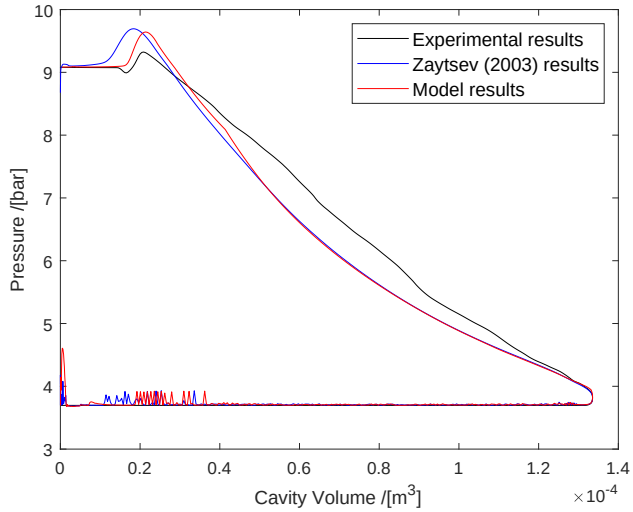

Figure 4.2: Comparison of experimental data from Zaytsev [20], his model and the current model results.

should be pointed out that the location of the discharge port was moved by two rotational degrees to better match the experimental data.

4.4 ANALYSIS AND DISCUSSION

In the following subsections the effects of the main operational parameters are further studied. Another field of study that is not discussed here is the optimization of the geometry of a twin screw compressor as has been done by e.g. Stosic et al. [110]. As mentioned in the previous section, experiments with a new screw compressor prototype are planned in the near future. Unfortunately the detailed geometry is not available therefore the same geometry as defined by Zaytsev is used for the analysis. One uncertainty of the new prototype are the clearances. The two rotors are kept apart by timing gears and additionally the

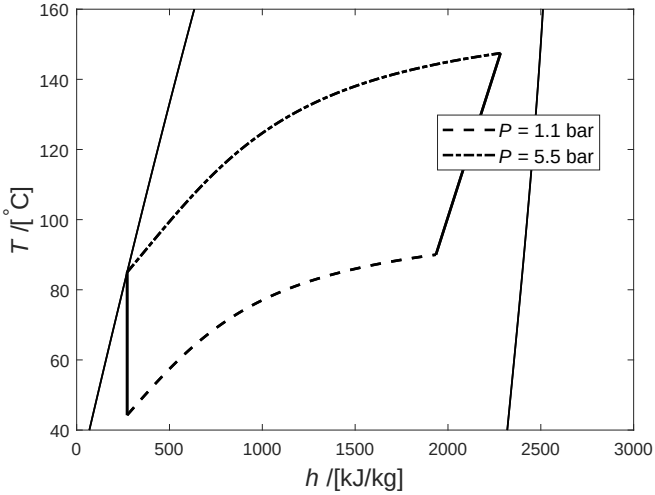

Figure 4.3: *T-h* diagram of a CRHP, using wet compression, for 30 wt.% NH_3. The compression process is entirely in the two phase region from the lower to the higher pressure level. The resorption happens at the higher pressure level, 5.5 bar in this case, then isenthalpic expansion is assumed and the desorption process is at 1.1 bar.

clearances can change during operation due to thermal expansion. However, the rotational speed will be significantly larger. The compressor in practice should be able to operate from around 10,000 until 32,000 rpm which is considerably higher than the 3500 rpm from Zaytsev's experiments. Even though during testing of the first prototype the higher limits will unlikely be tested it is interesting to see the effects on the efficiency and entropy production. Therefore, the effects of clearance size as well as different rotational speeds are investigated in the following sections.

For the prototype there is a minimum pressure limit of around 1.1 bar. This limit is because of the shaft seals that are used. If the pressure is lower there is a danger of oil leaking into the compressor and limiting its performance. In the analysis the discharge pressure is set to 5.5 bar. An example of the CRHP system for 30 wt.% NH_3 is shown in Figure 4.3. The temperature range could be suitable to many potential industrial applications. As mentioned by Chamoun et al. [92] large amount of waste heat at 80-90 °C is available in various industrial sectors where higher temperatures are needed, typically around 120-130 °C. Additionally, the production of steam where at the same time there is a heat source with a temperature glide is an attractive option for CRHP. The location of the discharge port is modified for each case so that it gives results close to perfect compression. The effects of under and over- compression are additionally analysed in the last subsection of this section. Ammonia concentrations in the range from 20 to 40 wt.% NH_3 are investigated since they are normally of interest for CRHP where the heat source and or heat sink have a large temperature glide. The analysed cases are listed in Table 4.4.

Table 4.4: Different operating cases that are investigated in this study.

Nr.	Average ammonia concentration, kg/kg	Clearance, μm	rpm	Inlet vapor quality
1	30	10	10,000	0.6
2	30	50	10,000	0.6
3	30	100	10,000	0.6
4	30	200	10,000	0.6
5	30	50	3,500	0.6
6	30	50	5,000	0.6
7	30	50	20,000	0.6
8	30	50	30,000	0.6
9	20	50	10,000	0.6
10	40	50	10,000	0.6
11	30	50	10,000	0.5
12	30	50	10,000	0.7

4.4.1 CLEARANCE SIZE

In this part the results from cases 1 – 4 from Table 4.4 are discussed. In Figure 4.4 the entropy production for each leakage path is shown as a function of the male rotor angle for average clearance of 10 μm and 100 μm. In Figure 4.5 the *P-V* diagrams of the same cases are shown. The results from case 2 are approximately in between the other two cases. In Table 4.5 the entropy production of leakages, the overall entropy production as well as the isentropic efficiencies are listed for the cases. As expected with larger clearances the efficiency decreases and the entropy production increases. In both cases a small cause of entropy production is at the start of the suction process. The suction process is approximately until male rotation angle of 400 º where the compression process starts until the discharge port is opened around an angle of 650 º. At the start of the suction process there is already a small volume available in the compressor before the suction cavity opens. When the clearances are small this causes a slight pressure and temperature drop. With larger clearances the leakages flows are large enough to maintain the pressure (see Figure 4.5). This shows the importance of a well located suction port. In both cases the largest losses are caused by leakages through the sealing line during the compression process. However, there is a large shift to the left (see Figure 4.4) during the compression process with increased clearance since larger amount leaks back. This can also be seen from the shift in pressure during the compression process in the *P-V* diagram in Figure 4.5. The

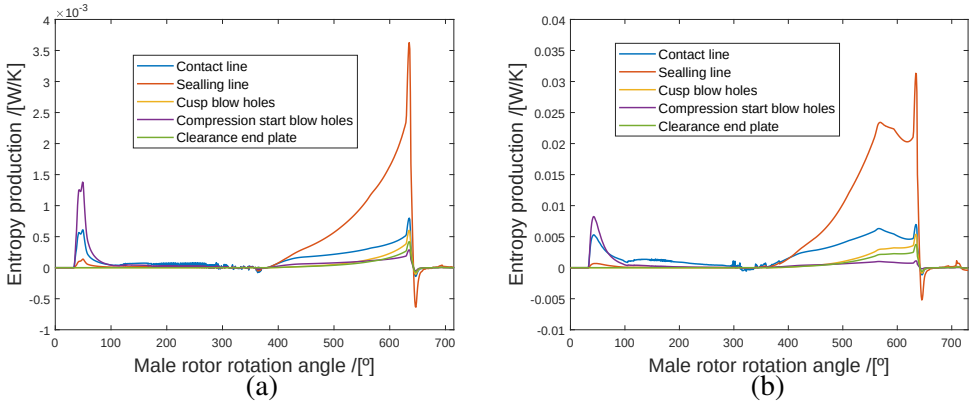

Figure 4.4: $\dot{\sigma}$ for each leakage path in the compressor, 10 μm (a) and 100 μm (b).

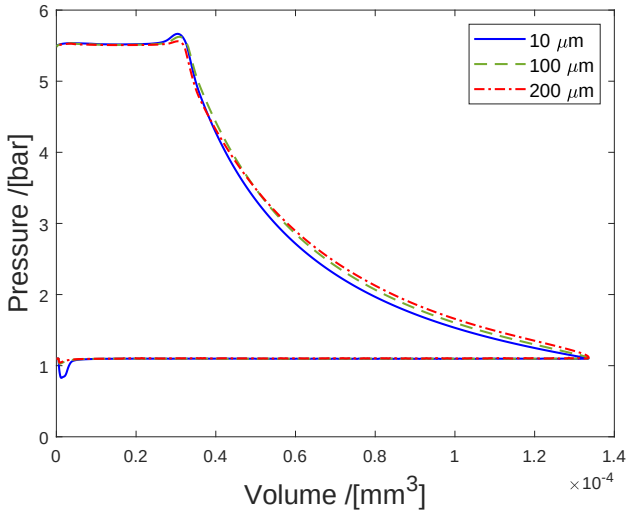

Figure 4.5: *P-V* diagram for 10 μm (blue solid line), 100 μm (green dashed line) and for 200 μm (red dash-dot line).

second largest contributor is leakage through the contact line of the two rotors. It should be noted that the contribution of the leakages are closely related to the clearance of each leakage path. Here an average clearance is assumed. The clearances can be different for each leakage path, along the leakage path and also vary throughout the compression process, for example, for the sealing line due to thermal expansion. Using locally measured clearances can modify these results. In Table 4.5 the main results are listed.

Table 4.5: Isentropic efficiencies, entropy production of the leakages and overall entropy production of cases 1 - 4 (see Table 4.4).

Nr.	Clearance, μm	η_{is}	$\eta_{is,total}$	$\dot{W}$, kW	Entropy production of leakages in, W/K	Entropy production of leakages out, W/K	Overall entropy production, W/K
1	10	0.78	0.73	21.8	0.4	0.2	10.9
2	50	0.71	0.66	22	2.5	1.1	13.6
3	100	0.63	0.58	22.4	5.8	2.8	16.6
4	200	0.45	0.43	22.5	11.8	6.2	18.3

Table 4.6: Isentropic efficiencies and overall entropy production of cases 2, 5-8 (see Table 4.4).

Nr.	Rotational speed, rpm	η_{is}	$\eta_{is,total}$	$\dot{W}$, kW	Entropy production of leakages in, W/K	Entropy production of leakages out, W/K	Overall entropy production, W/K
5	3500	0.57	0.53	7.9	2.3	3.4	7
6	5000	0.65	0.61	11.1	8.8	8.4	8.2
2	10000	0.71	0.65	22	2.5	1.1	13.6
7	20000	0.75	0.7	44	2.1	1	21.6
8	30000	0.73	0.67	67.2	3	1.9	26.9

4.4.2 ROTATIONAL SPEED

In Table 4.6 the isentropic efficiency as well as the overall entropy production for cases 2, 5 - 8 are listed. Chamoun et al. [92] investigated water vapor compression with injected liquid and similarly the efficiency increases with increased rotational speed. Similar trend can be seen here up to a certain point. This difference can be explained by the increase in mechanical losses. As mentioned earlier, experiments conducted by Arjeneh et al. [100] showed that the mechanical losses increase with the rotational speed. When the rotational speed increases also the flow of working fluid through the compressor increases. So in this case a larger entropy production (which follows from the larger flow) is not necessarily negative since there is also a larger displacement of working fluid. Here the isentropic efficiency gives a better indication of which operating condition is more advantageous. Nevertheless, also here the entropy production allows for identification of the major sources of irreversibility in the compressor and remains relevant.

Table 4.7: Isentropic efficiencies and overall entropy production of cases 2, 9 and 10 (see Table 4.4).

Nr.	NH_3 concentration, wt%	η_{is}	$\eta_{is,total}$	$\dot{W}$, kW	Entropy production of leakages in, W/K	Entropy production of leakages out, W/K	Overall entropy production, W/K
9	20	0.68	0.63	22.1	2.4	1	13.9
2	30	0.71	0.66	22	2.5	1.1	13.6
10	40	0.72	0.67	21.9	2.1	1.1	12.6

4.4.3 AMMONIA CONCENTRATION

Depending on each industrial application a specific ammonia concentration will give the optimum results for a CRHP. As mentioned earlier, for large number of industrial application cases the optimum ammonia concentration is in the range of 20 to 40 wt.% ammonia. In Table 4.7 the entropy production of leakages, the overall entropy production as well as the isentropic efficiencies are listed for the cases with different ammonia concentration. Even though the isentropic efficiency increases with increasing ammonia concentration as well as the overall entropy production decreases the effects of the leakages are similar for all 3 cases. Figure 4.6 displays the pressure as a function of the local enthalpy for 20 wt.% ammonia versus 40 wt.% ammonia. The different mixtures have of course quite different properties and with increasing ammonia concentration for a similar process it is clear from the figure that less work is needed for the same compression ratio. It should be noted that different concentrations will lead to different temperature levels. Therefore, this does not mean that for every application it is optimal to operate at higher concentration of ammonia. However, this might cause a slight shift in the optimal ammonia concentration.

4.4.4 VAPOR QUALITY

For CRHP the optimum outlet vapor quality is saturated vapor (quality = 1.0) if it is assumed that the compressor has a fixed isentropic efficiency (Van de Bor et al. [70]). In practice this might be difficult to reach since the temperature increases drastically if the working fluid goes into the superheated region. If the working fluid starts to superheat the temperature rises quickly and the compressor could be damaged because of thermal expansion. Reversed the compressor will also be damaged with excessive amounts of liquid. Higher inlet quality than 0.7 is not possible in this case since the outlet quality at the end of the compression process is close to being saturated vapor. For this reason only the inlet quality range 0.5 to 0.7 will be investigated.

In Table 4.8 the main results are listed. Cao et al. [89] performed experiments with varied gas volume fraction for an oil flooded twin screw compressor. Even though entirely a different mixture they obtained similar results, that is with a lower gas volume fraction the

Table 4.8: Isentropic efficiencies and overall entropy production of case 2, 11 and 12 (see Table 4.4).

Nr.	Vapor quality	η_{is}	$\eta_{is,total}$	$\dot{W}$, kW	Entropy production of leakages in, W/K	Entropy production of leakages out, W/K	Overall entropy production, W/K
11	0.5	0.72	0.67	21.6	2	1	14.1
2	0.6	0.71	0.66	22	2.5	1.1	13.6
12	0.7	0.7	0.65	22.4	3.4	0	13.1

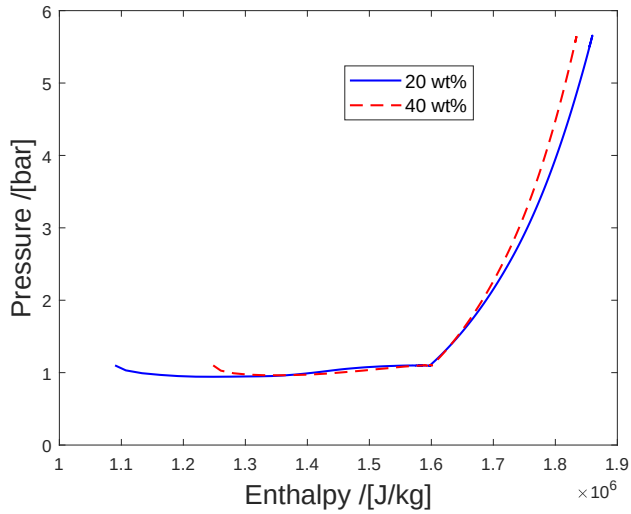

Figure 4.6: Pressure as a function of the local enthalpy, 20 wt.% (blue solid line) and 40 wt.% (red dashed line).

efficiency increased since the liquid partially blocks the leakage paths. In Figure 4.7 the entropy production is displayed for case 2 and 12. The differences are small, however, the difference can be most clearly seen in the decreased losses caused by the contact line during the suction period (until a male rotation angle of approximately 400 º). The entropy production caused by the leakages decreases at lower vapor qualities while the overall entropy production increases. The increase in the overall entropy production can be explained by a slight increase in the overall mass flow at lower inlet qualities. From these results it is clear that it is not satisfactory to use a fixed isentropic efficiency for evaluation of the performance of an CRHP.

Table 4.9: Isentropic efficiencies and overall entropy production of cases 2 with under and over compression (see Table 4.4).

Nr.	Compression	η_{is}	$\eta_{is,total}$	$\dot{W}$, kW	Entropy production of leakages in, W/K	Entropy production of leakages out, W/K	Overall entropy production, W/K
2	Under	0.7	0.66	22.4	2.3	1.1	13.7
2	-	0.71	0.66	22	2.5	1.1	13.6
2	Over	0.69	0.65	22.4	2.4	1.2	13.6

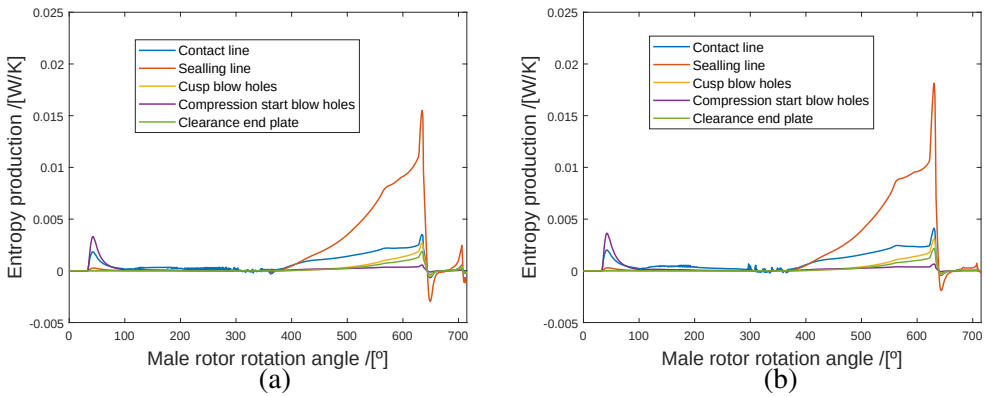

Figure 4.7: $\dot{\sigma}$ for each leakage path in the compressor, 0.6 inlet vapor quality (a) and 0.7 inlet vapor quality (b).

4.4.5 UNDER AND OVER-COMPRESSION

In Table 4.9 the main results from shifting the discharge port by 5 degrees to the left and right for case number 2 (from Table 4.4) are listed. The results are additionally shown in a *P-V* diagram in Figure 4.8. From under and over compressing the efficiency decreases slightly while the entropy production stays more or less the same. This results from slight differences in the overall mass flow. A small degree of under or over compressing should therefore not have a large impact on the overall performance. Of course with a larger deviation the performance will continue to decrease and therefore should be avoided at all cost.

4.5 SIMPLIFIED COMPRESSOR MODEL WITH NH_3-H_2O AND NH_3-CO_2-H_2O

A simplified compressor model based on the same mass and energy conservation equations was developed by Gudmundsdottir [111]. The model described in this chapter needs

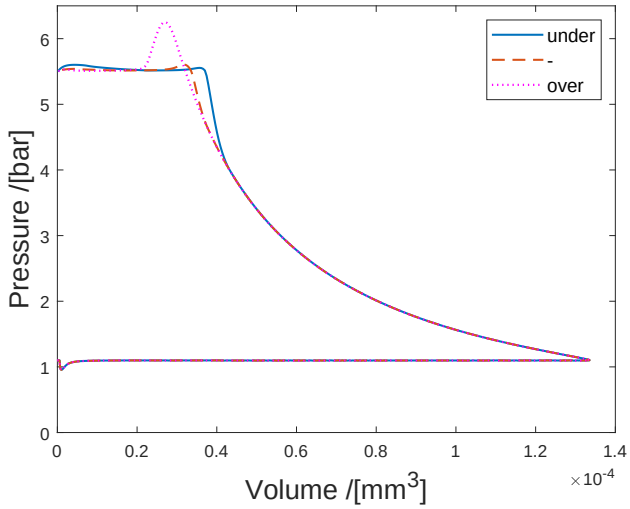

Figure 4.8: *P-V* diagram for under compression (blue solid line), close to perfect compression (red dashed line) and for over compression (magenta dotted line).

detailed information of the compressor geometry. However, this information is frequently not available. Therefore, her approach was to scale the volume and area curves (port and leakage areas) from Tang [112] and Zaytsev [20] to a specific volumetric capacity. Additional goal was to speed up the calculations to ease the use of the model in heat pump cycle calculations. Therefore, the solving method was simplified similar to the approach of Chamoun et al. [92]. Same leakage paths are considered as in the previously designed model, however, the mechanical efficiency is assumed constant or 0.9.

The model is implemented in Matlab. When operating with NH_3-H_2O the thermodynamic properties are calculated with the method developed by Rattner and Garimella [105]. This model was adapted to work with NH_3-CO_2-H_2O as well by Gruijthuijsen [113]. In that case the thermodynamic properties are implemented in table form from the new fit described in Chapter 2. A comparison of the isentropic efficiencies calculated with the previous model, the adaptation of Gudmundsdottir [111] and with 5 wt.% added CO_2 is listed in Table 4.10. From the table it is clear that the efficiencies are slightly higher with the simpler model. This is mainly since the heat loss due to sealing losses are not included and the total leakage areas of the generated profiles are slightly smaller than in the more detailed model. However, the same trends are seen and it can, therefore, be used to estimate the efficiency for different operating conditions. The main exception is that for case 8 the efficiency with the simpler model increases instead of decreases compared to case 7 since the mechanical efficiency is a constant and not a function of the rotational speed. The decrease in efficiency is also steeper when going from 30 wt.% to 20 wt.% with the more detailed model (case 7). With the added CO_2 again the same trends are noticed with

Table 4.10: Comparison of the isentropic efficiencies calculated with the detailed model from this chapter and a simplified version with and without CO_2 for the operating cases listed in Table 4.4

Nr.	Detailed model	Simplified model	Simplified model with 5 wt.% CO_2
	η_{is} / $\eta_{is,total}$	η_{is} / $\eta_{is,total}$	η_{is} / $\eta_{is,total}$
1	0.78 / 0.73	0.8 / 0.72	0.82 / 0.74
2	0.71 / 0.66	0.75 / 0.68	0.77 / 0.70
3	0.63 / 0.58	0.67 / 0.6	0.67 / 0.62
4	0.45 / 0.43	0.47 / 0.42	0.49 / 0.44
5	0.57 / 0.53	0.59 / 0.53	0.62 / 0.56
6	0.65 / 0.61	0.67 / 0.6	0.68 / 0.61
7	0.75 / 0.7	0.79 / 0.71	0.81 / 0.73
8	0.73 / 0.67	0.8 / 0.72	0.83 / 0.74
9	0.68 / 0.63	0.74 / 0.67	0.77 / 0.69
10	0.72 / 0.67	0.75 / 0.68	0.78 / 0.71
11	0.72 / 0.67	0.76 / 0.68	0.79 / 0.71
12	0.7 / 0.65	0.74 / 0.67	0.76 / 0.68

a small increase in the efficiencies. This indicates that there can be an even greater benefit of using the NH_3-CO_2-H_2O mixture than indicated in Chapter 2. This simplified model, with and without CO_2 will, therefore, be used in the subsequent chapter for cycle analysis.

4.6 CONCLUSIONS

This Chapter has introduced the use of local entropy generation to identify the causes of thermodynamic irreversibilities in twin-screw compressors operating oil-free with two-phase ammonia-water as working fluid:

- For identical clearance sizes, the sealing line losses lead to the largest thermodynamic losses of the twin-screw compressor;
- An increase of the clearance size from 10 to 100 μm leads to 10 times larger sealing line losses;
- Since the working fluid flow increases with the rotational speed of the compressor the overall entropy production also increases while the energetic performance may increase. In this case a larger entropy production is not necessarily disadvantageous;
- The effect of ammonia-water concentration on the entropy production losses is limited, higher concentration leads to a small decrease of the entropy production;
- A lower quality at the compressor inlet indicates that more liquid is available for limiting the leakages and so the entropy production;
- Small deviations of the position of the discharge port lead to small under- or over-compression with small changes of the entropy production and should be avoided at all costs.

This Chapter has additionally investigated, for a specific geometry, if a twin-screw compressor is capable of attaining isentropic efficiencies higher than 0.7 so that it will deliver competitive performance results when implemented in wet compression resorption heat pumps. The study has indicated that:

- Clearance sizes should be limited to 50 μm;
- Rotational speed should be maintained above 10000 rpm;
- Ammonia-water concentration should preferably be maintained in the range 30 to 40 wt.%;
- The vapor quality at the inlet of the compressor should be maintained in the range 0.5 to 0.7;

A simplified version of the model was developed as well, for NH_3-H_2O and NH_3-CO_2-H_2O, that shows the same trends as the detailed model but with slightly higher efficiencies. This model can be used more easily for heat pump cycle calculations.

In general, it can be concluded that the compressor efficiency will strongly depend on the operating conditions so that, when predicted the thermodynamic performance of wet compression resorption heat pumps, the specific efficiency needs to be taken into account.

5

TECHNICAL AND ECONOMIC ANALYSIS OF COMPRESSION-RESORPTION HEAT PUMPS

In the previous chapter models have been developed suitable to investigate wet compression in twin screw compressors. In this chapter the simplified models from that chapter are combined with simplified models of the other heat pump components to examine the thermodynamic and economic performance of two potential industrial cases operating with NH_3-H_2O and NH_3-CO_2-H_2O. The results are used to calculate the simple payback period, when a boiler is replaced by a CRHP, as a function of the predicted gas and electricity prices in the Netherlands from 2020 to 2030. As expected, the results are highly sensitive to the operating conditions of the heat pump cycle and the ratio of the gas and electricity price. However, it is clear that even for high temperature glides the payback period can be within acceptable limits, especially if the cost of CO_2 emissions is taken into account.

This chapter is adapted from Gudjonsdottir, V. and Infante Ferreira, C. A. „Technical and Economic analysis of Wet Compression-Resorption Heat Pumps." In: *International Journal of Refrigeration* (2020). Under review.

5.1 INTRODUCTION

As mentioned in the introduction, one of the main reasons why heat pumps are not used to a greater extent in industry is long payback periods, often in the range of 5-8 years or even more [7]. According to industrial sources in the Netherlands, they will only consider applying heat pumps if the payback period is less than three years. In this chapter we, therefore, study the economic performance of two industrial CRHP systems using wet compression.

With the increasing CO_2 allowance price the payback periods for heat pumps can improve significantly. The price set by the European Union Emission Trading System has increased dramatically in the recent years with a jump of around 200 % in 2018 alone [115] and it has kept on increasing in 2019. This has been a much steeper increase than predicted by, for example, ECN in 2017 [116]. They predicted that the price would be around 7 €/ton in 2020 and not go up to 25 €/ton until 2035, which it has already reached in 2019. This increase is positive news for heat pumps that can, as mentioned at the beginning of the introduction, significantly reduce CO_2 emissions in industry.

In recent years a large focus has been on high temperature applications since the potentials are vast in industry [9]. CRHPs are, as mentioned in the introduction, ideal for HTHP applications and both NH_3-H_2O and NH_3-CO_2-H_2O are low GWP working fluids. In this chapter, we therefore, explore two potential applications. The first one is; upgrading a waste heat stream from 90 to 130 ºC; and the second one to upgrade a waste heat stream from 60 to 140 ºC. To achieve this goal the simplified compressor models described in the previous chapter are combined with a simple heat pump model. Firstly, the thermodynamic models are discussed. Thereafter, the simple payback period for these systems compared to a boiler is investigated where sensitivity analysis based on the electricity and gas prices are performed. The cost of CO_2 is, as well, taken into account.

5.2 MODELLING APPROACH

A simplified model of the CRHP – similar to the one used by Van de Bor et al. [12] – is used to get initial guesses of the cycle variables to speed up the calculations. The main equations are listed in Table 5.1. In section 5.3, two application cases are investigated. For the second case to achieve more realistic pressure ratios two compressors are used in series. Where the outlet of the first one is the inlet of the second one and the pressure ratios are taken as equal so that the intermediate pressure is calculated with the following equation

$$P_{\text{interm}} = \sqrt{P_2 P_1} \tag{5.1}$$

The model assumes a fixed isentropic efficiency of the compressor, however, in reality it is a function of the cycle variables. As was shown in the previous chapter the difference

Table 5.1: Equations used to model the CRHP cycle.

$T_1 = [T_{cw} - \Delta T_{driving}]$
$T_3 = [T_{cw} + \Delta T_{driving}]$
$P_2, P_3, h_3, h_4 = f(T_3, q = 0)$
$T_2, h_2 = f(P_3, q = 1)$
$h_1, s_1 = f(P_1, T_1)$
$h_{2,s} = f(P_3, s_1)$
$h_2 = \frac{h_{2s} - h_1}{\eta_{is}} + h_1$

can be significant depending on the operating conditions. Therefore, first an isentropic efficiency is assumed, then it is calculated with the compressor model and iterated until the efficiency change is within 0.1 %. The following realistic assumptions are considered:

- Saturated liquid at the outlet of the resorber
- Isenthalpic expansion
- 5 K minimum temperature driving force in the resorber and desorber and no pressure drop
- Compressor mechanical efficiency of 0.9

The coefficient of performance (COP) when only considering heating demands is defined as the ratio of the heat delivered and the work required by the compressor (see figure 1.1 for reference states).

$$COP = \frac{h_2 - h_3}{h_2 - h_1} \tag{5.2}$$

When considering two compressors in series the required work is the sum from the work required from both compressors

$$COP_{2st} = \frac{h_2 - h_3}{(h_2 - h_{interm}) + (h_{interm} - h_1)} \tag{5.3}$$

When cooling demand is considered the COP is defined as the ratio of not only the heat delivered but additionally the cooling delivered and the work required by the compressor

$$COP_{comb} = \frac{(h_2 - h_3) + (h_1 - h_4)}{h_2 - h_1} \tag{5.4}$$

Table 5.2: Main geometrical characteristic of the compressor used in this study.

Maximum volume per cavity, m^3	$6.04 \cdot 10^{-5}$
Length of the compressor rotors, m	0.337
Rotational speed, rpm	10,000
Number of male rotor lobes	5
Number of female rotor lobes	6
Clearance, μm	50
Discharge opens at, º	690
Stop angle, º	760
Mechanical efficiency, %	90

5.2.1 THE COMPRESSOR MODEL

The compressor calculations are based on the approach developed by Gudmunsdottir [111]. This model is much faster than the detailed model described in Chapter 4 and, as discussed at the end of that chapter, it shows similar trends as the more detailed model. It is, therefore, ideal to investigate the performance of the entire heat pump cycle.

In that model the geometry calculations were simplified. Since it can be challenging to acquire detailed geometry data from compressor manufacturers her approach was to scale the volume and area curves (port and leakage areas) from Tang [112] and Zaytsev [20] to a specific volumetric capacity. The main geometrical characteristics that are used in this study are listed in Table 5.2. The thermodynamic model is a homogeneous model based on mass and energy conservations similar to that of Zaytsev [20]. However, the solving method was simplified similar to the approach of Chamoun et al. [92]. The mass and energy conservation equations are defined in equations 4.1 and 4.2.

The model takes into account the main leakage paths in a screw compressor, which are through:

- The contact line between the two rotors.
- The sealing line between the tip of the rotors and the housing.
- The cusp blowholes at compression side with high pressure.
- The compression-start blowholes at the suction side.
- The discharge end clearance.

Initially, the compression process is solved without any leakages and then including the main leakages. The iteration goes on until the difference in the pressure of each iteration

step at 530 º, during the compression process, converges to a value with less than 1 Pa difference.

The model is implemented in Matlab. When operating with NH_3-H_2O the thermodynamic properties are calculated with the method developed by Rattner and Garimella [105]. The compressor model was adapted to work with NH_3-CO_2-H_2O as well by Gruijthuijsen [113]. In that case the thermodynamic properties are implemented in table form from the new fit described in Chapter 2.

5.2.2 ECONOMIC CALCULATIONS

To determine the simple payback time the methodology is adapted from Jensen et al. [117]. The payback time is calculated based on a CRHP replacing a gas burner:

$$PBP = \frac{TCI_{\mathrm{HP}}}{(FC_{\mathrm{NG}} - FC_{\mathrm{HP}}) + (OMC_{\mathrm{NG}} - OMC_{\mathrm{HP}}) \cdot CRF} \tag{5.5}$$

Where the total cost of investment is determined as

$$TCI_{\mathrm{HP}} = \sum_{k=1}^{K} PEC_k \cdot 3.11 \tag{5.6}$$

Where the factor 3.11, same as used by van de Bor and Infante Ferreira [21], accounts for additional cost such as installation. And the cost of each component is determined as

$$PEC_Y = PEC_W \left(\frac{X_Y}{X_W} \right)^{\gamma} \tag{5.7}$$

Where the PEC_W is the cost at base capacity X_W and γ is the cost function exponent. In Table 5.3, an overview of the cost correlations for each equipment are given. The heat exchanger geometry from Jensen et al. [117] is used and also their cost correlation for a low pressure ammonia chevron plate heat exchanger. From the thermodynamic calculations the necessary area is obtained. For the compressor the same correlation is also used, however, it is multiplied by a factor of 2 to take into account the use of oil-free compressor instead of an oil lubricated one. The factor 2 was advised by industrial partners of the project.

The annual cost for the fuel consumption is estimated for the heat pump as

$$FC_{\mathrm{HP}} = \frac{\dot{Q}}{COP}(c_{\mathrm{el}} + c_{CO_2,el})H \tag{5.8}$$

Where H is the total operating hours per year, c_{el} is the cost of electricity and $c_{CO_2,el}$ is the cost of CO_2, which is estimated from the CO_2 emission factor for electricity and the cost of CO_2 per ton. In a similar way the fuel cost per year is estimated for natural gas as:

$$FC_{\mathrm{NG}} = \frac{\dot{Q}}{\eta_{\mathrm{NG}}}(c_{\mathrm{NG}} + c_{CO_2,NG})H \tag{5.9}$$

Table 5.3: Cost correlations for the heat exchangers and compressor [117]

Equipment	PEC_W (€)	X_W	γ
Heat exchangers	15,526	42.0 [m^2]	0.8
Compressor	11,914 · 2	178.4 [m^3h^{-1}]	0.66
Electrical motor	10,710 · 2	250 [kW]	0.65

Both the cost of electricity and natural gas are varied depending on the predictions made by ECN [116] for the Netherlands in 2020 to 2035. The CO_2 emission factor for natural gas is based up on the values for the Groningen gas field in the Netherlands [118] and the electricity factor is based up on the value from 2010 which was based on the integral method as defined by Harmelink et al. [119]. Since then this factor has increased slightly since use of coal has increased in the Netherlands. However, in the near future the part of renewables will be increased, therefore, this value might give a good estimate for the coming years. These values are all location sensitive and will differ from country to country and should therefore be taken with caution.

The operation and maintenance cost (OMC) is calculated in the same way as Jensen et al., that is assumed 20 % of the total investment cost, and therefore 0 for the gas burner. The capital recovery factor, CRF, is calculated as

$$CRF = \frac{i^{\text{eff}}(1+i^{\text{eff}})^{LT}}{(1+i^{\text{eff}})^{LT}-1} \tag{5.10}$$

Where the effective interest rate is

$$i^{\text{eff}} = \frac{1+i}{1+i_L} - 1 \tag{5.11}$$

Table 5.4 gives an overview of the parameters and the values used for the cost calculations.

5.3 RESULTS AND DISCUSSION

5.3.1 APPLICATION CASES

As mentioned by Chamoun et al. [92] large amount of waste heat at 80-90 °C is available in various industrial sectors where higher temperatures are needed, typically around 120-130 °C. This is partly confirmed by a market study conducted by Spoelstra et al. for the EU28 countries [121]. For most of the applications researched by them the source temperature varies from 50 to 110 °C, and the sink from 70 to 170 °C. There are specifically

Table 5.4: Parameters used for the cost calculations and sources.

Parameter	Sign	Value	Source
Interest rate	i	7 %	[117]
Inflation rate	i_L	2 %	[117]
Technical lifetime	LT	15 years	[117]
Operating time	H	8600 h/year	Industrial sources
Gas burner efficiency	η_{NG}	0.9	[117]
Electricity price	c_{el}	0.03 - 0.05 €/kWh	[116]
Average electricity price (reference case)	$c_{el,avg}$	0.04 €/kWh	
Natural gas price	c_{NG}	0.0134 - 0.034 €/kWh	[116]
Average natural gas price (reference case)	$c_{NG,avg}$	0.0237 €/kWh	
CO_2 price	c_{CO_2}	25 €/ton	[120]*
CO_2 electricity emission factor	$c_{CO_2,el}$	0.460 kg/kWh	[119]
CO_2 natural gas emission factor	$c_{CO_2,NG}$	0.202 kg/kWh	[118]

*Based on values from May, 2019

quite a number of applications having a source temperature of approximately 60 °C and a sink of 140 °C. As remarked in the introduction, CRHP, are ideal for high temperature applications. The first type of application that is considered is, therefore, heating of a waste heat stream from 90 - 130 °C, called case 1 from now on. It is assumed in that case that the inlet of the compressor is at 85 °C. And the second application with a larger temperature increase, from 60 °C to 140 °C, called case 2. For both cases it is assumed that the heat source and sink have a linear glide as a function of the heat load, as is the case with pressurized water. For both cases the focus is on upgrading the heat sink. Therefore, for each set of operating conditions the desorber outlet temperatures will vary. The only restriction is that the temperature pinch is kept as 5 K. The results are as well limited to a minimum pressure of 0.3 bar and maximum of 30 bar. These limits are chosen since operating at lower or higher pressure levels requires specialized and more expensive equipment according to industrial sources. For the NH_3-CO_2-H_2O the thermodynamic property model is not reliable above approximately 50 wt% NH_3 [22]. Therefore, the results with added CO_2 are only calculated until that limit.

The thermodynamic performance of both cases are presented first in the following section and in the subsequent section the economic results. All results are presented as a function of the NH_3 concentration. This is due to the reason that the mixture thermodynamic properties change significantly depending on the NH_3 concentration. It will be clear from the following sections that due to this difference the optimal thermodynamic case does not necessarily represent the optimum economic one.

5.3.2 THERMODYNAMIC PERFORMANCE

When assuming a fixed isentropic efficiency of the compressor it was shown by van de Bor et al. [56] for over 50 industrial cases that the ideal configuration for CRHP is to have close to saturated conditions at the compressor outlet. However, when taking into account operating condition dependent compressor efficiency the outcome can be quite different. Even though twin screw compressors, as assumed in this case, can handle quite some liquid there is a limit. Therefore, the minimum vapor quality is kept as 0.5. To make sure that no superheating occurs the highest tested vapor quality is kept at 0.98, instead of 1. In figure 5.1 the COP is shown as a function of the NH_3 concentration for various compressor outlet vapor qualities for both cases, and in figures 5.2 and 5.3 the pressure ratio and isentropic efficiency, respectively. The solid lines are the results for NH_3-H_2O and to dotted lines with added 5 wt% CO_2. For case 2, using a single compressor results in pressure ratios in the range of 10 to 20. Therefore, as mentioned in the model section, two compressors in series are utilized for case 2. In that case the isentropic efficiencies shown in figure 5.3 are the average from both compressors. The results for each compressor vary slightly, in the range of 1-2 %.

It is clear that the thermodynamic performance differs significantly for the two cases. For case 1, the lower the quality the higher the isentropic efficiency and as well the COP. In this case the thermodynamic optimum is when the resorber temperature glide is fit as closely as possible, that is at low NH_3 concentrations or around 0.15 - 0.2 kg/kg, depending on the vapor quality. With 5 wt% added CO_2 the pressure ratio is slightly lower and both the isentropic efficiency and the COP increase. For case 2, a similar trend is seen with the added CO_2 concerning the isentropic efficiency and the pressure ratio, however, the COP decreases. In case 2, the temperature glide in the resorber is much larger, 80 K instead of 40 K. With the added CO_2 the temperature glide of the mixture decreases, this is beneficial in the first case, however, in the second case this has negative effects. The same reason is why there is a limit to the increase in COP with decreased vapor quality. By lowering the vapor quality the temperature glide of the mixture decreases as well, resulting at some point in lower COP (see figure 5.1). For this case the optimum when considering the NH_3 concentration is also higher, for the same reason. At higher concentrations, up to a certain limit (ca. 50 wt% NH_3), the temperature glide increases. Therefore, to get a good fit in the resorber higher ammonia concentrations are needed in case 2 than in case 1. In this case the highest COPs are around 0.35 - 0.4 wt% NH_3. Note that where the lines are cut off is where the pressure is lower than 0.3 bar or higher than 30 bar.

Above the main focus was on the heat sink. And in case 1 the heat source was cooled down from 90 °C to 60 - 80 °C, depending on the concentration. Those temperature levels are still too high for traditional cooling applications. In case 2, however, for NH_3 concentrations above 0.5 kg/kg the heat source is cooled down to around 15 - 20 °C (assuming a temperature difference of 5 K in the desorber). These streams can be suitable for cooling if there are any cooling needs at the site. Therefore, additional benefits can be obtained

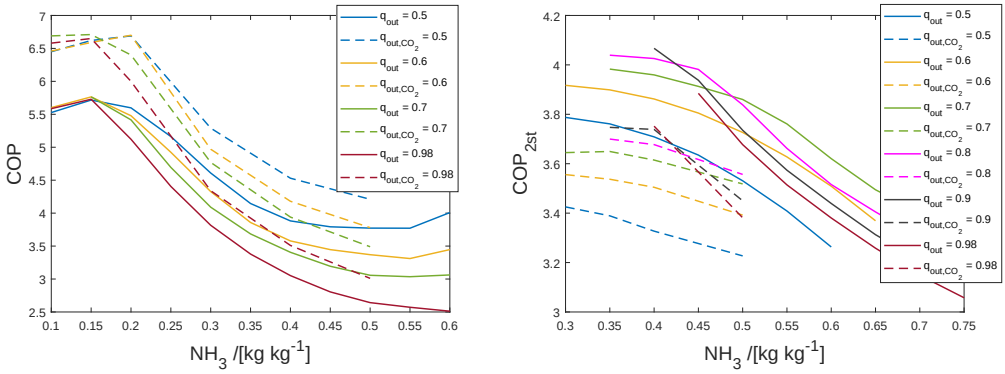

Figure 5.1: COP as a function of the NH_3 concentration for various compressor outlet vapor qualities when a waste heat stream is heated from 90 to 130 °C (a) and from 60 to 140 °C (b). The solid lines are the results for NH_3-H_2O and the dotted lines with added 5 wt% CO_2.

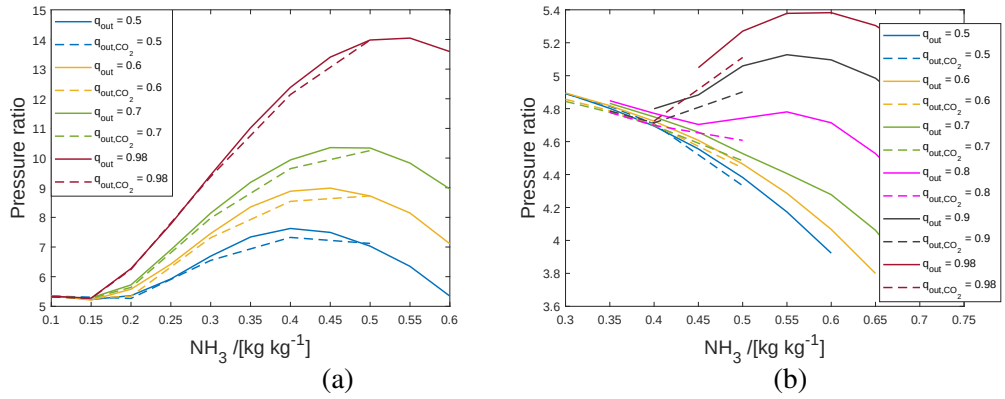

Figure 5.2: Pressure ratio as a function the NH_3 concentration for various compressor outlet vapor qualities when a waste heat stream is heated from 90 to 130 °C (a) and from 60 to 140 °C (b).The solid lines are the results for NH_3-H_2O and the dotted lines with added 5 wt% CO_2.

using these concentrations. Figure 5.4 shows the combined COP for case 2. In this case the COP with the added CO_2 is comparable or slightly lower than without. The difference in COP decreased mainly due to the benefits of the predicted increase in isentropic efficiency with the added CO_2.

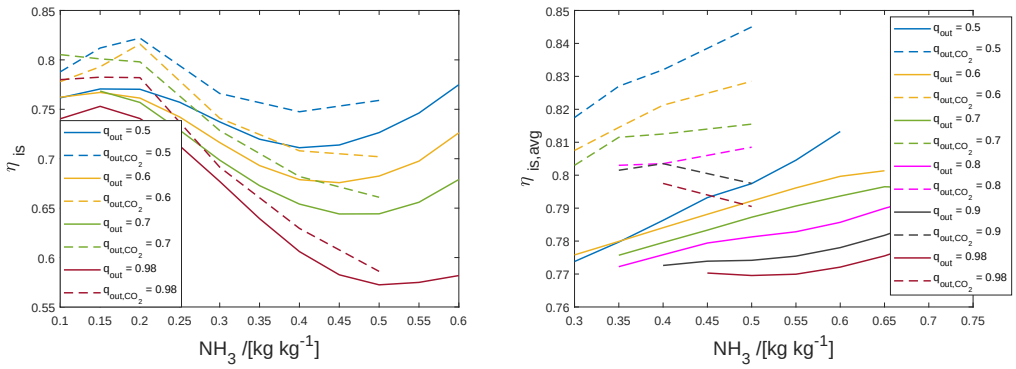

Figure 5.3: η_{is} as a function of the NH_3 concentration for various compressor outlet vapor qualities when a waste heat stream is heated from 90 to 130 °C (a) and from 60 to 140 °C (b).The solid lines are the results for NH_3-H_2O and the dotted lines with added 5 wt% CO_2.

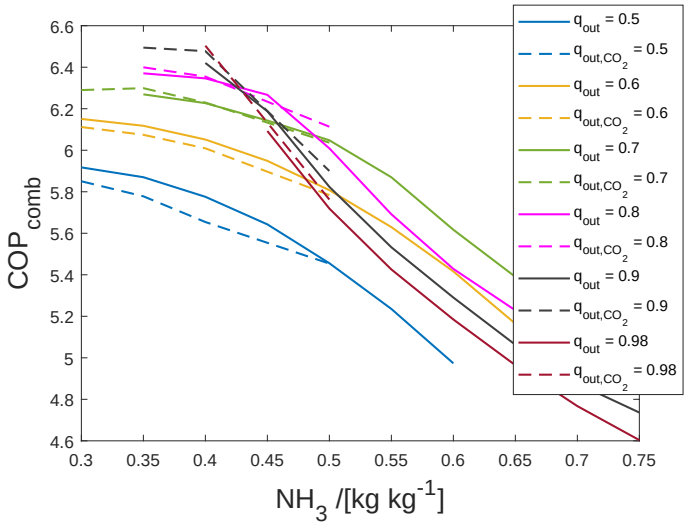

Figure 5.4: COP_{comb} as a function of NH_3 concentration for various compressor outlet vapor qualities when a waste heat stream is heated from 60 to 140 °C.The solid lines are the results for NH_3-H_2O and the dotted lines with added 5 wt% CO_2.

5.3.3 ECONOMIC PERFORMANCE

In the report from Spoelstra et al. [121] where 4065 heat pump installations were identified in the EU28 countries, the vast majority were found within thermal output of 10 MW. With many installations in the 1-2 MW range. Therefore, in the following analysis 1 MW, 5 MW and 10 MW installations are investigated. For case 2 only the NH_3-H_2O mixture is considered since in that case the added CO_2 did not show any additional benefits. It

Table 5.5: Mixture composition, pressures, compressor inlet density, volumetric flow at the inlet of the compressor and COP results for the cases showing the best thermodynamic or economic performance.

		(kg/kg)		q_{out}	P_{low}	P_{high}	$\rho_{comp,in}$	$\dot{m}_{vol,comp,in}$	COP
Case Nr.	NH_3	H_2O	CO_2		(bar)	(bar)	(kg/m^3)	(m^3/s)	
1	0.181	0.819	0	0.7	0.79	4.14	0.74	4.70	5.76
1	0.55	0.45	0	0.5	4.00	25.23	4.74	1.29	3.81
1	0.188	0.762	0.05	0.7	0.84	4.39	0.91	1.79	6.74
1	0.1	0.85	0.05	0.5	0.75	4.02	1.22	1.46	6.45
2	0.4	0.6	0	0.9	0.31	1.51	0.27	9.44	4.07
2	0.65	0.35	0	0.6	1.88	27.1	2.05	2.47	3.37

should also be noted that it is assumed that the same components can be used for both mixtures. In reality specialized absorbers might be necessary when operating with the NH_3-CO_2-H_2O mixture, as explained in Chapter 3. Therefore, the NH_3-CO_2-H_2O results should be taken with caution.

Figure 5.5 shows the simple payback time (without taking into account the cost of CO_2) for the average electricity and gas price from Table 5.4 and 1 MW thermal output. The same case is displayed in figure 5.6 including the cost of CO_2. When these two figures are compared it is clear that it is crucial to account for the cost of CO_2. The payback periods are approximately two times shorter.

For case 1, the payback period decreases with decreased vapor quality. For the NH_3-H_2O mixture, the payback period in general decreases with increased NH_3 concentration. This is mainly due to the fact that with increased NH_3 concentration a smaller compressor is needed since the density increases. With the added CO_2 the trend is slightly different, this is mostly due to the very high COPs at low NH_3 concentrations. The increase in density at higher concentrations is, therefore, not sufficient to decrease the payback period as much. For outlet compressor quality of 0.98 the trend is slightly different. In that case the pressure ratio and efficiency are too unfavorable at higher concentrations, due to a poor temperature fit in the resorber and high compressor outlet temperatures for higher concentrations. For case 2, these trends are even more prominent, that is the payback periods decrease with increased NH_3 concentration and decreased vapor quality. Similar results are seen for 5 and 10 MW thermal output, see figures 5.7 and 5.8, with decreasing cost for increased capacity.

For case 2, the payback period is much longer as expected, since the COP is lower. However, as mentioned at the end of the last section, for this case there might be opportunities to use the heat source for cooling purposes. If that is the case, additional economical benefits can be obtained.

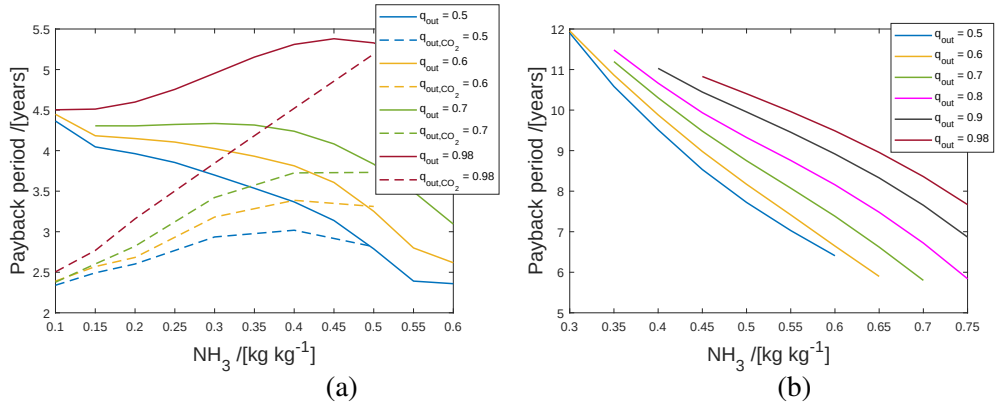

Figure 5.5: The simple payback time as a function of the NH_3 concentration for various compressor outlet vapor qualities, assuming 1 MW thermal output, when a waste heat stream is heated from 90 to 130 °C (a) and from 60 to 140 °C (b).The solid lines are the results for NH_3-H_2O and the dotted lines with added 5 wt% CO_2.

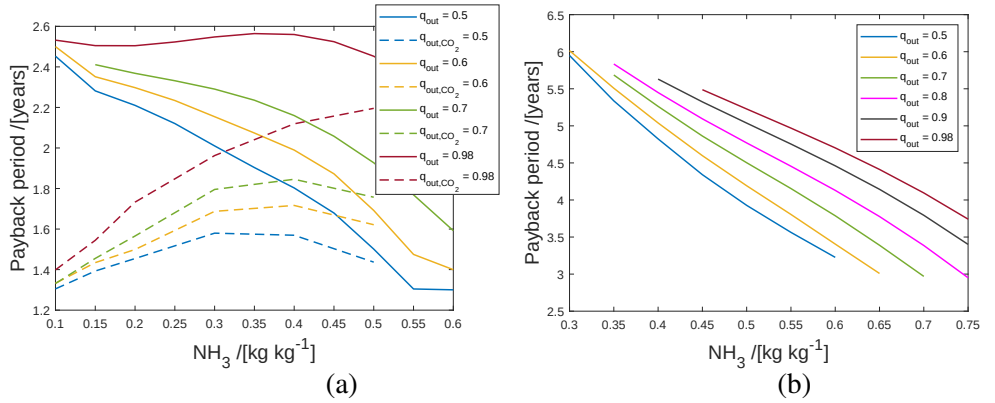

Figure 5.6: The simple payback time taking the cost of CO_2 into account as a function of the NH_3 concentration for various compressor outlet vapor qualities, assuming 1 MW thermal ouput, when a waste heat stream is heated from 90 to 130 °C (a) and from 60 to 140 °C (b).The solid lines are the results for NH_3-H_2O and the dotted lines with added 5 wt% CO_2.

Tables 5.5 and 5.6 compare the cases that showed the best performance either thermodynamically or economically. Note that for case 2, where two compressors are used, the compressor cost and the motor cost is the combined cost for both compressors. Table 5.6 shows that the compressor is by far the most expensive component. The larger the volumetric flow (see Table 5.5), the larger compressor is needed. The cost of the heat exchangers depend on their areas, which are closely linked to the temperature difference inside the heat exchangers. Figure 5.9 shows example of temperature glides for different NH_3 concentrations. For concentrations around 0.5 kg/kg the glide most closely follows the glide

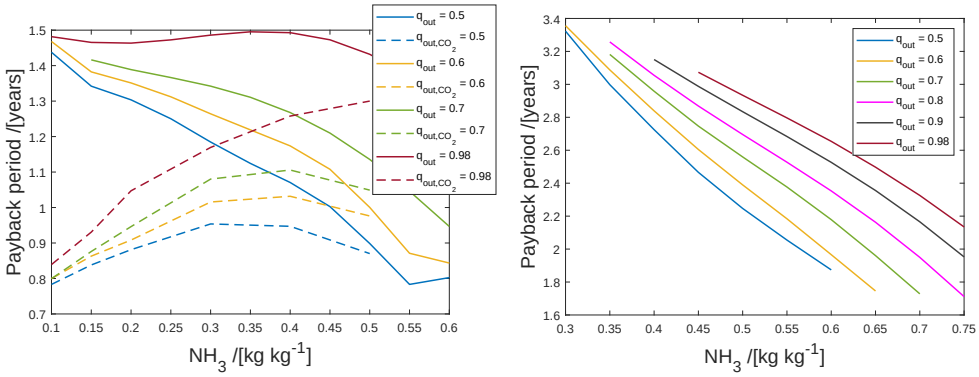

(a) (b)

Figure 5.7: The simple payback time taking the cost of CO_2 into account as a function of the NH_3 concentration for various compressor outlet vapor qualities, assuming 5 MW thermal output, when a waste heat stream is heated from 90 to 130 °C (a) and from 60 to 140 °C (b).The solid lines are the results for NH_3-H_2O and the dotted lines with added 5 wt% CO_2.

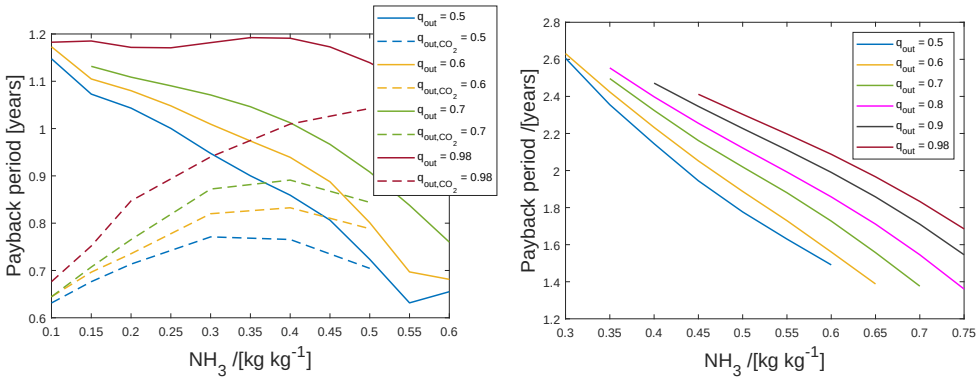

(a) (b)

Figure 5.8: The simple payback time taking the cost of CO_2 into account as a function of the NH_3 concentration for various compressor outlet vapor qualities, assuming 10 MW thermal output, when a waste heat stream is heated from 90 to 130 °C (a) and from 60 to 140 °C (b).The solid lines are the results for NH_3-H_2O and the dotted lines with added 5 wt% CO_2.

of pressurized water (that is linear as a function of the heat load). In those cases larger and, therefore, slightly more expensive heat exchangers are needed than when the temperature fit is poorer.

Figure 5.10 shows the simple payback time results for vapor quality of 0.5 and NH_3 concentration of 0.55 for 5 MW thermal output for case 1 as a function of the gas and electricity price. Figure 5.11 shows similar result, however, for case 2. In this case the

Table 5.6: Mixture composition, component cost (without installation cost) and the average simple payback time (assuming 5 MW thermal output) for the cases showing the best thermodynamic or economic performance.

		(kg/kg)		PEC_{res}	PEC_{des}	PEC_{comp}	PEC_{motor}	PBP_{avg}(5 MW)
Case Nr.	**NH_3**	**H_2O**	**CO_2**	**(k€)**	**(k€)**	**(k€)**	**(k€)**	**(years)**
1	0.181	0.819	0	45.0	58.9	481	48.1	1.50
1	0.55	0.45	0	44.9	65.7	205	63.0	0.77
1	0.188	0.762	0.05	47.7	60.0	255	43	0.90
1	0.1	0.85	0.05	34.6	57.5	222	44.7	0.78
2	0.4	0.6	0	34.8	33.7	1069	76.8	3.15
2	0.65	0.35	0	47.2	40.0	455	86.8	1.75

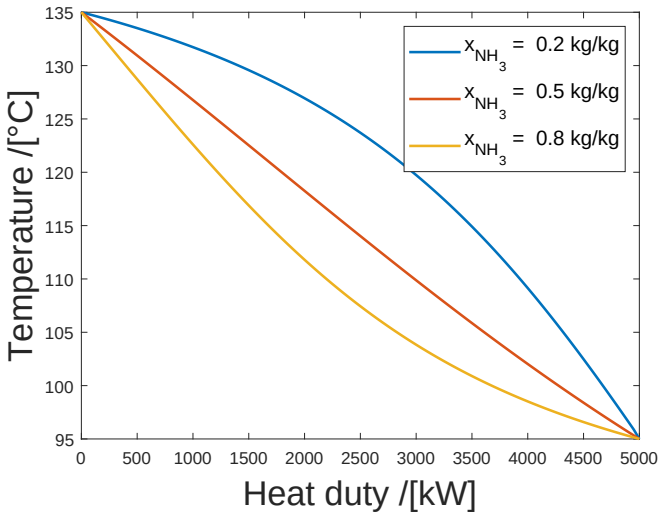

Figure 5.9: Example temperature glides as a function of the heat load for NH_3 concentrations of 0.2 kg/kg, 0.5 kg/kg and 0.8 kg/kg.

vapor quality is chosen as 0.6 and NH_3 concentration of 0.65 for 5 MW thermal output. It is clear in both cases that the payback time is highly sensitive to those prices, especially the gas price. The gas price has been predicted to rise in the following years according the study done by ECN [116]. If this holds true the business case for CRHP will keep on improving. Both figures also emphasize the need to account for the price of CO_2. The difference can be up to 8 times better, depending on the electricity and gas price.

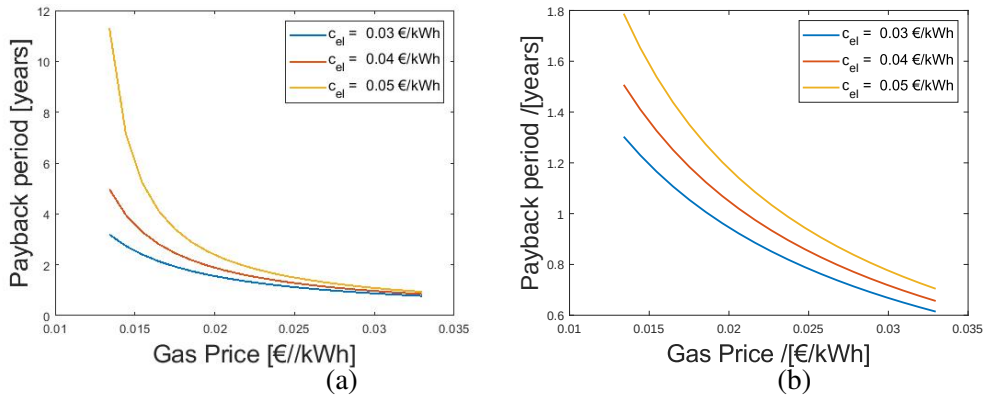

Figure 5.10: The simple payback period as a function of the gas and electricity price for a compressor outlet vapor quality of 0.5 and NH_3 concentration of 0.55, when waste heat stream is heated from 90 to 130 °C, assuming 5 MW thermal output. Not taking into account the cost of CO_2 (a), taking into account the cost of CO_2 (b)

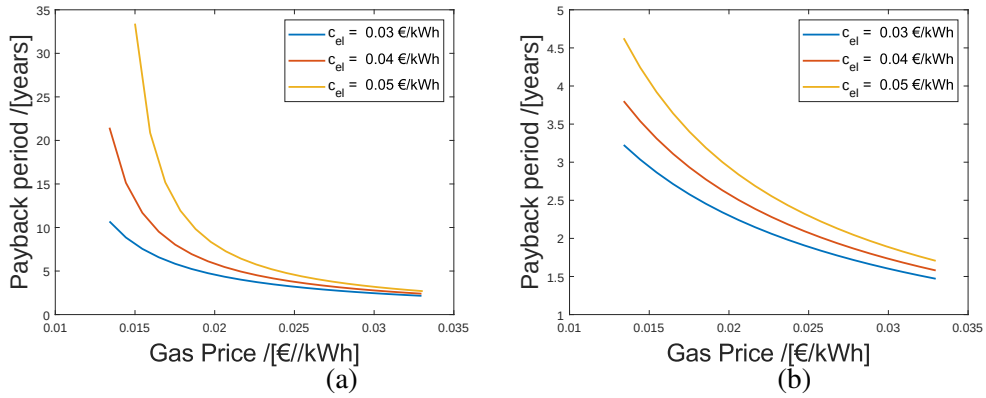

Figure 5.11: The simple payback period as a function of the gas and electricity price for a compressor outlet vapor quality of 0.6 and NH_3 concentration of 0.65, when waste heat stream is heated from 60 to 140 °C, assuming 5 MW thermal output. Not taking into account the cost of CO_2 (a), taking into account the cost of CO_2 (b)

5.4 CONCLUSIONS

It is clear that CRHP are a very promising option to upgrade waste heat streams. This study shows that the payback period can very well be within acceptable limits, even for large temperature glides of 80 K. The results are, however, highly sensitive to the gas, electricity and CO_2 price as expected. It is also quite clear from the results that the thermodynamic optimum is far from being the most economical option in most cases. In general the following conclusions can be drawn from the results:

- The thermodynamic optimum depends on the temperature fit of the resorber when only focusing on heating applications for CRHP.
- It is crucial to account for the price of CO_2 emissions when investigating the business case for heat pumps.
- In general the simple payback period decreases with decreased vapor quality and increased NH_3 concentration.
- For CRHP the compressor is by far the most expensive component of the heat pump system.
- It depends on the application case if it is beneficial to use NH_3-H_2O or NH_3-CO_2-H_2O mixture as a working fluid for CRHP. If the temperature glide is very high, as it is for case 2 investigated in this study, then no additional benefits are attained from the added CO_2. For lower temperature glides, added CO_2 can increase both the thermodynamic and economic performance significantly. Quantitative results will depend on each specific application.

6

CONCLUSIONS & FUTURE PERSPECTIVES

6.1 CONCLUSIONS

The goal of this thesis was to investigate the potential of CRHP utilizing wet compression to upgrade industrial waste streams. Additional focus was to explore how the performance can be further improved. It can be concluded that for high temperature applications with a large temperature glide, CRHP are a very promising option both from a thermodynamic, environmental and economic point of view. To further improve the performance of CRHPs two different paths were taken. The first one was to investigate an alternative working fluid, and the second to explore wet compression in more detail.

Chapters 2 and 3 focused on the first goal by investigating the potential of operating a CRHP with NH_3-CO_2-H_2O, instead of NH_3-H_2O. In Chapter 2, a suitable thermodynamic property model was identified and used to confirm the mixture potentials. To achieve accurate thermodynamic properties a new fit was developed of the existing e-NRTL model available in the Aspen Plus software. The SLE was improved and the application range was extended from 30 wt% NH_3 to around 50 wt% NH_3. Thereafter, simple heat pump calculations showed that for a heating application the COP could be increased by 5 %, and the operating pressure levels and pressure ratio became more favorable compared to NH_3-H_2O. However, when the heat pump must also deliver certain level of cooling then the benefits of added CO_2 appeared insignificant.

To partly validate the findings of Chapter 2, absorption experiments were performed in a mini-channel heat exchanger with NH_3-CO_2-H_2O and NH_3-H_2O. Those findings were displayed in Chapter 3. The main finding were that a heat load increase of approximately 5 % was observed with the added CO_2. However, pumping instabilities limited the operating range and comparable pressure ranges were not accomplished. Additionally, it was confirmed that the best configuration when using a mini-channel heat exchanger for absorption of ammonia in NH_3-H_2O or NH_3-CO_2-H_2O, is to keep the mixture on the tube side and use downward absorption. The performance increased by approximately 10 % compared to upward absorption.

As mentioned in the introduction the benefits of CRHPs are only obtained if the isentropic efficiency of the compressor is high enough. Hence, in Chapter 4, the focus shifts to the compressor performance. In that chapter, twin screw compressor models suitable for wet compression are presented. A detailed model including the local entropy production showed that for identical clearance sizes, the sealing line losses lead to the largest thermodynamic losses in twin screw compressors. The losses decreased with increasing NH_3 concentration and decreased vapor quality and clearance size. The isentropic efficiency also increased to a certain limit with increased rotational speed. In general, it can be concluded that for CRHP the efficiency will largely depend on the operating conditions. Therefore, assuming a fixed efficiency will not give acceptable results. A simplified version of this model was developed that can easily operate with both NH_3-H_2O and NH_3-CO_2-H_2O, and is significantly faster. The simplified version still showed the same trends as the more detailed model, and could therefore be used for heat pump system estimations.

The last chapter evaluated the thermodynamic and economic performance of two high temperature heat pump applications. To achieve that goal, the simplified compressor model was combined with a simple heat pump cycle model to get realistic estimations of the performance. The main results were that the thermodynamic optimum was far off, in both cases, from the economic one. For limited temperature glides NH_3-CO_2-H_2O showed significant thermodynamic benefits over NH_3-H_2O. These benefits, however, disappeared for larger glides. The most expensive component of the system was the compressor and in general the payback period decreased with decreased vapor quality and increased NH_3 concentration. Moreover, it was shown that accounting for the CO_2 allowance price is crucial for the business case of heat pumps. Including the CO_2 allowance price the simple payback time was predicted, even for a large temperature glide, to be within 3 years in most cases. These results are still highly dependent on the gas and electricity price.

To conclude, the thermodynamic and environmental advantages of utilizing heat pumps are irrefutable and the business case, in general, keeps on improving. This will hopefully speed up the implementations of heat pumps in industry. For high temperature applications with a temperature glide, CRHP utilizing wet compression is a very promising option. However, still a couple of extra steps need to be taken before they can be implemented in industry. The following section will address these further actions that are needed.

6.2 FUTURE PERSPECTIVES

To ensure implementation of CRHP in industry the compressor performance has to be validated. At this point a set-up to test wet compression has been built at Delft University of Technology and global experiments at low compressor speeds have been initiated, operating with NH_3-H_2O. At this point, only the inlet and outlet conditions of the compressor are measured. The initial data already partly confirms the trends shown by the compressor models introduced in Chapter 4. That is, with increasing rotational speed and decreasing vapor quality the performance improves. However, more data points are needed to validate the models. Further work is needed to install pressure sensors in order to attain the $P-V$ diagram from the compressor. With such data the compressor models can be further validated and the compressor can be further optimized to operate efficiently in the two phase region.

If the compressor experiments are successful, one of the participating companies of this project is planning to build a pilot plant where the entire heat pump cycle can be investigated. This will help to further identify the challenges and opportunities for CRHP when applied at industrial sites. One of the main challenges will be the control of the system; especially if the process streams are not constant and not at constant temperatures.

Regarding the NH_3-CO_2-H_2O mixture there are still many questions unanswered. Simulations (Chapter 2 and 5) indicate that for certain applications, adding just a small amount of CO_2, can significantly improve the thermodynamic and economic performance. This,

however, is really case specific. The absorption experiments, even though indicating benefits of the added CO_2, were limited by pumping instabilities. This indicates that specialized equipment might be necessary when operating with the NH_3-CO_2-H_2O mixture, which could lead to additional cost. This could be partly confirmed by conducting compressor experiments with NH_3-CO_2-H_2O, and that is indeed the plan after the NH_3-H_2O experiments have been finalized.

REFERENCES

[1] Thunberg, G. n/a. Speech at United nations Climate Action Summit, New York. https://news.un.org/en/story/2019/09/1047052. 2019.

[2] UNCC. The Paris Agreement. https://unfccc.int/process/the-paris-agreement/what-is-the-paris-agreement. 2016.

[3] European Council. Climate and energy policy framework. 2014.

[4] European Environment Agency. Final Energy consumption by sector and fuel. https://www.eea.europa.eu/data-and-maps/indicators/final-energy-consumption-by-sector-9/assessment. 2015.

[5] Kiss, A. A. and Infante-Ferreira, C. A. Heat pumps in chemical process industry. CRC-Press (Taylor & Francis Group), US, 2016.

[6] Wolf, S. and Blesl, M. Contribution of industrial heat pumps to the European climate change mitigation strategy. ECEEE Industrial Summer Study Proceedings. 2016.

[7] IEA. Application of industrial heat pumps. Technical report. https://www.energiteknologi.dk/sites/energiteknologi.dk/files/slutrapporter/annex_xiii_part_a.pdf. 2014.

[8] Arpagaus, C., Bless, F., Schiffmann, J. and Bertsch, S. S. „Multi-temperature heat pumps: A literature review." In: *International Journal of Refrigeration* 69 (2016), pp. 437–465.

[9] Arpagaus, C., Bless, F., Uhlmann, M., Schiffmann, J. and Bertsch, S. S. „High temperature heat pumps : Market overview, state of the art, research status, refrigerants, and application potentials." In: *Energy* 152 (2018), pp. 985–1010.

[10] Bamigbetan, O., Eikevik, T. M., Nekså, P. and Bantle, M. „Review of vapour compression heat pumps for high temperature heating using natural working fluids." In: *International Journal of Refrigeration* 80 (2017), pp. 197–211.

[11] Srikhirin, P., Aphornratana, S. and Chungpaibulpatana, S. „A review of absorption refrigeration technologies." In: *Renewable and Sustainable Energy Reviews* 5 (2001), pp. 343–372.

[12] van de Bor, D. M., Infante Ferreira, C. A. and Kiss, A. A. „Low grade waste heat recovery using heat pumps and power cycles." In: *Energy* 89 (2015), pp. 864–873.

[13] Itard, L. C. M. and Machielsen, C. H. M. „Considerations when modeling compression/resoprtion heat pumps." In: *International Journal of Refrigeration* 17 (1994), pp. 453–460.

[14] Mikielewicze, O. and Wajs, J. „Performance of the very high-temperature heat pump with low GWP working fluids." In: *Energy* 182 (2019), pp. 460–470.

[15] Fukuda, S., Kondou, C., Takata, N. and Koyama, S. „Low GWP refrigerants R1234-ze(E) and R1234ze(Z) for high temperature heat pumps." In: *International Journal of Refrigeration* 40 (2014), pp. 161–173.

[16] Kondou, C. and Koyama, S. „Thermodynamic assessment of high-temperature heat pumps using Low-GWP HFO refrigerants for heat recovery." In: *International Journal of Refrigeration* 53 (2015), pp. 126–141.

[17] Zhang, Y., Zhang, Y., Yu, X., Guo, J., Deng, N., Dong, S., He, Z. and Ma, X. „Analysis of a high temperature heat pump using BY-5 as refrigerant." In: *Applied Thermal Engineering* 127 (2017), pp. 1461–1468.

[18] Xiaohui, Y., Yufeng, Z., Na, D., Chengmin, C., Lijun, M., Lipin, D. and Yan, Z. „Experimental performance of high temperature heat pump with near-azeotropic refrigerant mixture." In: *Energy and Buildings* 78 (2014), pp. 43–49.

[19] Itard, L. C. M. „Wet compression versus dry compression in heat pumps working with pure refrigerants or non-azetropic mixtures." In: *International Journal of Refrigeration* 18 (1995), pp. 495–504.

[20] Zaytsev, D. Development of wet compressor for application in compression-resorption heat pumps. PhD thesis, Delft University of Technology. 2003.

[21] van de Bor, D. M. and Infante Ferreira, C. A. „Quick selection of industrial heat pump types including the impact of thermodynamic losses." In: *Energy* 53 (2013), pp. 312–322.

[22] Gudjonsdottir, V., Infante Ferreira, C. A., Rexwinkel, G. and Kiss, A. A. „Enhanced performance of wet compression-resorption heat pumps by using NH_3-CO_2-H_2O as working fluid." In: *Energy* 124 (2017), pp. 531–542.

[23] Zhao, B., Su, Y., Tao, W., Li, L. and Peng, Y. „Post-combustion CO_2 capture by aqueous ammonia: A state-of-the-art review." In: *International Journal of Greenhouse Gas Control* 9 (2012), pp. 355–371.

[24] Ten Asbroek, N. and Rexwinkel, G. Improved heat pump and process of heat pumping, Frames Renewable Energy Solutions B.V., Patent application number N2016303. 2016.

[25] Vorster, P. P. J. and Meyer, J. P. „Wet compression versus dry compression in heat pumps working with pure refrigerants or non-azeotropic binary mixtures for different heating applications." In: *International Journal of Refrigeration* 23 (2000), pp. 292–311.

[26] Carlson, E. C. „Don't gamble with physical properties for simulations." In: *Chemical Engineering Progress* 92 (1996), pp. 35–46.

[27] Kurz, F., Rumpf, B. and Maurer, G. „Vapor-liquid-solid equilibria in the system NH_3-CO_2-H_2O from around 310 to 470 K: New experimental data and modeling." In: *Fluid Phase Equilibria* 104 (1995), pp. 261–275.

[28] Thomsen, K. and Rasmussen, P. „Modeling of vapor-liquid-solid equilibrium in gas-aqueous electrolyte systems." In: *Chemical Engineering Science* 54 (1999), pp. 1787–1802.

[29] Chen, C. C., Britt, H. I., Boston, J. F. and Evans, L. B. „Local composition model for excess gibbs energy of electrolyte systems. 1. Single solvent, single completely dissociated electrolyte systems." In: *AICHE Journal* 28 (1982), pp. 588–596.

[30] Darde, V., Thomsen, K., van Well, W. J. M., Bonalumi, D., Valenti, G. and Macchi, E. „Comparison of two electrolyte models for the carbon capture with aqueous ammonia." In: *International Journal of Greenhouse Gas Control* 8 (2012), pp. 61–72.

[31] Darde, V., Well, W. J., Stenby, E. H. and Thomsen, K. „Modeling of carbon dioxide absorption by aqueous ammonia solutions using the extended UNIQUAC model." In: *Industrial Engineering Chemistry Research* 49 (2010), pp. 12663–12674.

[32] Darde, V. CO_2 capture using aqueous ammonia. PhD thesis, Technical University of Denmark. 2011.

[33] Que, H. and Chen, C. C. „Thermodynamic modeling of the NH_3-CO_2-H_2O system with electrolyte NRTL model." In: *Industrial Engineering Chemistry Research* 50 (2011), pp. 11406–11421.

[34] Niu, Z., Guo, Y., Zeng, Q. and Lin, W. „A novel process for capturing carbon dioxide using aqueous ammonia." In: *Fuel Processing Technology* 108 (2013), pp. 154–162.

[35] Zhang, M. and Guo, Y. „A comprehensive model for regeneration process of CO_2 capture using aqueous ammonia solution." In: *International Journal of Greenhouse Gas Control* 29 (2014), pp. 22–34.

[36] Liu, J., Gao, H. C., Peng, C. C., Wong, D. S. H., Jang, S. S. and Shen, J. F. „Aspen Plus rate-based modeling for reconciling laboratory scale and pilot scale CO_2 absorption using aqueous ammonia." In: *International Journal of Greenhouse Gas Control* 34 (2015), pp. 117–128.

[37] Maribo-Mogensen, B. Development of an electrolyte CPA equation of state for applications in the petroleum and chemical industries. PhD thesis, Technical University of Denmark. 2014.

[38] Aspen Physical Property System. Version 8.8. Aspen Tech, Cambridge, MA. 2015.

[39] Aspen Physical Property System. Aspen Plus: Rate-based model of the CO_2 capture process by NH_3 using Aspen Plus. Aspen Tech, Cambridge, MA. 2011.

[40] Aspen Physical Property System. Aspen Plus: Rate-based model of the CO_2 capture process by NH_3 using Aspen Plus. Aspen Tech, Cambridge, MA. 2012.

[41] Kim, Y. J., You, J. K., Hong, W. H., Yi, K. B., Ko, C. H. and Kim, J. „Characteristics of CO_2 absorption into aqueous ammonia." In: *Separation Science and Technology* 43 (2008), pp. 766–777.

[42] Park, H., Jung, Y. M., You, J. K., Hong, W. H. and Kim, J. N. „Analysis of the CO_2 and NH_3 reaction in an aqueous solution by 2D IR COS: formation of bicarbonate and carbamate." In: *Journal of Physical Chemistry A* 112 (2008), pp. 6558–6562.

[43] Janecke, E. „Über die Löslickeit von ammonbicarbonat in wasser bis zum schmeltzpunkt." In: *Zeitschrift für Electrochemie* 35 (1929), pp. 332–334.

[44] Göppert, U. and Maurer, G. „Vapor-liquid equilibria in aqueous solutions of ammonia and carbon dioxide at temperatures up to 7 MPa." In: *Fluid Phase Equilibria* 41 (1988), pp. 153–185.

[45] Müller, G., Bender, E. and Maurer, G. „Das dampf-flüssigkeitsgleichgewicht des ternären systems ammoniak-kohlendioxid-wasser bei hohen wassergehalten im bereich zwischen 373 und 474 Kelvin." In: *Berichte der Bunsengesellschaft für Physikalische Chemie* 92 (1988), pp. 148–160.

[46] Yanagisawa, Y., Harano, T. and Imoto, T. „Vapor-liquid equilibrium for ternary system of ammonia-carbon dioxide-water at 70-99 ºC." In: *Nippon Kagaku Kaishi* 2 (1975), pp. 271–274.

[47] Shen, H. M. „VLE measurement and calculation of NH_3-H_2O-CO_2-N_2-H_2 system under high pressure." In: *Huagong Xuebao* 4 (1990), pp. 196–206.

[48] Pexton, S. and Badger, E. H. M. „The examination of aqueous solutions containing only NH_3 and CO_2." In: *Journal of the Society of Chemical Industry* 57 (1938), pp. 107–110.

[49] Jilvero, H., Jens, K. J., Normann, F., Andersson, K., Halstensen, M., Eimer, D. and Johnsson, F. „Equilibrium measurements of the NH_3-CO_2-H_2O system-measurement and evaluation of vapor-liquid equilibrium data at low temperatures." In: *Fluid Phase Equilibria* 385 (2015), pp. 237–247.

[50] Pawlikowski, E. M., Newman, J., and Prausnitz, J. M. „Phase equilibria for aqueous solutions of ammonia and carbon dioxide." In: *Industrial Engineering Chemistry Process Design and Development* 21 (1982), pp. 764–770.

[51] Trypuc, M. and Kielkowska, U. „Solubility in the NH_4HCO_3 + $NaHCO_3$ + H_2O System." In: *Journal of Chemical Engineering Data* 43 (1998), pp. 201–204.

[52] Toporescu, U. „Sur la Préparation du bicarbonate de sodium." In: *Comptes Rendus* 175 (1922), pp. 268–270.

[53] Lichtfers, U. Spektroskopische untersuchungen zur ermittlung von speziesverteilungen im system ammoniak - kohlendioxid - wasser. PhD thesis, Kaiserslautern Univeristy of Technology. 2000.

[54] Rumpf, B., Wyrich, F. and Maurer, G. „Enthalpy changes upon partial evaporation of aqueous solutions containing ammonia and carbon dioxide." In: *Industrial Engineering Chemistry research* 37 (1998), pp. 2983–2995.

[55] Infante Ferreira, C. A., Zamfirescu, C. and Zaytsev, D. „Twin screw oil-free wet compressor for compression–absorption cycle." In: *International Journal of Refrigeration* 29 (2006), pp. 556–565.

[56] van de Bor, D. M., Infante Ferreira, C. A. and Kiss, A. A. „Optimal performance of compression-resorption heat pump systems." In: *Applied Thermal Engineering* 65 (2014), pp. 219–225.

[57] Lemmon, E. W., Huber, M. L. and McLinden, M. O. NIST Standard Reference Database 23: Reference Fluid Thermodynamic and Transport Properties-REFPROP, Version 9.1, National Institute of Standards and Technology, Standard Reference Data Program, Gaithersburg. 2013.

[58] Choi, Y. S. and Nešić, S. „Determining the corrosive potential of CO_2 transport pipeline in high pCO_2-water environments." In: *International Journal of Greenhouse Gas Control* 5 (2011), pp. 788–797.

[59] Krzemień, A., Więckol-Ryk, A. and Smoliński, A. „Assessing the risk of corrosion in amine-based CO2 capture process." In: *Journal of Loss prevention in the Process Industry* 43 (2016), pp. 189–197.

[60] Gudjonsdottir, V., Shi, L. and Infante Ferreira, C. A. „Experimental investigation of the upward or downward absorption process of NH_3-CO_2-H_2O in a mini-channel heat exchanger." In: *International Journal of Heat and Mass Transfer* (2019). Under review.

[61] Qasem, N. A. A. and Zubair, S. M. „Compact and microchannel heat exchangers: A comprehensive review of airside friction factor and heat transfer correlations." In: *Energy Conversion and Management* 173 (2018), pp. 555–601.

[62] Khan, M. G. and Fartaj, A. „A review on microchannel heat exchangers and potential applications." In: *International Journal of Energy Research* 35 (2011), pp. 553–582.

[63] Amaris, C., Vallès, M and Bourouis, M. „Vapour absorption enhancement using passive techniques for absorption cooling/heating technologies: A review." In: *Applied Energy* 231 (2018), pp. 826–853.

[64] Trichè, D., Bonnet, S., Perier-Muzet, M., Boudèhenn, F., Demasles, H. and Caney, N. „Experimental and numerical study of a falling film absorber in an ammonia-water absorption chiller." In: *International Journal of Heat and Mass Transfer* 111 (2017), pp. 374–385.

[65] Nagavarapu, A. K. and Garimella, S. „Experimentally validated models for falling-film absorption around microchannel tube banks: Hydrodynamics." In: *International Journal of Heat and Mass Transfer* 134 (2019), pp. 815–827.

[66] Kang, Y. T., Akisawa, A. and Kashiwagi, T. „Analytical investigation of two different absorption modes: falling film and bubble types." In: *International Journal of Refrigeration* 23 (2000), pp. 430–443.

[67] Castro, J., Oliet, C., Rodrǵuez, I. and Oliva, A. „Comparison of the performance of falling film and bubble absorbers for air-cooled absorption systems." In: *International Journal of Thermal Sciences* 48 (2009), pp. 1355–1366.

[68] van Leeuwen, J. Absorption and desorption of ammonia-water mixtures in mini-channel heat exchangers, Master thesis, Delft University of Technology. 2011.

[69] Garimella, S., Determan, M. D., Meacham, J. M., Lee, S. and Ernst, T. C. „Microchannel component technology for system-wide application in ammonia/water absorption heat pumps." In: *International Journal of Refrigeration* 34 (2011), pp. 1184–1196.

[70] van de Bor, D. M., Vasilescu, C. and Infante Ferreira, C. A. „Experimental investigation of heat transfer and pressure drop characteristics of ammonia–water in a mini-channel annulus." In: *Experimental Thermal and Fluid Science* 61 (2015), pp. 177–186.

[71] Amaris, C., Bourouis, M. and Vallès, M. „Effect of advanced surfaces on the ammonia absorption process with $NH_3/LiNO_3$ in a tubular bubble absorber." In: *International Journal of Heat and Mass Transfer* 72 (2014), pp. 544–552.

[72] Yoon, J. I., Phan , T. T., Moon , Ch. G., Lee, H. S. and Jeong, S. K. „Heat and mass transfer characteristics of a horizontal tube falling film absorber with small diameter tubes." In: *Heat Mass Transfer* 44 (2008), pp. 437–444.

[73] Stephan, P. and Kabelac, S. and Kind, M. and Marting, H. and Mewes, D. and Schaber, K. VDI Heat Atlas. 2nd. Springer, Berlin, 2010.

[74] Nefs, C. W. M., van de Bor, D. M. and Infante Ferreira, C. A. „Laminar single phase flow distribution in a multi-tube mini-channel heat exchanger using fractal distribution." In: *Chemical Engineering and Processing: Process Intensification* 80 (2014), pp. 29–37.

[75] van de Bor, D. M. Mini-channel Heat Exchangers for Industrial Distillation Processes. PhD thesis, Delft University of Technology. 2014.

[76] Lee, K. B., Chun, B. H., Lee, G. C. and Kim, S. H. „Experimental analysis of bubble mode in a plate-type absorber." In: *Chemical Engineering Science* 57 (2002), pp. 1923–1929.

[77] Lee, S., Bohra, L. K., Garimella, S. and Nagavarapu, A. K. „Measurement of absorption rates in horizontal-tube falling-film ammonia-water absorbers." In: *International Journal of Refrigeration* 35 (2012), pp. 613–632.

[78] Cerezo, J., Best, R., Bourouis, M. and Coronoas, A. „Comparison of numerical and experimental performance criteria of an ammonia–water bubble absorber using plate heat exchangers." In: *International Journal of Heat and Mass Transfer* 53 (2010), pp. 3379–3386.

[79] Kang, Y. T., Akisawa, A. and Kashiwagi, T. „Experimental correlation of combined heat and mass transfer for NH_3–H_2O falling film absorption." In: *International Journal of Refrigeration* 22 (1999), pp. 250–262.

[80] Ozgur, C. Demonstration plant design: two conventional distillation columns integrated with two novel heat pumps. PDEng report, Delft University of Technology. 2012.

[81] Park, Y. G., Liu, L. and Jacobi, A. M. „Rational approaches for combining redundant, independent measurements to minimize combined experimental uncertainty." In: *Experimental Thermal and Fluid Science* 34 (2010), pp. 720–724.

[82] Taylor, J. Introduction to error analysis, the study of uncertainties in physical measurements. University Science Books, US, 1997.

[83] Park, C. W., Kim, S. S., Cho, H. C. and Kang, Y. T. „Experimental correlation of falling film absorption heat transfer on micro-scale hatched tubes." In: *International Journal of Refrigeration* 26 (2003), pp. 758–763.

[84] Sparrow, E. M. and Patankar, S. V. „Relationships among boundary conditions and Nusselt numbers for thermally developed duct flows." In: *Journal of Heat Transfer* 99 (1977), pp. 483–484.

[85] Miyatake, O. and Iwashita, H. „Laminar-flow heat transfer to a fluid flowing axially between cylinders with a uniform wall heat flux." In: *International Journal of Heat and Mass Transfer* 34 (1991), pp. 322–327.

[86] Bhagwat, S. M. and Ghajar, A. J. „Similarities and differences in the flow patterns and void fraction in vertical upward and downward two phase flow." In: *Experimental Thermal and Fluid Science* 39 (2012), pp. 213–227.

[87] Kim, J. K., Park, C. W. and Kang, Y. T. „The effect of micro-scale surface treatment on heat and mass transfer performance for a falling film H_2O/LiBr absorber." In: *International Journal of Refrigeration* 26 (2003), pp. 575–585.

[88] Gudjonsdottir, V., Infante Ferreira, C. A. and Goethals, A. „Wet compression model for entropy production minimization." In: *Applied Thermal Engineering* 149 (2019), pp. 439–447.

[89] Cao, F., Gao, T., Li, S., Xing, Z. and Shu, P. „Experimental analysis of pressure distribution in a twin screw compressor for multiphase duties." In: *Experimental Thermal and Fluid Science* 35 (2011), pp. 219–225.

[90] Shen, J., Xing, Z., Zhang, K., He, Z. and Wang, X. „Development of a water-injected twin-screw compressor for mechanical vapor compression desalination systems." In: *Applied Thermal Engineering* 95 (2016), pp. 125–135.

[91] Tian, Y., Yuan, H., Wang, C., Wu, H. and Xing, Z. „Numerical investigation on mass and heat transfer in an ammonia oil-free twin-screw compressor with liquid injection." In: *International Journal of Thermal Sciences* 120 (2017), pp. 175–184.

[92] Chamoun, M., Rulliere, R., Haberschill, P. and Peureux, J. „Modelica-based modeling and simulation of a twin screw compressor for heat pump applications." In: *Applied Thermal Engineering* 58 (2013), pp. 479–489.

[93] Jianfeng, L., Huagen, W., Bingming, W., Ziwen, X. and Pengcheng, S. „Research on the performance of water-injection twin screw compressor." In: *Applied Thermal Engineering* 29 (2009), pp. 3401–3408.

[94] Seshaiah, N., Ghosh, S. K., Sahoo, R. K. and Sarangi, S. K. „Mathematical modeling of the working cycle of oil injected rotary twin screw compressor." In: *Applied Thermal Engineering* 27 (2007), pp. 125–135.

[95] Tian, Y., Shen, J., Wang, C., Xing, Z. and Wang, X. „Modeling and performance study of a water-injected twin-screw water vapor compressor." In: *International Journal of Refrigeration* 83 (2017), pp. 75–87.

[96] Kennedy, S., Wilson, M. and Rane, S. „Combined numerical and analytical analysis of an oil-free twin screw compressor numerical analysis of an oil-free twin screw compressor using 3D CFD and 1D multi-chamber thermodynamic model." In: *IOP Conference Series: Materials Science and Engineering* 232 (2017).

[97] Zaytsev, D. and Infante Ferreira, C. A. „Profile generation method for twin screw compressor rotors based on the meshing line." In: *International Journal of Refrigeration* 28 (2005), pp. 744–755.

[98] Stosic, N., Milutinovic, L., Hanjalic, K. and Kovavacevic, A. „Investigation of the influence of oil injection upon the screw compressor working process." In: *International Journal of Refrigeration* 15 (1992), pp. 206–220.

[99] Arbon, I. M. The design and application of rotary twin-shaft compressors in the oil and gas industry. Mechanical Engineering Publications, 1994.

[100] Arjeneh, M., Kovacevic, A., Rane, S., Manorils, M. and Stosic, N. „Numerical and experimental investigation of pressure losses of a twin screw compressor." In: *IOP Conference Series: Materials Science and Engineering* 90 (2015), p. 012006.

[101] SKF. Bearing friction, power loss and starting torque. Retrieved from http://www.skf.com/group/products/bearings-units-housings/principles/bearing-selection-process/operating-temperature-and-speed/friction-powerloss-startingtorque/index.html. n. d.

[102] Parker Hannifin Corporation. Rotary Seals: Rotary Seals Design Guide. Catalog EPS 5350/USA. 2017.

[103] Beardmore, R. Gear efficiency. Retrieved from http://www.roymech.co.uk/Useful_Tables/Drive/Gear_Efficiency.html. 2013.

[104] Moran, M. J. and Shapiro, H. N. Fundamentals of Engineering Thermodynamics. John Wiley and Sons, 6th edition, 2010.

[105] Rattner, A. S. and Garimella, S. „Fast, stable computation of thermodynamic properties of ammonia-water mixtures." In: *International Journal of Refrigeration* 62 (2015), pp. 39–59.

[106] Nannan, J. R. Analysis of the leakage flow through the labyrinth seal of the ammonia-water two-phase screw compressor, Master thesis, Delft University of Technology. 2004.

[107] Eser, D. and Kazakia, J. Y. „Air flow in cavities of labyrinth seals." In: *International Journal of Engineering Science* 30 (1995), pp. 2309–2326.

[108] Fujiwara, M. and Osada, Y. „Performance analysis of an oil-injected screw compressor and its application." In: *International Journal of Refrigeration* 18 (1995), pp. 220–227.

[109] Prins, J. and Infante Ferreira, C. A. „Quasi one-dimensional steady-state models for gas leakage part II: improvement of the viscous modeling." In: *International Compressor Enginering Conference* (1998). Purdue University, Indiana.

[110] Stosic, N., Smith, I. K. and Kovacevic, A. „Optimisation of screw compressors." In: *Applied Thermal Engineering* 23 (2003), pp. 1177–1195.

[111] Gudmundsdottir, K. Theoretical and experimental investigation of a wet compression process operating with ammonia-water in the application of a CRHP. Master thesis, Delft University of Technology. 2018.

[112] Tang, Y. Computer aided design of twin screw compressors. PhD thesis, University of Strathclyde. 1995.

[113] Gruijthuijsen, D. A. W. Development of a wet screw compressor model operating with NH_3-CO_2-H_2O. Master thesis, Delft University of Technology. 2019.

[114] Gudjonsdottir, V. and Infante Ferreira, C. A. „Technical and Economic analysis of Wet Compression-Resorption Heat Pumps." In: *International Journal of Refrigeration* (2020). Under review.

[115] Król, J. and Oclon, P. „Sensitivity analysis of hybrid combined heat and power plant on fuel and CO_2 emission allowances price change." In: *Energy Conversion and Management* 196 (2019), pp. 127–148.

[116] ECN. Nationale Energieverkenning 2017. Technical report, Amsterdam/Petten, Netherlands. 2017.

[117] Jensen, J. K., Ommen, T., Markussen, W. B., Reinholdt, L. and Elmegaard, B. „Technical and economic working domains of industrial heat pumps: Part 2 - Ammonia-water hybrid absorption-compression heat pumps." In: *International Journal of Refrigeration* 5 (2015), pp. 183–200.

[118] PBL. Uncertainty in the Netherlands' greenhouse gas emissions inventory: Estimation of the level and trend uncertainty using the IPCC Tier 1 approach. Technical report, Bilthoven, the Netherlands. 2009.

[119] Harmelink, M., Bosselaar, L., Gerdes, J., Boonekamp, P., Segers, R., Pouwelse, H. and Verdonk, M. Berekening van de CO_2-emissies, het primair fossiel energiegebruik en het rendement van elektriciteit in Nederland. Technical report, the Netherlands. 2012.

[120] EUA. EU Emission Allowances | Secondary Market. Retrieved, 22nd of May 2019 from https://www.eex.com/en/market-data/environmental-markets/spot-market/european-emission-allowances#!/2019/05/22. 2019.

[121] Spoelstra, S. and Wemmers, A. and Groen, R. Dutch program for the Acceleration of sustainable Heat Management in industry, Scoping study final report. 2017.

ACKNOWLEDGMENTS

There are so many people I need to thank for support during the course of my PhD and for making my time in Delft an unforgettable time of my life. Thankfully, I had great people around me that were there to guide me or, when needed, distract me from my work.

First of all I want to thank my promotor and daily supervisor, Carlos. I had the privilege of doing my master thesis under his supervision and knowing how good he is as a supervisor, it was an easy decision to go for a PhD with him as well. He will always make time to give valuable feedback to any question, even with his busy schedule. Thank you for your advice and your encouragement during these past years! I would also like to thank my promotor, Thijs, for his remarks that helped improve this thesis, and the other committee members, Prof. dr. A. Kovacevic, Prof. Dr. D. M. J. Smeulders, Prof. dr. L. C. M Itard for taking their time to evaluate this work. Special thanks to Prof. dr. Tony Kiss, another committee member, and a valuable part of the project at the start. Thank you for interesting discussions and great feedback to my work.

I also have to thank all the participating companies. Without their knowledge and advice this work would not be where it is at the moment: Nick and Glenn from Frames, special thanks for advice regarding the set-up and the NH_3-CO_2-H_2O mixture; Robert and Peter from IBK, for advice regarding equipment and the setup; Lawien from Nouryon for interesting discussion about the heat exchanger experiments and potential application cases; Kees from Dow, for all the great advice concerning equipment and the financial aspects; Klaartje and Agata from ISPT for making sure the project ran smoothly; and finally, Anton from Atlas Copco. This has been a roller coaster for sure. In your own words from March last year: "It seems like it is just not meant to be. Never had so much misfortune in a project before and this should have been a straight forward engineering task." I'm grateful for all your time and that you did not give up. Finally we are seeing some results!

During these four years many days were spent in the lab at P&E. Without the technicians the current compressor set-up would not be there at all. I want to thank all of them for their hard work and for providing their knowledge that helped improve the setup. I would especially like to thank Gerard who basically built the setup from scratch! Also Martijn for all the electrical work and great discussion about many details regarding the setup, and Bas for helping me out when the others were not available. Jan and Will, thank you for the labview implementations for both set-ups.

I was lucky to have great master students during the course of my PhD that gave valuable inputs to this work. Stefan, Liang, Kristín, Dionne and Varun, it was a pleasure to work with you and I wish Varun good luck with continuing the compressor experiments!

I would also like to thank all the ETH group members for enjoyable discussions and group meetings. I would especially like to thank Mang and Xuan for all the great discus-

sions and the conference trips we went on together. I would also like to thank Remco for the Dutch summary. And our final secretary, Leslie, that was always helpful and super quick to arrange everything from lunches to new contracts.

I would also like to thank the members of the 3ME PhD council, present and past, and Mascha from the 3ME Graduate school. It was a pleasure to work with all of you organizing lunches, events, company visits and trying to solve and discuss various problems that PhDs encounter in our department. It was nice to get a glimpse of the "behind the scenes" of the Graduate school.

I was very lucky to get to know a lot of amazing people during my stay in Delft. Starting with all the friends I made during the masters and made it an easy decision to decide to stay in Delft like Alex, Venky, Patrick, Salah, Liona and Birgit. Thank you for all the great times we spent together! Then when I started the PhD I was fortunate to end up in the best office in P&E which made the transition of starting the PhD even smoother. Thanks to all the 34-K-1-290 people! Nikos, Carla, Samira, Fatma, Hakan, Luis, Ursa, Karsten, Reza, Vincent, Jelle, Johan, Elyas, Simone, Stefan and Rishabh. Not forgetting my paranymphs, Gustavo, almost as annoying as myself, and Noura! I will miss you guys so much and I'm afraid future office mates will not be able to be as amazing as you! We have shared so many amazing moments together, not just coffee and ping pong breaks but also many unforgettable evenings, brunches and even weddings! I would also like to thank all my other friends from Delft, like my former roommates, Maaike, Fay, Federica and Dhruv, and newly made ones, Marco and Filippo. You will probably not miss my cooking skills but I will for sure miss yours! These last years have been so much fun due to all of you guys! I hope we will never loose touch and you know you are always welcome to visit me in Iceland!

I would also like to thank my family and friends from back home. I know I will always have your support and I'm looking forward to join you again in Iceland. It has been especially nice to have my sister, Sólrún, in the same town these last 5 years. Thank you for all the talks and nice dinners! After you and Maggi defend your own PhDs this year (thanks to him as well) we should keep up the tradition of regular dinners! I also have to specially thank my friend Margrét! You helped me get through a very difficult time in my life at the start of my PhD and many other tough ones along the way. I will forever be grateful for having you as a friend and cannot wait to be able to spend more time with you and your little ones in Iceland.

Last but not least. Pedro, I need to thank you for always being there for me and motivating me to keep going during all the times I felt like given up. Obrigada amorzinho!

Vilborg Guðjónsdóttir
January 2020

CURRICULUM VITÆ

PERSONAL INFORMATION

FULL NAME: Vilborg Guðjónsdóttir

BIRTH DATE: 09-05-1990

NATIONALITY: Icelandic

EDUCATION

2015-2019: PhD Researcher, Process & Energy Dpt., Delft University of Technology, The Netherlands.

2013-2015: MSc in Mechanical Engineering, Energy Technologies, Delft University of Technology, The Netherlands.

2010-2013: BSc in Mechanical Engineering, University of Iceland, Iceland; Exchange Student, Virginia Tech, United States (in 2012, for six months).

LIST OF PUBLICATIONS

Publications included in this thesis:

[1] Gudjonsdottir, V. Infante Ferriera, C. A., Rexwinkel, G. and Kiss A. A. "Enhanced performance of wet compression-resorption heat pumps by using NH_3-CO_2-H_2O as working fluid." In: *Energy* 124 (2017), pp. 531-542.

[2] Gudjonsdottir, V., Infante Ferreira, C. A. and Goethals, A. "Wet compression model for entropy production minimization." In: *Applied Thermal Engineering* 149 (2019), pp. 439-447.

[3] Gudjonsdottir, V., Shi, L. and Infante Ferreira, C. A. "Experimental investigation of the upward or downward absorption process of NH_3-CO_2-H_2O in a mini-channel heat exchanger." In: *International Journal of Heat and Mass Transfer*. Under review.

[4] Gudjonsdottir, V. and Infante Ferreira, C. A. "Technical and Economic analysis of Wet Compression-Resorption Heat Pumps." In: *International Journal of Refrigeration*. Under review.

Publications not included in this thesis:

[1] Gudjonsdottir, V. and Infante Ferreira, C. A. "*Comparison of models for calculation of the thermodynamic properties of NH_3-CO_2-H_2O mixture*." Paper presented at the 16th International Refrigeration and Air Conditioning Conference, Purdue, (2016).

[2] Shi, L., Gudjonsdottir, V., Infante Ferreira, C. A. and Rexwinkel, G. and Kiss, A. A. "*Absorption of CO_2-NH_3-H_2O mixture in mini-channel heat exchangers.*" Paper presented at the 12th IEA Heat Pump Conference, Rotterdam, (2017).

[3] Aarts, S. P., Gudjonsdottir, V., Infante Ferreira, C. A and Kiss, A. A. "*Entropy production minimization of a CRHP*." Paper presented at the 5th IIR International Conference on Thermophysical Properties and Transfer Processes of Refrigerants, Seoul, (2017).

[4] Gudjonsdottir, V., Infante Ferreira, C. A., Goethals, A. and Kiss, A. A. "*Measures to minimize entropy production in compression-resorption heat pumps*." Paper presented at the 13th IIR Gustav Lorentzen conference on natural refrigerants, Valencia, (2018).

[5] Gruijthuijsen, D., Gudjonsdottir, V. and Infante Ferreira, C. A. "*Wet compression with NH_3-CO_2-H_2O*." Paper presented at the 25th IIR International congress of refrigeration, Montreal, (2019).